University of Louisville

ThinkIR: The University of Louisville's Institutional Repository

Electronic Theses and Dissertations

12-2022

Alpha, beta-unsaturated aldehydes: the underrepresented markers of disease.

Saurin Sutaria
University of Louisville

Recommended Citation

α,β-UNSATURATED ALDEHYDES:
THE UNDERREPRESENTED MARKERS OF DISEASE

By

Saurin R. Sutaria
B.S., Indiana University Southeast, 2017
M.S., University of Louisville, 2019

A Dissertation
Submitted to the Faculty of the
College of Arts & Sciences of the University of Louisville
in Partial Satisfaction of the Requirements
for the Degree of

Doctor of Philosophy in Chemistry

Department of Chemistry
University of Louisville
Louisville, Kentucky

December 2022

α,β-UNSATURATED ALDEHYDES:
THE UNDERREPRESENTED MARKERS OF DISEASE

By

Saurin R. Sutaria
B.S., Indiana University Southeast, 2017
M.S., University of Louisville, 2019

A Dissertation Approved

August 29th, 2022

By the following Dissertation Committee:

_____

Dissertation Director: Dr. Michael H. Nantz

_____

Dr. Gerald B. Hammond

_____

Dr. Francis P. Zamborini

_____

Dr. Sanjay Srivastava

DEDICATION

This dissertation is dedicated to my incredible wife

Ashley Marie Sutaria,

without whom I would never have found this path and accomplished all that we have.

ACKNOWLEDGEMENTS

ABSTRACT

α,β-UNSATURATED ALDEHYDES:
THE UNDERREPRESENTED MARKERS OF DISEASE

Saurin R. Sutaria

August 29th, 2022

The peroxidation of unsaturated fatty acids is a widely recognized metabolic process that creates a complex mixture of volatile organic compounds including aldehydes. Elevated levels of reactive oxygen species in cancer cells promote random lipid peroxidation, which leads to an increase in a variety of aldehydes. Many of these volatile aldehydes are exhaled and are of interest as potential markers of disease. Chapter 1 presents a review of reported aldehydes in the exhaled breath of lung cancer patients. α,β-Unsaturated aldehydes, detected primarily when derivatized during exhaled breath preconcentration, are underreported in the reviewed articles. Chapter 1 concludes with our hypothesis that better methods for detection of exhaled α,β-unsaturated aldehydes are needed and will translate into more accurate diagnoses of disease.

Chapter 2 details a new approach to selectively derivatize, concentrate and analyze the underrepresented subset of carbonyl-containing VOC metabolites produced by cells under oxidative stress, namely α,β-unsaturated aldehydes. We examined, using

a peristaltic pump and gas dispersion tube, passing gaseous breath samples through solutions containing thiol derivatization reagents. Thiol reagents were prepared and investigated for their ability to chemoselectively react with α,β-unsaturated carbonyls. The goal of targeting α,β-unsaturated aldehydes via thiol-Michael addition was not achieved, likely due lack of phase transfer of VOCs and slow reaction rate of the 1,4 addition.

Chapter 3 describes a novel breath analysis approach that couples established carbonyl preconcentration technology with UV-Vis spectroscopy to constitute a fast, inexpensive, and noninvasive test for disease. The underlying principle of this work exploits the characteristic absorbance of conjugated α,β-unsaturated aldehydes in the UV spectrum. An increase in cellular oxidative stress, as happens in diseased cells, will result in even higher levels of aldehydes, including unsaturated compounds, in exhaled breath. Thus, we explored UV spectral detection of the unsaturated metabolite fraction within the complex breath carbonyl mixture. A pilot study comparing 10 healthy and 10 symptomatic COVID-19 positive patient breath samples was performed to test the hypothesis that the distinct absorbances of unsaturated carbonyls could be used as a diagnostic indicator. Breath samples were preconcentrated using silicon microreactor technology known to isolate carbonyl compounds as oxime ether adducts. Solvent elution from the microreactor provided sample solutions that then were directly analyzed by UV-Vis spectroscopy. The data indicate that even trace amounts of α,β-unsaturated aldehyde adducts increase UV absorptions in the presence of higher concentration saturated analogs. A significant elevation in UV absorptions from COVID-19 positive

samples was observed, a result that may be due to increases in concentrations of α,β-unsaturated aldehyde metabolites from lipid peroxidation in the positive cohort. On comparing the averaged absorbance from the healthy group to averaged absorbance from the COVID-19 positive group, with plus or minus one standard deviation, at wavelengths from 235 to 305 nm, we noted a clear distinction between the error ranges for the two groups. The data suggests that a UV absorbance threshold could be established, an absorbance above which is indicative of SARS-CoV-2 infection. Application to other diseases may be possible, especially if related to cellular oxidative stress conditions.

As α,β-unsaturated aldehydes are known to elicit harmful effects through alkylation of DNA, proteins, and other biomacromolecules, we explored the toxic effects of a well-known metabolite of benzene, muconaldehyde. For this work we developed a new synthesis. Chapter 4 describes a new synthesis of (E,E)-muconaldehyde, an open-ring metabolite of benzene, from muconic acid. Several syntheses of muconaldehyde have been reported, each requiring multiple steps with the best synthesis having an overall yield of 32%. By our method, muconaldehyde was prepared in 71% yield using a one-pot procedure by selective DIBAL-H-mediated mono-reduction of muconic acid activated as a bis(*N*-acyl-*N*,*N*'-diisopropylurea). The method was demonstrated on gram scale (1.14 g muconaldehyde was prepared in 65% yield).

Finally, Chapter 5 provides the experimental details and spectral characterizations of compounds synthesized during the course of my PhD research.

TABLE OF CONTENTS

LIST OF TABLES

LIST OF FIGURES

LIST OF SCHEMES

CHAPTER 1

LIPID PEROXIDATION PRODUCES A DIVERSE MIXTURE OF SATURATED AND UNSATURATED ALDEHYDES IN EXHALED BREATH — DETECTING THESE ALDEHYDES MIGHT PROVE USEFUL FOR DIAGNOSIS OF DISEASE

1.0. Introduction

This PhD dissertation summarizes my efforts toward developing new methods for breath analysis. My research in the Nantz Group in the Department of Chemistry and close collaboration with the Fu Group in the Department of Chemical Engineering, both at University of Louisville, has been focused on the detection and quantification of exhaled volatile carbonyl compounds. The particular focus on carbonyl compounds stems from the close link between breath carbonyl compounds and the state of oxidative stress in given cells, which in turn may signal a developing or established disease. This relationship is the main topic of Chapter 1. The hypothesis that has driven my research becomes clear after reviewing the origins of aldehydes in breath, as outlined next.

1.1 What is the Interconnection Between Oxidative Stress, Exhaled Carbonyl Compounds, and Disease, Such as Lung Cancer?

Perturbations of oxidant levels, such as reactive oxygen species (ROS), in the cellular matrix arise due to endogenous or xenobiotic processes that are either a cause or effect of various disease states. The oxidative stress (OS) related to such perturbations has been extensively studied and reported in the literature.[1,2,3,4,5] Redox imbalance is directly implicated in lung carcinogenesis; in particular, oxidative cleavage of lung tissue lipids is attributed either to systematic ROS or their presence in the lung organs.[6] Lipid peroxidation (LPO) is a widely accepted free radical process used to describe the oxidative destruction of unsaturated fatty acids. The products of such peroxidation have been confirmed in various biological matrices using a variety of techniques.[7] The wide interest

in LPO-derived metabolites is due in part to the potential of these small, volatile organic products to serve as indicators of early-stage lung cancer.[8]

Lung cancer (LC) is the most common form of malignancy in the world. A reported 142,080 people died from LC in the United States in 2018.[9] The advent of computed tomography (CT) scanning has allowed for the large-scale screening for lung cancer. The surveillance and early diagnosis of LC leads to timely treatment and higher survival rates.[10] However, the disadvantages of repeated exposure to radiation from CT or positron emission tomography (PET) scans, the high false positive rates associated with this primary modality of LC screening, and the need for subsequent, more invasive technologies to confirm diagnoses have limited the wider application of these tests. It is therefore imperative to evaluate alternative methods of LC detection. One promising alternate modality is to analyze the exhaled breath of patients to detect products of LPO and thereby diagnose the presence, extent, and possibly even the type of LC.[11]

While the existence of volatile LPO products in exhaled breath have been known since the 1970s, reports differ in terms of assigning the origin of the volatilome, the mechanism of oxidative breakdown, and the predictive value of exhaled markers for the clinical diagnosis of disease.[12] We have therefore examined the reports that correlate exhaled volatile organic compounds (VOCs) with incidences of LC. This study is aimed to investigate the reports of LPO products while also providing an explanation for the existence and predictive efficiency of individual markers in breath as they relate to lung cancer detection. Although systemic LPO is well established in the literature,[13] the focus here is to evaluate the aldehyde volatilome originating in the lungs. Other LPO-derived

VOC families, such as alkanes, alkenes, and alcohols, have been discussed elsewhere and are not addressed further.[14,15] Limiting this study to aldehydes allowed the focus to be on the particular species of markers that is expected in higher concentrations in exhaled breath, namely volatile aldehydes generated from the oxidative cleavage of mono-, di- and polyunsaturated lipids, which constitute nearly 69% of all phosphatidylcholines—the major lipid class in lung tissue.[16] The LPO products generated within the lungs are expected to better survive the endogenous environment compared to those originating systemically because they can rapidly exchange across the liquid–air interface within the alveoli as they are generated and then be exhaled.

To enumerate the source and predict potential aldehyde candidates of LPO due to lung disease, a systematic approach was followed:

(a) identify common unsaturated fatty acids found in lung tissue.

(b) based on the free radical mechanism of LPO, simulate oxidative cleavage of the identified panel of unsaturated lipids.

(c) list potential aldehyde products of LPO generated by the simulation.

(d) conduct a literature search for reports of the LPO products in exhaled breath and document the analytical techniques used to detect them.

1.2 Lipid Composition of Lung Tissue

To understand the origin of exhaled LPO products, it is first important to understand the source of these oxidative byproducts—the lipidome. The lipid composition of lung tissue is well understood.[17] The human lung is composed of a variety of cell types, and

each cellular membrane contains a signature combination and high percentage of phospholipids.[17] The variations in phospholipids arise from a multitude of possible configurations involving different polar headgroups and types of fatty acid (FA) hydrophobic domains. FAs are incorporated in the cellular membranes and may be either saturated, monounsaturated, or polyunsaturated depending on the biochemical pathway activated for their de novo synthesis. The activation of such pathways may be triggered in response to endogenous or xenobiotic stimulus and may vary widely between individuals. Consequently, the resulting biosynthesis of lipids and the incorporated FAs vary accordingly. While there are abundant studies on the activation of biochemical pathways that result in the selective, enzymatic incorporation of specific FAs in the phospholipid framework, it is outside the scope of this work. The focus was on the most common FAs reported in the lung tissue for the further evaluation of their respective LPO products.[18]

Unlike other organs, lung epithelium (alveolar type II cells) also secretes a surfactant, composed mainly of lipids (90%) and protein (10%), that lines the surface and promotes alveolar stability by lowering surface tension.[16] Lung surfactant may be further classified based on its physical form; namely, tubular myelin, a monolayer at the air-liquid interface, or micellar lipid form. The levels of fatty acids in surfactant are also in a state of constant flux and vary from person to person. Lung surfactant has no unique phospholipids (PL); however, the combinations of fatty acids vary extensively. The PL composition of surfactant is more than three-quarters phosphatidylcholine (PC), and half of these PC lipids are polyunsaturated.[19] Due to the fact that excess ROS also react with

surfactant lipids, leading to a weakened surface tension and the breakdown of lung surfactant as well as LPO products,[20] the composition of surfactant lipids will have a bearing on the aldehyde volatilome. The commonly reported FAs found in human lung tissue and lung surfactant are provided in Table 1.1,[18] and the breakdown of lipids comprising lung tissue is shown in Figure 1.1.[16]

Table 1.1. Commonly reported FAs in lung tissue and lung surfactant.[16,21]

Saturated FA		Monounsaturated FA (MUFA)		Polyunsaturated FA (PUFA)	
12:0 [a]	Lauric acid	16:1	Palmitoleic acid	18:2	Linoleic acid
14:0	Myristic acid	18:1	Oleic acid	18:3	Linolenic acid
16:0	Palmitic acid	20:1	Eicosenoic acid	20:2	Eicosadienoic acid
18:0	Stearic acid			20:3	Eicosatrienoic acid
				20:4	Arachidonic acid
				22:6	Docosahexaenoic acid

[a] XX:Y = number of carbons comprising the FA: number of double bonds in FA.
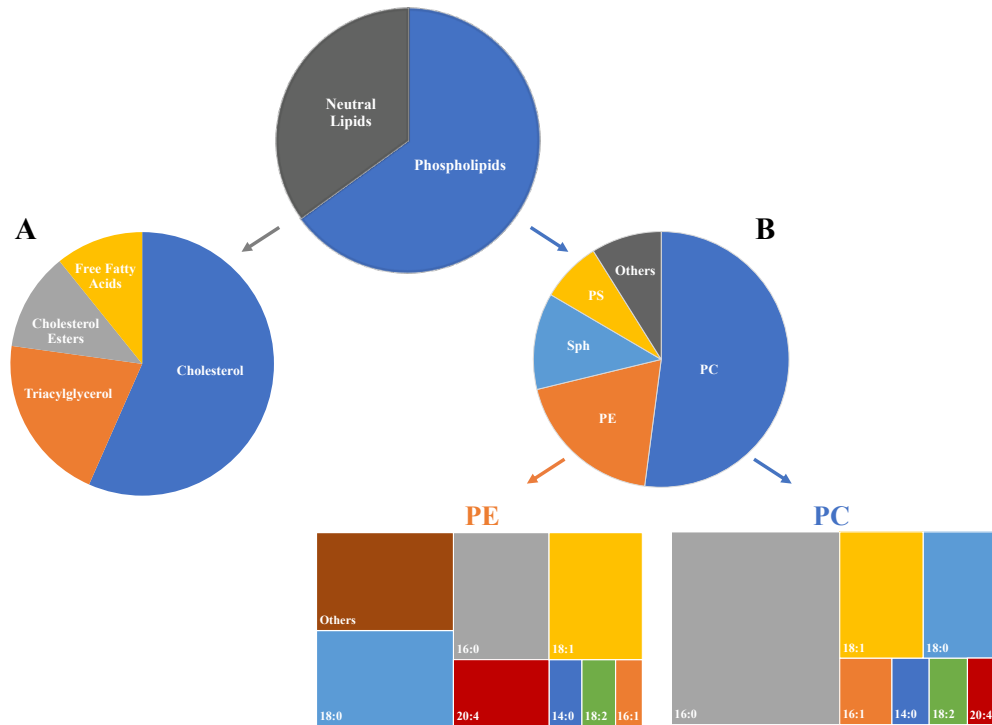
Figure 1.1. Lipid composition of lung tissue. (**A**) Neutral lipid breakdown; (**B**) phospholipid breakdown and relative fatty acid compositions (treemap charts) for the major phosphatides phosphatidylethanolamine (PE) and phosphatidylcholine (PC). For a key to abbreviations, see list at end of article.

To determine the potential aldehyde volatilome that could be generated as a result of LPO in lung tissue, we applied the free radical oxidative cleavage mechanism of LPO to the relevant FAs (Table 1.1) as described in the next section.[14,22] This simulation generated a number of saturated aldehydes, α,β-unsaturated aldehydes, and hydroxyaldehydes. A thorough review of the literature for these compounds required further classification of the LPO-derived aldehydes as those that were either detected in exhaled breath or those that were subjected to discriminatory analyses and deemed to be indicators—biomarkers—of lung cancer.

1.3 Lipid Peroxidation

To understand the random mixture of aldehydes that is formed under LPO conditions, consider the representative reactions of the ω-6 fatty acids linoleic and eicosadienoic, **1a** and **1b**, respectively (Figure 1.2). While 2–5% of major pulmonary phospholipids are linoleic,[23] eicosadienoic is not as prevalent but still common.[24] For reasons related to free radical stability,[25] hydrogen atom abstraction by ROS generated under oxidative stress predominantly occurs at the bis-allylic methylene position to produce the doubly resonance-stabilized free radical **2**. Resonance delocalization leads to the scrambling of alkene stereochemistry to afford isomeric mixtures of *E* and *Z* alkenes at carbons 9-12 for **2a** and carbons 11-14 for **2b**. The subsequent reaction with molecular oxygen generates peroxyl radicals, which afford corresponding pentadienylic hydroperoxides, such as **3a,b** and **5a,b**, as well as bis-allylic hydroperoxides,[26] such as **4a,b**, on hydrogen atom transfer from resident hydrogen donors that include neighboring PUFAs,[27] resulting in the propagation of the free radical-mediated process.

The peroxyl radicals derived from PUFAs with high degrees of unsaturation often undergo cyclization reactions to generate cyclic peroxides,[28] leading to complex mixtures on subsequent cleavage.[29] Redox active metals, such as Fe(II),[30] V(IV) or V(V),[31] and Cu(I),[32] deplete hydroperoxides by generating alkoxy radicals[33,34,35] that undergo carbon–carbon bond scission to release corresponding aldehyde and alkyl radical products.[36] Conversely, hydroperoxide activation via enzyme-mediated (e.g., phospholipid hydroperoxide glutathione peroxidase (phGPx),[37,38] cytochromes P450 (CYP2S1, CYP3A4))[39] or acid-induced processes actuate Hock–Criegee rearrangements[40,41]—peroxide O–O cleavage via neighboring group 1,2-migration—to deliver the mixture of hemiacetals **6**-**9**. Each hemiacetal dissociates to two aldehydes, with the lipid tail-derived fragments (in red, Figure 1.1) producing the more volatile aldehyde fraction consisting of hexanal, heptanal, 2-octenal, and 2-nonenal. In the case of nonenal, the unsaturated aldehyde may be formed with β,γ-unsaturation that subsequently undergoes isomerization to the thermodynamically preferred α,β-position or react with ROS to produce hydroxylated products (e.g., 4-hydroxy-2-nonenal, 4-HNE), as discussed next.[22]

In addition to aldehydes derived from lipid mono-peroxidation, bis-peroxidation processes also contribute to diversify the mixture of volatile aldehydes generated under LPO conditions.[22] As examples, a reduction in lipid hydroperoxides **3a,b** delivers dienyl alcohols **10a,b** that undergo subsequent radical-mediated reactions with diatomic oxygen at various positions to afford hydroperoxides **11a,b** and **14a,b** after hydrogen atom transfers (Figure 1.3). These adducts then are transformed as noted above via hemiacetals **12a,b** and **15a,b** into the hydroxyaldehyde products 4-hydroxynonenal (4-

HNE) and 2-hydroxyheptanal, respectively. Peroxyl radical additions to dienyl intermediates, such as **10a,b**, also occur to generate new radical species that can react with oxygen, as exemplified by the formation of **13a,b**. The subsequent fragmentation of the 1,2-bishydroperoxides produces 4-HNE. [42]
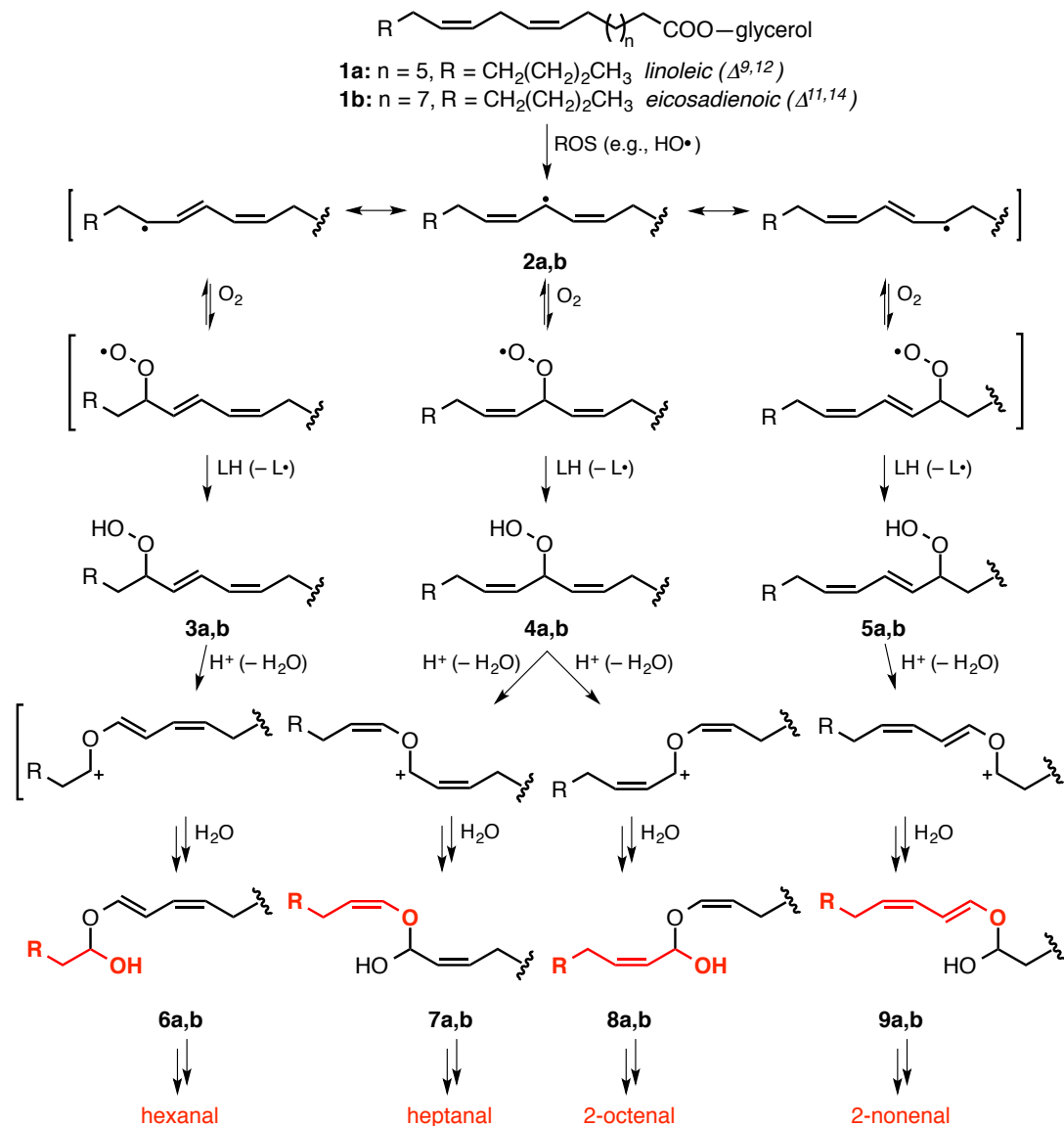
Figure 1.2. Polyunsaturated fatty acyl sidechain oxidation via free radical-mediated hydro-peroxide formation and decomposition leads to mixtures of saturated and unsaturated aldehydes (ROS = reactive oxygen species; LH = neighboring lipid). Atoms in red give rise to the aldehydes generated on hemiacetal equilibrium.

As shown in Figure 1.3, a principal 2-hydroxyaldehyde formed under oxidative stress is 2-hydroxyheptanal.[43,44] Whereas short-chain 2-hydroxyaldehydes are known as products of lipid peroxidation,[43,45] detecting them in exhaled breath presents a considerable challenge due to their facile dimerization, a consequence of the higher carbonyl reactivity imparted by the inductive effect of the adjacent C-OH group.[46] α,β-Unsaturated aldehydes, such as 2-octenal, 2-nonenal, and 4-HNE (aldehydes formed in Figures 1.2 and 1.3), are also more reactive than saturated counterparts, as they are electrophilic at both the carbonyl carbon and the β-carbon and able to undergo both 1,2- and 1,4-addition reactions.[47] Unsaturated aldehydes react with nucleophilic moieties of proteins and nucleic acids, modifying those molecules and effecting their function.[36] Substitution at the γ-carbon (4-position), as in 4-HNE and 4-hydroxy-2-hexenal (4-HHE), somewhat diminishes 1,4-addition reactivity due to steric and electronic considerations and thus confers a longer lifetime.[48] Indeed, 4-HNE is among the most detected and studied LPO products.[49,50]
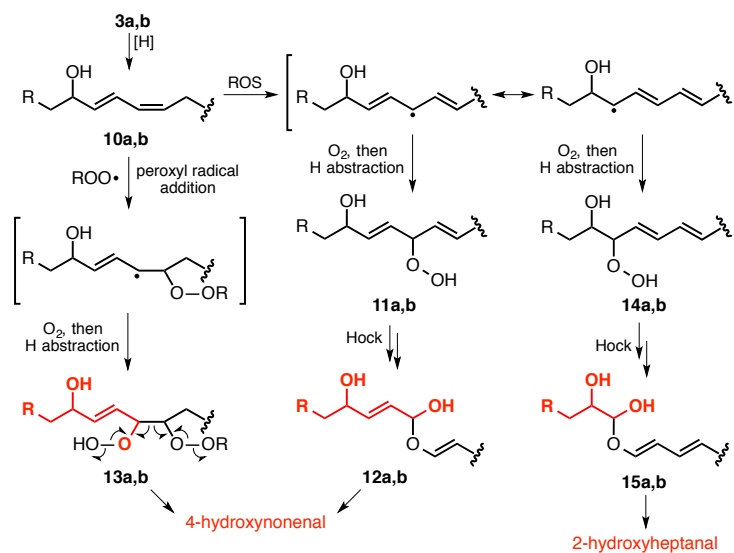
Figure 1.3. Bis-peroxidation pathways leading to the formation of 2- and 4-hydroxyaldehydes. Atoms in red give rise to the aldehydes generated by the indicated processes.

Figures 1.2 and 1.3 illustrate the mixture of aldehydes and aldehyde types that can be formed under LPO conditions. The application of this process to a wider, representative selection of ω-3, -6, -7, and -9 unsaturated FAs taken from Table 1.1 creates a diverse panel of aldehydes, listed in Table 1.2, a result of the random nature of LPO.

Table 1.2. Predicted LPO-derived aldehydes from a selection of unsaturated fatty acyl chains present in common ω-3 to ω-9 lung phosphatides.

Fatty Acid Sidechain	Aldehydes Predicted as LPO Products		
	Saturated	Unsaturated	Hydroxy
ω–3 n = 5: α-linolenic acid ($\Delta^{9,12,15}$) n = 7: eicosatrienoic acid ($\Delta^{11,14,17}$)	propanal butanal	2-pentenal 2-hexenal	2-hydroxybutanal
		4-hydroxyhexenal (4-HHE)	
ω–6 n = 5: linoleic acid ($\Delta^{9,12}$) n = 7: eicosadienoic acid ($\Delta^{11,14}$)	pentanal hexanal heptanal	2-octenal 2-nonenal	2-hydroxyheptanal
		4-hydroxynonenal (4-HNE)	
ω–7 n = 5: palmitoleic (Δ^{9})	hexanal heptanal octanal	2-octenal	2-hydroxyheptanal
ω–9 n = 5: oleic acid (Δ^{9}) n = 7: eicosenoic acid (Δ^{11})	octanal nonanal decanal	2-decenal	2-hydroxynonanal
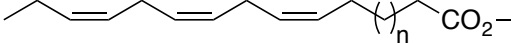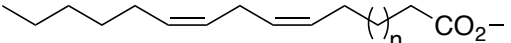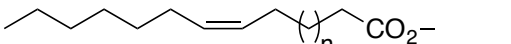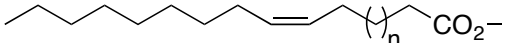
Efforts that have experimentally mimicked LPO conditions in vitro on MUFAs and PUFAs report many of these aldehydes. Tamura et al. carried out oxidations of mono- and polyunsaturated fatty acids with Fe(II) and hydrogen peroxide at 37 °C and found all but two of the α,β-unsaturated aldehydes listed in Table 1.2.[51] In 2007, Kawai et al. reported 33 aldehyde products from in vitro lipid peroxidations at pH 7.4 and 37 °C matching four of the seven α,β-unsaturated aldehydes and four of the five hydroxyaldehydes listed in Table 1.2.[52]

Not shown in Table 1.2 are several low-molecular weight (C1–C3) aldehydes arising from lipid over-oxidation, secondary aldehyde oxidations, or amino acid metabolism; these include formaldehyde, acetaldehyde, hydroxyacetaldehyde, propenal (acrolein), and malondialdehyde (MDA). With the exception of MDA, these aldehydes are common in breath, often as a result of alcohol and tobacco use,[53,54] and as such are not reliable as biomarkers of lung cancer. MDA, however, is a product of LPO and a well-established[55] marker of OS and will be discussed in a later section. Hydroxyacetaldehyde, a reported marker of lung cancer,[56] is more closely linked to serine metabolism than lipid peroxidation.[57,58]

1.4. Search Method and Results

Literature searches for the putative lung LPO-derived aldehydes were performed using the SciFinder[n] and PubMed[®] databases, last searched 25 May 2022, with no restrictions on date of publication. The searches used combinations of the keywords and phrases: lung cancer, breath, and marker. The PubMed[®] searches had no exclusions,

while SciFinder[n] marked 70,178 reports to be ineligible using an automation tool due to a low relevance to the searched terms. Titles and abstracts were screened for reports of exhaled breath related to lung cancer. Those that passed the initial screening process and reported aldehydes were collected for this work. Table 1.3 is a summary of the results. Specifically, 16,378 records were screened by the author SRS, 114 were assessed for eligibility, and 44 studies spanning 34 years, from 1988–2022, were selected. Tabulated data from these 44 reports was reviewed by the Zhenzhen Xie and J.D. Morris. Given the timespan of the reports in this study and differences in patient details reported, the analysis of the data does not include patient age, sex, or race. Smoking history, reported by some studies but not all, is also not tabulated in this analysis and is another limitation of this work.

Table 1.3. Study details and exhaled aldehydes reported in breath analysis articles reviewed [a].

Year	Study [b]	Patients [c]	Stage [d]	Breath Collection	Preconcentration Method	Analytical Instrument	Saturated Aldehydes	Unsaturated Aldehydes
1988	O'Neill[59]	8	NR	Teflon bag	Tenax TA	GC-MS	propanal, octanal, nonanal	
1999	Phillips[60]	108	I-IV	10 L collection apparatus	activated carbon	GC-MS	**hexanal, heptanal**	
2004	Deng[61]	10	I	sampling bulb	CAR/PDMS	GC-MS	**hexanal, heptanal**	
2005	Chen[62]	24	NR	Tedlar bag	SPME (unspecified)	GC-SAW sensor	**hexanal, heptanal**	
2007	Chen[63]	29	NR	Tedlar bag	PDMS	GC-FID	**hexanal, heptanal**	
2009	Bajtarevic[64]	285 [e]	NR	Tedlar bag	CAR/PDMS	PTR-MS/ GC-MS	**pentanal**	
2009	Gaspar[65]	18	IV	Tedlar bag	PDMS	GC-MS	hexanal, heptanal	
2009	Ligor[66]	65	NR	Tedlar bag	CAR/PDMS	GC-MS	pentanal	
2010	Fuchs[67]	12	III-IV	Tedlar bag	PDMS/DVB (PFBHA derivatization)	GC-MS	propanal, butanal, **pentanal, hexanal**, heptanal, **octanal, nonanal**, decanal	
2010	Kischkel[68]	31	II-IV	Tedlar bag	CAR/PDMS	GC-MS	**propanal**, butanal, pentanal, hexanal, heptanal, octanal	2-butenal
2010	Poli[8]	40	I-III	Bio-VOC tube	PDMS/DVB (PFBHA derivatization)	GC-MS	pentanal, **butanal**, **pentanal, hexanal, heptanal, octanal, nonanal**	
2011	Rudnicka[69]	23	NR	Tedlar bag	CAR/PDMS	GC-MS	propanal, butanal, pentanal	
2011	Ulanowska[70]	137	NR	Tedlar bag	CAR/PDMS	GC-MS	**propanal, pentanal, hexanal**	
2011	Buszewski[71]	115	NR	Tedlar bag	CAR/PDMS	GC-MS	propanal, pentanal, hexanal	
2012	Buszewski[72]	29	NR	Tedlar bag	CAR/PDMS	GC-MS	propanal, **butanal**	
2012	Peled[73]	53	I-IV	Mylar bag	Tenax PA	GC-MS	decanal	

[a] Aldehydes in **bold** were identified as biomarkers of LC, whereas aldehydes in normal typeface were detected but not directly correlated with LC; [b] first author of report and literature citation; [c] number of cancer patients examined; [d] lung cancer stage (NR = not reported); [e] 220 samples analyzed by PTR-MS, 65 samples analyzed by GC-MS;

Table 1.3. Study details and exhaled aldehydes reported in breath analysis articles reviewed [a]. (continued)

Year	Study [b]	Patients [c]	Stage [d]	Breath Collection	Preconcentration Method	Analytical Instrument	Saturated Aldehydes	Unsaturated Aldehydes
2014	Bousamra[74]	107	I-IV	Tedlar bag	Si microreactor (ATM derivatization)	FT-ICR-MS		**4-HHE**
2014	Filipiak[75]	36	NR	Tedlar bag	Tenax TA/CAR	GC-MS	butanal, pentanal, hexanal, nonanal, decanal	
2014	Fu[56]	97	I-IV	Tedlar bag	Si microreactor (ATM derivatization)	FT-ICR-MS	pentanal, hexanal, octanal, nonanal	**4-HHE,** 4-HNE
2014	Handa[76]	50	I-IV	—	expiration into spirometer	IMS	**hexanal, heptanal,** nonanal	
2014	Rudnicka[77]	108	I-IV	Tedlar bag	CAR/PDMS	GC-MS	propanal, pentanal, **hexanal**	
2015	Corradi[78]	71	I-IV	Bio-VOC tube	CAR/PDMS or PDMS/DVB (PFBHA derivatization)	GC-MS	propanal, butanal, pentanal, hexanal, **heptanal,** octanal, nonanal	2-hexenal, 2-heptenal, **2-nonenal**
2015	Li[79]	85	I-IV	Tedlar bag	Si microreactor (ATM derivatization)	FT-ICR-MS	**pentanal**	MDA, **4-HHE, 4-HNE**
2015	Ligo[80]	123	III-IV	Tedlar bag	CAR/PDMS	GC-MS	propanal	
2015	Schumer[81]	156	0-IV	Tedlar bag	Si microreactor (ATM derivatization)	FT-ICR-MS		**4-HHE**
2016	Feinberg[82]	22	III-IV	QuinTron bag	aliquot[f]	PTR-MS	butanal, pentanal, hexanal	
2016	Schallschmidt[83]	37	NR	gas bulb and fleece tube	CAR/PDMS	GC-MS	**propanal, butanal,** pentanal, hexanal, heptanal, octanal, nonanal, **decanal**	
2016	Schumer[84]	31	0-IV	Tedlar bag	Si microreactor (ATM derivatization)	FT-ICR-MS		**4-HHE**
2016	Shehada[85]	149	I-IV	Tedlar bag	Tenax TA	Si nanowire sensor	**propanal, pentanal**	
2017	Callol-Sanchez[86]	81	I-IV	Bio-VOC tube	Tenax TA/graphitized carbon black/carbonized mol. sieve	GC-MS	hexanal, heptanal, octanal, nonanal	
2017	Jouyban[87]	7	IV	1 L glass sphere	breath condensate	GC-FID	hexanal, heptanal, **octanal,** decanal	2-decenal

[a] Aldehydes in **bold** were identified as biomarkers of LC, whereas aldehydes in normal typeface were detected but not directly correlated with LC; [b] first author of report and literature citation; [c] number of cancer patients examined; [d] lung cancer stage (NR = not reported); [f] an aliquot of the collected sample was removed for analysis, no preconcentration;

15

Table 1.3. Study details and exhaled aldehydes reported in breath analysis articles reviewed [a]. (continued)

Year	Study [b]	Patients [c]	Stage [d]	Breath Collection	Preconcentration Method	Analytical Instrument	Saturated Aldehydes	Unsaturated Aldehydes
2017	Sakumura[88]	107	I-IV	analytical barrier bag	breath condensate	GC-MS	nonanal	
2018	Wang[89]	233 [g]	NR	Tedlar bag	PDMS/Tenax TA	GC-MS	octanal, nonanal, decanal	
2019	Rudnicka[90]	108	I-IV	Tedlar bag	CAR/PDMS	GC-MS	propanal, pentanal, hexanal	
2020	Koureas[91]	51	NR	Tedlar bag	CAR/PDMS	GC-MS	hexanal, octanal, nonanal	
2020	Munoz-Lucas[92]	107	NR	Bio-VOC tube	Tenax TA/graphitized carbon black/carbonized mol. sieve	GC-MS	hexanal, heptanal, nonanal	
2021	Chen[93]	160	I-IV	Tedlar bag	Tenax TA	GC-MS	**hexanal, heptanal** butanal, **pentanal**,	
2021	Gashimova[94]	40	I-IV	Tedlar bag	Tenax TA	e-nose sensor and GC-MS	**hexanal**, heptanal, octanal, nonanal, decanal	
2021	Li[95]	6	NR	Tedlar bag	AgNP-coated chromatography paper	GC-MS	**propanal, butanal, pentanal, hexanal, heptanal**, octanal, nonanal, decanal	
2021	Long[96]	116	I-IV	Tedlar bag	DVB/CAR/PDMS	GC-MS	**nonanal, decanal**	
2021	Zou[97]	60	I-IV	Tedlar bar	Tenax TA	GC-MS	**octanal**	
2022	Larracy[98]	100	NR	—	Tenax TA	CRDS	hexanal	
2022	Soufi[99]	5	NR	Tedlar bag	POSS naphthalene diimine	GC-MS	pentanal, octanal, nonanal	
2022	Zou[100]	60	I-IV	Tedlar bag	Tenax TA	GC-MS	**hexanal**, octanal, nonanal	

[a] Aldehydes in **bold** were identified as biomarkers of LC, whereas aldehydes in normal typeface were detected but not directly correlated with LC; [b] first author of report and literature citation; [c] number of cancer patients examined; [d] lung cancer stage (NR = not reported); [g] 108 samples were collected in Tedlar bags and preconcentrated by PDMS SPME, 125 samples were collected and preconcentrated using Tenax TA SPME.

16

1.5 Aldehydes Observed in the Exhaled Breath of Cancer Patients

The large variations in the reported median concentrations of the exhaled aldehydes in Table 1.3 are common and can be attributed to differences in VOC capture technology, particularly with respect to the different solid-phase microextraction (SPME) materials that were used (e.g., Carboxen-polydimethylsiloxane (CAR/PDMS) or divinylbenzene-Carboxen-PDMS (DVB/CAR/ PDMS) vs. Tenax extraction). Differences in SPME fiber exposure times, differences in desorption protocols and analysis processes, differences in the patient populations examined, especially with respect to LC staging, and differences in the type of lung cancer studied (non-small cell lung cancer (NSCLC) vs. small cell lung cancer (SCLC)) also contributed to widening the concentration ranges noted for aldehyde biomarkers.[101] Biomarker quantification is further complicated by the nature of the VOC mixture. Brunton et al. compared the adsorptions of aldehydes to different fibers and found that aldehyde recovery by Carbowax/DVB fiber, for example, was lowered by a factor of seven when exposed to an aldehyde mixture compared to recovery on exposure to singular aldehydes.[102] Concentration variations in a population of samples can also be due to environmental effects. Exogenous sources of aldehydes include food consumption, tobacco use, and even inhaled aldehydes from aging building and floor materials in indoor environments,[6,103] thus requiring careful control measurements.

From Table 1.3, when plotting both the incidence of aldehyde detection in lung cancer patient breath and when the presence of a given aldehyde was determined to be

a biomarker of lung cancer for that study, a qualitative assessment of LPO-derived aldehydes as indicators of lung cancer becomes evident (Figure 1.4). Saturated aldehydes are particularly well represented, and their presence is often significantly different in the EB of LC patients relative to healthy control (HC) subjects (Figure 1.4, red bars). In contrast, hydroxyaldehydes and unsaturated aldehydes, which are derived from the same lipids and random LPO processes, are not widely observed, possibly a result of their higher intrinsic reactivity resulting in lower, trace concentrations in exhaled breath. Below are study details for the aldehydes summarized in Table 1.3.
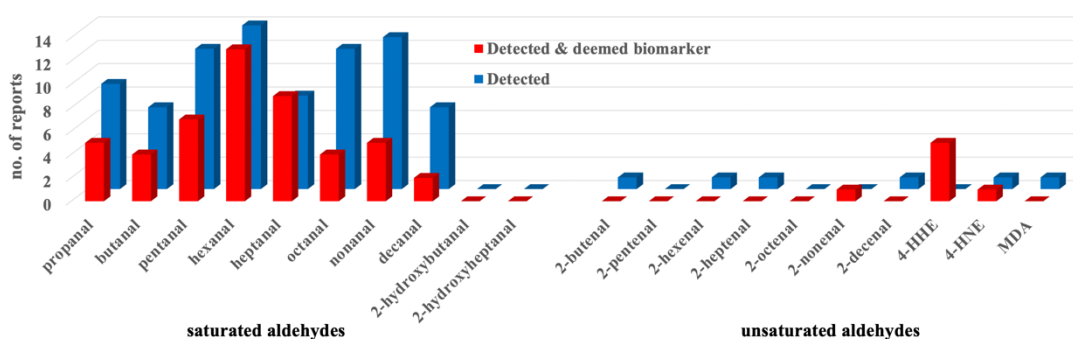
Figure 1.4. Number of literature reports for each aldehyde that was either detected (blue) in the exhaled breath of lung cancer patients or deemed a biomarker (red) of lung cancer. The term biomarker denotes a statistically significant increase in the EB of LC patients compared to healthy controls. Total reports for a given aldehyde are the sum of the red and blue columns.

1.6   Saturated Aldehydes

1.6.1 *Propanal*

The LPO source of propanal is ω-3 FAs. Six independent studies reported that propanal is significantly elevated in the EB of the LC patients relative to levels in HCs and smokers. Kischkel et al. reported a median concentration of propanal in LC patients of 0.34 nmol/L.[68] In comparison, the median propanal levels in HCs and smokers were both

reported as 0.00 nmol/L. Poli et al. noted significantly higher levels of propanal relative to HCs, with mean concentrations of 0.054 nmol/L and 0.031 nmol/L, respectively.[8] Schallschmidt et al. reported a median propanal concentration of 1.01 nmol/L in LC patients and significantly lower levels of propanal in HCs.[83] Ulanowska et al. also observed higher levels of propanal in LC patients, reporting an average propanal concentration of 7.8 ppb, while measuring lower levels of propanal in the breath of HCs at an average concentration of 6.9 ppb.[70] Shehada et al. analyzed breath using silicon nanowire field effect transistors and identified propanal as a biomarker.[85] In 2021, Li et al. reported propanal as a biomarker with a significant increase in its concentration when comparing the breath of LC patients to that of HCs using a non-traditional on-paper derivatization SPME coupled with GC-MS analysis.[95] Similarly, Ligor et al. concluded that propanal was elevated in the EB of LC patients but did not claim that propanal could serve as a LC biomarker.[80] Rudnicka et al. (2011) reported propanal in the EB of LC patients having a concentration range of 0.66-3.74 ppb but not as a marker of LC.[69] In summary, propanal was reported in 34% of the studies collected for this work, and 40% of these studies determined propanal is a biomarker of LC. These investigations suggest that elevated levels of propanal may indeed be indicative of an underlying disease. However, one issue that complicates using propanal as a biomarker of cancer is its presence in ambient air,[104] tobacco smoke,[105] food,[106] and other exogenous sources, such as car exhaust.[107,108]

1.6.2 *Butanal*

The formation of butanal via LPO is restricted to the oxidation of ω-3 fatty acids. Several studies have measured butanal in EB.[67] Buszewski et al. measured butanal levels

in LC patients at 1.32–2.55 ppb relative to concentrations in HCs at 1.35–1.87 ppb.[72] Similarly, Rudnicka et al. found butanal in EB at concentrations in the range of 0.78–2.55 ppb.[69] Kischkel et al. found the median butanal concentration of 1.81 nmol/L to be higher in LC patients only relative to the levels observed in smokers, while they noted no significant difference in comparison to levels in HCs, who presented higher median concentrations of butanal than LC patients.[68] In contrast, Poli et al.[8] observed butanal to be a reliable marker of NSCLC, and the mean butanal concentration was measured at 0.026 nmol/L compared to the mean level measured in HCs at 0.011 nmol/L. Schallschmidt et al. found butanal to be significantly elevated in the EB of LC patients, with a median level 0.014 nmol/L relative to a median level in HCs of 0.007 nmol/L.[83] Li et al. also recently reported butanal to be a biomarker of LC.[95] Similar to the challenge of using propanal as a biomarker, the numerous exogenous sources of butanal complicate the characterization of butanal as a biomarker. Common ambient butanal sources include tobacco smoke[109] and food.[110] Butanal is a principal VOC emitted from municipal solid waste treatment plants.[111] Whereas butanal was reported in only 25% of the studies reviewed, it was determined as a biomarker in 36% of those cases.

1.6.3 Pentanal

Pentanal is generated from ω-6 FAs. It was reported in 45% of the studies collected for this work, of which 40% noted significantly elevated levels in the EB of LC patients relative to HCs, making pentanal the second most reported aldehyde in this work. Fu et al. investigated both SCLC and NSCLC patients in comparison to patients with benign pulmonary nodules and HCs and found significantly higher pentanal levels only in SCLC

patients.[56] In a follow-up study, the same group noted a statistically significant difference in pentanal levels between HCs, patients with benign pulmonary nodules, and those with LC, who had the highest levels of pentanal, with concentration thresholds ranging from 1.1–1.315 nmol/L.[79] Fuchs et al. observed the median pentanal concentration in LC patients to be 0.019 nmol/L relative to median levels in both HCs and smokers at 0.002 and 0.000 nmol/L, respectively.[67] Poli et al. reported a mean pentanal concentration in the breath of NSCLC patients of 19.1 pM in comparison to a mean concentration in HCs of 7.6 pM.[8] Ulanowska et al. measured the average concentration of pentanal in LC patients at 5.9 ppb and found that the HCs, which included healthy smokers, non-smokers, and past smokers, had an average concentration of 0.0 ppb.[70] Gashimova et al. reported the pentanal/acetonitrile ratio as a biomarker.[94] Three other groups reported pentanal as a biomarker of LC: Bajtarevic et al. in 2009,[64] Shehada et al. in 2016,[85] and Li et al. in 2021.[95] Based on the differences in disease and control groups noted in these studies, there is good evidence that pentanal appears to be a breath biomarker of LC.

1.6.4 *Hexanal*

The LPO of both ω-6 and ω-7 FAs can lead to the formation of hexanal. It is the most widely reported LPO-derived aldehyde. Of the 44 reports collected for this work, 61% detected hexanal, of which 48% determined that hexanal is a biomarker of LC. Hexanal was observed using every reported technique of preconcentration and analysis method. Phillips et al. were the first to label hexanal as a biomarker of LC in EB in 1999.[60] Fuchs et al. reported hexanal as an LC biomarker with an LC patient median concentration of 0.010 nmol/L compared to a HC median concentration at 0.00 nmol/L.[67] Ulanowska et al.

determined hexanal as a biomarker with an average LC patient concentration of 4.5 ppb, also compared to a HC average concentration of 0.0 ppb.[70] Poli et al. reported hexanal in LC patients with a mean concentration of 0.037 nmol/L, significantly higher than the levels in HCs at 0.009 nmol/L.[8] Poli's findings were cited and corroborated by Li et al. in finding hexanal to be an EB biomarker of LC.[95] Deng et al. found hexanal to be in the EB of LC patients but not in the EB of HCs.[61] Handa et al. deemed hexanal a biomarker; their report was one of the few not to use a preconcentration method and the only report using ion mobility spectrometry to detect VOCs.[76] In 2005, Chen et al. reported hexanal as a biomarker and were the only report to use a novel GC-SAW sensor for analysis.[62] In 2007, Chen et al. highlighted the VOCs present in the headspace, and in another, much larger, study with 160 LC patients in 2021, found hexanal to once again rise to the level of a biomarker of LC.[93] Rudnicka et al.,[77] Gashimova et al.,[94] and Zou et al.[100] also reported hexanal to be an EB biomarker of LC. Whereas Kischkel et al. measured hexanal to have a greater median concentration in the EB of LC patients (0.59 nmol/L) than that of healthy smokers (0.31 nmol/L), the concentration in LC patients was less than the median concentration they measured in HCs (0.63 nmol/L).[68] Despite a few potential exogenous sources of hexanal,[103,112] the number of reports detecting hexanal clearly suggest hexanal must be considered when evaluating for EB biomarkers of LC. Chen et al. reported that the headspace VOCs of stage I and II lung tumor tissue are the same as those in the headspace from stage III and IV lung tumor tissue. They found that hexanal is one of the headspace VOCs and subsequently determined hexanal to be a biomarker in the EB of LC patients.[63]

1.6.5 *Heptanal*

Heptanal is a possible LPO product of both ω-6 and ω-7 FAs. It is the second most reported biomarker of LC from the papers collected for this study. Phillips et al. was the first to identify heptanal in exhaled breath as a biomarker of LC in 1999.[60] Chen et al. reported heptanal as a biomarker of LC in 2005,[62] stating that while heptanal is less likely to be present in the EB of LC patients than hexanal, differences in heptanal concentrations between LC and HCs are significant to signify heptanal as a biomarker of LC.[63] Poli et al. reported a 13.9 pM median concentration of heptanal in the EB of LC patients compared to 6.1 pM in HCs, a significant difference that also identified heptanal as a biomarker of LC.[8] Corradi et al. was the only group to identify heptanal as a biomarker of LC in EB without also noting hexanal as a biomarker.[78] Deng et al. found heptanal in the EB of LC patients but not in the EB of HCs.[61] Three other reports deemed heptanal to be a biomarker of LC in EB: Handa et al.[76] in 2014 and Chen et al.[93] and Li et al.,[95] both in 2021. Heptanal was reported in 39% of the papers collected for this work, and 53% of those studies considered heptanal to be biomarker of LC.

1.6.6 *Octanal*

Octanal is a possible LPO product of both ω-7 and ω-9 FAs. It was detected in the EB of LC patients in 36% of the papers collected for this study, 25% of which determined octanal to be a biomarker of LC. Fuchs et al. measured octanal as a biomarker in EB with a median concentration of 0.052 nmol/L in LC patients vs. a median concentration of 0.011 nmol/L in HCs.[67] Poli et al. reported similar results, with an octanal median concentration of 0.023 nmol/L in LC patients compared to a median concentration of

0.010 nmol/L in HCs.[8] Jouyban et al. reported an average concentration of octanal in the EB of LC patients to be 7.8 nmol/L, while HCs and patients undergoing treatment had levels lower than the LoD for the analytical method used; thus, they deemed octanal to be a biomarker of LC.[87] In 2021, Zou et al. also reported octanal as a biomarker of LC using a gradient boost decision trees algorithm on collected GC-MS data.[97]

1.6.7 *Nonanal*

Nonanal, the third most detected aldehyde among the reports collected for this work, is formed by the LPO of ω-9 FAs. Fuchs et al. reported a median concentration of nonanal in the EB of LC patients of 0.239 nmol/L compared to a median concentration of 0.033 nmol/L in HCs.[67] Poli et al. reported somewhat lower nonanal median concentrations of 0.044 nmol/L in LC patients and 0.013 nmol/L in the EB of HCs.[8] Based on these results, both groups considered nonanal to be a biomarker of LC. Handa et al. not only reported nonanal as an EB biomarker of LC but also stated that its EB concentration can be used to distinguish between adenocarcinoma and squamous cell carcinoma.[76] More recently, Li et al.[95] and Long et al.[96] both identified nonanal as an EB biomarker of LC. Nonanal was reported in 41% of papers collected for this work, of which 28% determined nonanal is a biomarker of LC in EB.

1.6.8 *Decanal*

Decanal is an LPO product of ω-9 FAs. It was the least reported saturated aldehyde, both overall (20%) and as a biomarker when observed (22%). Schallschmidt et al.[83] and Long et al.[96] were the only groups to identify decanal as a biomarker of LC. Schallschmidt

et al. reported a median concentration of decanal of 12.2 pmol/L in LC patients and 5.1 pmol/L in HCs. The high boiling point of decanal at 207 °C does require particular attention when establishing protocols for analysis by GC.

1.7 Unsaturated Aldehydes

1.7.1 *2-Propenal (Acrolein) and 2-Butenal (Crotonaldehyde)*

2-Propenal is the most reactive α,β-unsaturated aldehyde because it is unsubstituted in the β-position. Consequently, 2-propenal readily disrupts cell functions due to facile reactions with biological nucleophiles, such as DNA, proteins, glutathione, and others.[113] 2-Butenal is similar to 2-propenal in terms of associated toxicity and readily reacts with DNA and proteins.[114] Both aldehydes were detected in the EB of LC patients by Kischkel et al.,[68] and 2-propenal was determined by Rudnicka et al.[69] to be a biomarker of LC. Whereas both of these aldehydes are known products of LPO, their merit as biomarkers is limited by the many other endogenous and exogenous sources.[36,113,114] In particular, among the largest contributing sources is smoking tobacco. Given that more than 88% of people with lung cancer recently surveyed were, or currently are, smokers,[115] measurements of 2-propenal and 2-butenal in EB must be carefully considered in the context of patient history.

1.7.2 *2-Hexenal, 2-Heptenal and 2-Nonenal*

The only reports of 2-hexenal, 2-heptenal, and 2-nonenal in the EB of LC patients come from Corradi et al.,[78] who used a Bio-VOC tube for EB collection. This approach

allowed for the targeted collection of alveolar breath, which helps to exclude many exogenous VOCs and environmental interferences. Only 4 of the 44 studies reviewed used Bio-VOC tubes for EB collection. Using this approach, Corradi et al. determined 2-nonenal to be a biomarker of LC.

1.7.3 *2-Decenal*

2-Decenal was reported in association with LC only once, but not as a biomarker. Jouyban et al. detected aldehydes in the EB of LC patients by using a cold condensation tube and co-liquification protocol. As a result, they observed 2-decenal for the first time.[87]

1.7.4 *4-Hydroxy-2-hexenal (4-HHE)*

4-HHE is a well-known product of LPO arising from the reaction of ω-3 FAs.[116] However, it has only been detected in the EB of LC patients by using one particular collection–analysis protocol, namely, derivatization to an oxime ether during preconcentration followed by analysis using FT-ICR-MS.[56] Fu et al. disclosed 4-HHE as a breath biomarker of LC and that 4-HHE concentration thresholds could be used to distinguish squamous cell carcinoma from adenocarcinoma and other NSCLCs.[56] Bousamra et al. also reported 4-HHE as a breath biomarker of LC and noted that after tumor resection, levels of 4-HHE in EB are significantly reduced and returned to levels found in HCs.[74] Li et al., in addition to reporting 4-HHE as an LC biomarker, reported that threshold concentrations of 4-HHE can be used to distinguish LC patients from patients with benign nodules (0.0073 nmol/L), smoking controls (0.0073 nmol/L), and non-smoking controls (0.0067 nmol/L).[79] In 2015, Schumer et al. reported a median

concentration of 4-HHE in HCs (0.001 nmol/L) compared to elevated concentrations of 4-HHE in early-(0.007 nmol/L) and late-stage cancer patients (0.009 nmol/L).[81] In 2016, Schumer et al. also determined that the 4-HHE concentration in EB is reduced after tumor resection, reporting no significant difference between median concentrations in post-resection patients and HCs.[84] Of the papers collected for this work, only 11% observed 4-HHE in EB, but all those noted 4-HHE as a biomarker of LC. Though present in low concentrations, with proper preconcentration and analysis techniques, 4-HHE can be an excellent biomarker of LC due to its LPO origins and complete lack of environmental or other endogenous sources.

1.7.5 *4-Hydroxy-2-nonenal (4-HNE)*

4-HNE is derived from the LPO of ω-6 FAs.[116] Li et al. reported 4-HNE as a breath biomarker of LC, reporting threshold concentrations to distinguish LC from benign pulmonary nodules.[79] When comparing LC to patients with benign nodules, the threshold for LC is 0.00175 nmol/L, but when comparing LC to smoking controls or HCs, the thresholds are lower and at concentrations of 0.000285 and 0.000255 nmol/L, respectively.[79] In another study, Fu et al. observed significant differences in the 4-HNE concentrations that distinguish between SCLC and NSCLC in patients.[56] 4-HNE was reported in two of the papers collected for this work (5%), only one of which determined it to be a LC biomarker.

1.7.6 *Malondialdehyde (MDA)*

Tamura et al.[51] and Kawai et al.[52] both reported MDA as one of the many aldehydes produced during in vitro lipid peroxidation experiments, with its yield maximized when carried out at 37 °C.[51] In 2015, Li et al. disclosed the only report on MDA detected in the EB of LC patients but did not determine it as a biomarker.[79] In this study, MDA was detected by derivatization during preconcentration to a less reactive, cationic oxime ether analog, which may explain the ability of the researchers to detect this highly reactive enol-aldehyde. Interestingly, the large majority of studies reporting MDA in the EB of patients—patients with asthma,[117] COPD,[118,119] chronic airway inflammation,[120] pulmonary disease,[121] occupational hazard exposure,[122,123,124,125] and air pollution exposure[126]—or in the EB from healthy subjects[127,128,129,130,131] relied on the chemical derivatization of MDA with either 2,4-dinitrophenylhydrazine (DNPH) or thiobarbituric acid (TBA) after the collection of exhaled breath condensate. Condensing MDA in this manner, converting it into more stable adducts, and then analyzing the adducts by LC-MS avoids the exposure of this highly reactive, thermally sensitive metabolite to heat. The thermal desorption step associated with SPME, the principal analytical technique employed in the Table 1.3 studies, likely precludes the detection of MDA, and possibly other unsaturated aldehyde metabolites, due to inducing reactions and/or decomposition.

1.8 Conclusion

Cancerous cells have increased metabolic activity and cellular dysfunction, leading to elevated levels of ROS. The excess ROS react with unsaturated lipids to form aldehyde

metabolites via LPO. On considering the principal unsaturated fatty acids present in lung tissue and lung surfactant, it is reasonable to expect a panel of LPO-derived aldehydes consisting of saturated C3-C10 aldehydes, hydroxyaldehydes, and α,β-unsaturated aldehydes. This chapter examined all reports of volatile aldehydes in the EB of LC patients to summarize the efficacy of using the LPO-derived aldehyde panel as biomarkers of LC. The incidence of saturated aldehydes correlated often with LC, particularly in the case of pentanal, hexanal, and heptanal, which exhibited statistically significant elevations in concentration relative to HCs in near 50% of the studies that reported them. In contrast, there is a dearth of articles reporting hydroxyaldehydes or α,β-unsaturated aldehydes in the EB of LC patients, even though their formation via the random LPO process is also likely. 4-HHE was the most reported α,β-unsaturated aldehyde and was deemed a biomarker of LC 100% of the times it was detected. The studies reporting 4-HHE, as well as the other unsaturated biomarkers 2-nonenal and 4-HNE, all used chemical derivatization during preconcentration and analysis. The methods of preconcentration and analysis clearly impact not only the concentration ranges measured for the aldehyde metabolites, but also which classes of aldehydes are detected. The quantification of reactive α,β-unsaturated aldehydes including MDA appears to require derivatization methods for accurate assessment as biomarkers.

1.9 Hypothesis

In the two decades that followed the first reported aldehyde in LC patient breath in 1988, only four additional studies documented elevated levels of aldehydes in the EB of

LC patients. Since 2008, however, there have been 39 studies on the EB of LC patients showing the merit of exhaled aldehydes as biomarkers. To fully realize the potential in using this class of LPO-derived metabolites as biomarkers of LC, the integration of chemoselective capture technology specific to aldehyde functionality with methods of analysis that take into account the sensitive nature of the more reactive α,β-unsaturated aldehydes is needed. This is the underlying concept that drove the research presented in this dissertation.

We hypothesize that a method to enhance detection and quantification of the 'overlooked' fraction of exhaled breath aldehydes, namely α,β-unsaturated aldehydes, will improve the accuracy of breath analysis for diagnosis of disease. Lung cancer is not the only disease for which exhaled breath aldehydes can be used as biomarkers. Many other respiratory diseases are associated with OS,[132,133,134] and with the outbreak of SARS-CoV-2, the global pandemic demands the innovation of a rapid non-invasive diagnostic test for this disease. We expect that better methods for detection of unsaturated aldehydes in exhaled breath will improve the sensitivity and specificity associated with breath-based diagnostic tests.

Abbreviations used in Chapter 1:

AgNP	silver nanoparticle
ATM	2-aminooxy-N,N,N-trimethylethan-1-ammonium iodide
CAR	Carboxen
CRDS	cavity ring-down spectroscopy
DNPH	dinitrophenylhydrazine
DVB	divinylbenzene

EB	exhaled breath
e-nose	electronic nose
FA	fatty acid
FT-ICR-MS	Fourier-transform ion cyclotron resonance mass spectrometry
GC-MS	gas chromatography-mass spectrometry
HC	healthy control
4-HHE	4-hydroxy-2-hexenal
4-HNE	4-hydroxy-2-nonenal
IMS	ion mobility spectrometry
LC	lung cancer
LoD	limit of detection
LPO	lipid peroxidation
MDA	malondialdehyde
MUFA	monounsaturated fatty acid
NSCLC	non-small cell lung cancer
NR	not reported
OS	oxidative stress
PC	phosphatidylcholine
PDMS	polydimethylsiloxane
PE	phosphatidylethanolamine
PFBHA	(pentafluorobenzyl)hydroxylamine
PG	phosphatidylglycerol
PL	phospholipid
POSS	polyhedral oligomeric silsesquioxane
PS	phosphatidylserine
PTR-MS	proton transfer reaction-mass spectrometry
PUFA	polyunsaturated fatty acid
ROS	reactive oxygen species
SAW	surface acoustic wave
SCLC	small cell lung cancer
Sph	sphingomyelin
SPME	solid-phase microextraction
TBA	thiobarbituric acid
VOC	volatile organic compound

CHAPTER 2

DEVELOPMENT OF A GAS-TO-LIQUID PHASE TRANSFER APPARATUS FOR THIOL-MICHAEL DERIVATIZATION OF VOLATILE UNSATURATED CARBONYLS

2.0   Introduction

As discussed in Chapter 1, there is great interest in developing methods of breath analysis for disease diagnosis and to search for volatile biomarkers of disease. Some applications are already in use; for example, a urea breath test has been used to noninvasively predict the presence of *Helicobacter pylori.*[1] Electronic nose technology has been used to detect nitric oxide in exhaled breath as a means to predict childhood asthma.[2] In 2015, the US Food and Drug Administration approved monitoring gastric emptying using a stable isotope breath test, an approach first reported in 2012 by Bharucha *et al.*[3] These are just a few of the many versatile applications of breath analysis for diagnosis of disease.

In pursuit of a diagnostic technique for early detection of lung cancer, one that is noninvasive and relatively inexpensive, breath analysis has emerged as a potentially powerful diagnostic tool.[4] Lung cancer is one of the leading causes of cancer death, but early detection leads to higher survival rates.[5] Unfortunately, symptoms of lung cancer are usually not apparent until the cancer has already progressed to an advanced stage.[6] The five-year survival rate after diagnosis and treatment is only 18% for patients with advanced stage lung cancer; thus, early detection is the key to increasing lung cancer survival rates.[5] One means to detect lung cancer is screening by either computed tomography (CT scan) or chest X-ray analysis. However, the National Lung Screening Trial of 2011, in which persons at high risk for lung cancer were screened by either CT or X-ray, resulted in more than 95% false positive diagnosis.[4] Patients with a positive screening result then required, often unnecessarily, secondary procedures with greater associated

risk to the patient. A diagnostic technique for accurate, early detection of lung cancer, one that ideally is noninvasive and relatively inexpensive, is still needed.

The detection of lung cancer by measurement of biomarkers in exhaled breath is being widely studied.[3,7] Though putative biomarker VOCs vary among the studies, researchers agree that cancerous cells are under oxidative stress and exposed to excess reactive oxygen species (ROS), leading to generation of VOCs. [8,9,10] In 2000, Khyshiktuev *et al.* reported unsaturated and polyunsaturated lipid deficiencies in malignant and tumor-adjacent lung tissue.[11] This is a substantial finding — the deficiencies in unsaturated lipids can be attributed to ROS-mediated consumption of the lipids, generally constituents of cell membranes, via lipid peroxidation processes. As outlined in Chapter 1, the product lipid peroxides are unstable and form secondary products, principally saturated and α,β-unsaturated aldehydes. [12,13,14] These carbonyl VOCs tend to have low solubility in blood and, consequently, are exhaled in breath. [15,16,17]

Well known ATM-coated silicon microreactor-based breath analysis method is one ongoing approach to detect lung cancer by analyzing volatile, exhaled carbonyls. [18,19,20] While ATM excels at oximating saturated carbonyls, its 1,2-addition reactions with α,β-unsaturated carbonyls, an important subset of lipid peroxidation-derived VOCs, are relatively sluggish. [21] In an attempt to address this shortcoming, Ogunwale *et al.* developed a new hydrazine-based reagent, 2-hydrazinyl-*N,N,N*-trimethylethan-1-ammonium iodide (HTM) that has a lower activation energy for capture of α,β-unsaturated carbonyl VOCs compared to ATM.[21] Work is ongoing to increase the capture

efficiency of volatile α,β-unsaturated carbonyls in breath, an important direction to further improve breath analysis as a diagnostic tool.

2.1 A Different Method for Carbonyl Capture — Conjugate Addition

With the insight that targeting (i.e., preconcentrating) α,β-unsaturated compounds via 1,2-addition, as in the ATM approach, was sluggish, we considered an alternate approach of isolating exhaled breath carbonyls. Since conjugated carbonyls can undergo both 1,2- and 1,4-additions by nucleophiles (Figure 2.1), we hypothesized that a 1,4-selective approach might be more efficacious for trapping this important subset of VOCs.
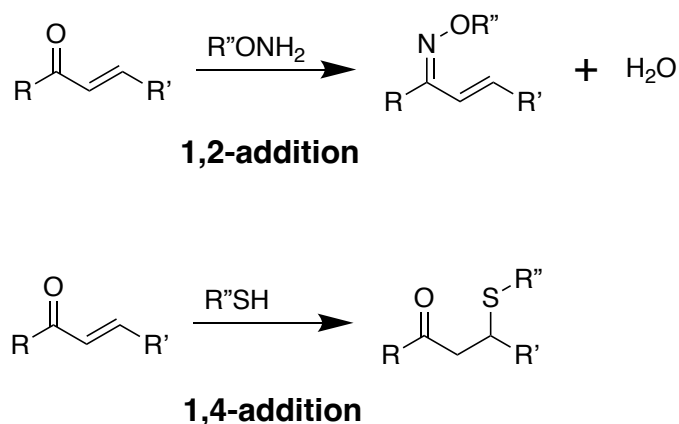
Scheme 2.1. Example of 1,2-addition of an aminooxy functionality to an α,β-unsaturated carbonyl and 1,4-addition of a thiol functionality to an α,β-unsaturated carbonyl.

Thiol-Michael Addition. The 1,4-conjugate addition of thiols is a well-known click chemistry reaction (Scheme 2.1), commonly referred to as the thiol-Michael addition, where a nucleophilic thiol attacks an electrophilic beta-carbon of an α,β-unsaturated carbonyl compound to form a β-sulfido-carbonyl adduct.[22] Exploiting the thiol-Michael addition reaction to chemoselectively target α,β-unsaturated aldehyde VOCs in exhaled

breath gave inspiration of a new cationic thiol reagent to exploit the 1,4-conjugate addition reaction.

There are many examples of thiol Michael addition reactions found in the literature. For example, Senter *et al.* reported the facile coupling of cysteine from an antibody with maleimide-functionalized drugs. [23] Gopal *et al.* reported facile and high-yielding 1,4-conjugate addition of thiols to α,β-unsaturated carbonyls in water without any catalyst,[24] a promising result considering exhaled breath is saturated with water.[25]

entry	enone	thiol	rxn time (min)	yield (%)
1			5	90
2			10	90
3			5	90
6			10	95
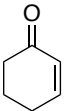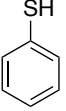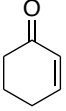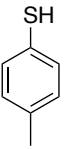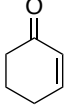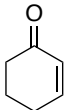
Table 2.1. Selected entries from Gopal *et al*. on thiol reactions with α,β-unsaturated carbonyls.[24]

An interesting observation from the work of Gopal *et al*. (see entry 3, Table 2.1) is that an electron-deficient thiol reacts faster than slightly more nucleophilic thiols (entry 2). This observation is rather counterintuitive; textbook organic chemistry would suggest

nucleophiles with more thiol electron density should react faster. In another observation from Table 2.1, the alkyl thiol entry 4 is slightly higher yielding, but it too had a slower reaction rate relative to entries 1 and 3. As our breath analysis techniques have used cationic reagents for mass spectrometry analysis in the past, the data from Gopal *et al*. publication inspired us to prepare two cationic thiol reagents. First a cationic aryl thiol because the *p*-nitrothiophenol from Table 2.1 had a fast reaction time and second, a cationic alkyl thiol because the ethanethiol from Table 2.1 had the highest yield. The aryl cationic thiol reagent we decided to make was 4-mercapto-*N,N,N*-trimethylbenzenammonium iodide (MBA) and the alkyl cationic thiol reagent was 2-mercapto-*N,N,N*-trimethylethanammonium iodide (MTA), shown in Figure 2.1.
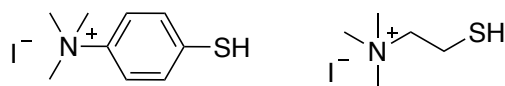
Figure 2.1. Cationic aryl thiol reagent MBA and cationic alkyl thiol reagent MTA.

Thiol reagents had been tested previously as derivatization agents using the silicon microreactor technology in breath analysis for capture of unsaturated carbonyls.[21] However, the results showed that thiols captured no carbonyls in the solid phase–gas phase experiments — these qualitative results suggest that the thiol 1,4 addition has a slower reaction rate relative to aminooxy 1,2 additions. In addition to the new thiol derivatization reagent, a new method for breath preconcentration was developed.

Bubbler apparatus. We developed a peristaltic pump-driven gas dispersion apparatus (Figure 2.2) to pass exhaled breath gas through a solution of cationic thiol reagent to derivatize and preconcentrate volatile α,β-unsaturated aldehydes. This gas-to-liquid phase reaction proposes to deliver exhaled breath α,β-unsaturated aldehydes as non-volatile, charged compounds suitable for analysis by liquid chromatography and high-resolution mass spectrometry (LC-HRMS). This is a unique approach as we could find no reports using a thiol-Michael reaction to isolate VOCs from breath. The selectivity simplifies analysis because all other classes of VOCs are not derivatized. Importantly, this subset of VOCs is mechanistically linked to cancer, thus, the method targets metabolites produced by the cancer ROS environment. The thiol reagent is far less likely to be contaminated by exogenous VOCs relative to reagents that rely on reactions with carbonyl VOCs, as α,β-unsaturated aldehydes are typically far less present in most environments. Furthermore, the gas-to-liquid approach allows the use of other reagents (e.g., catalysts) to improve capture efficiencies, while solid phase approaches (micro-preconcentrators, or 2,4-DNPH on absorbents) cannot be aided in this way because of site isolation issues. There is also the possibility with this apparatus of looping the sample or using duplicate setups in series to maximize VOC capture.
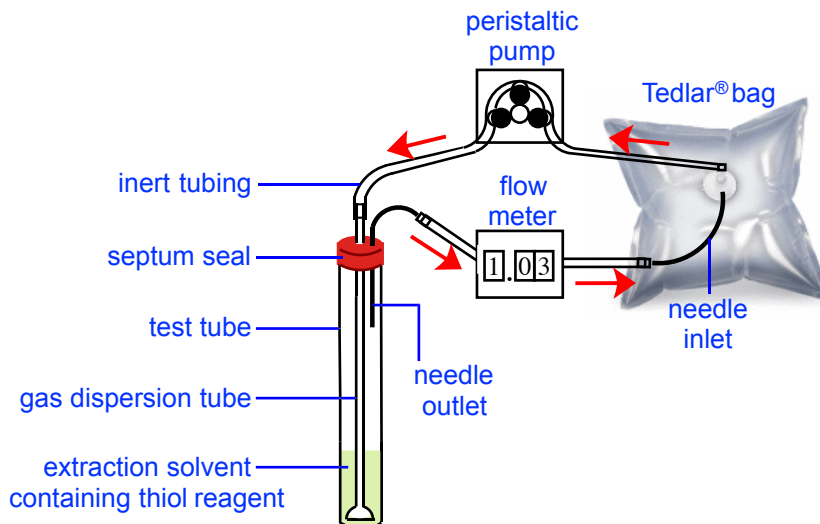
Figure 2.2. Experimental set-up used to capture $\alpha, \beta-$unsaturated aldehydes from breath samples (not to scale; bubbler apparatus enlarged to show detail). Air flow indicated by red arrows.

2.2   Thiol Reagent Synthesis

The aryl ammonium thiol reagent MBA was prepared using a route different from that reported in the literature (Scheme 2.2). [26] Attempts were made to prepare MBA via the reported synthesis by DePamphilis *et al*.[25] without success. A balancing act between thiol alkylation vs. incomplete amine alkylation in the reported synthesis proved it to be unsuitable in our hands. A more straightforward synthesis route was developed from commercially available 4-(dimethylamino)thiophenol. Thiol protection as a thioester was a high yielding reaction, followed by amine exhaustive alkylation and then ester hydrolysis afforded MBA. The *N*-exhaustive alkylation was the lowest yielding step with a 74% yield, also due of incomplete alkylation and thiol alkylation side products. The hydrolysis was high yielding at 94%. Figure 2.3 is a ^{1}H NMR spectrum taken of MBA. The ammonium

methyl 9H singlet at d 3.56 ppm and the thiol proton at d 5.99 ppm in the ^{1}H NMR spectrum confirms formation of MBA.
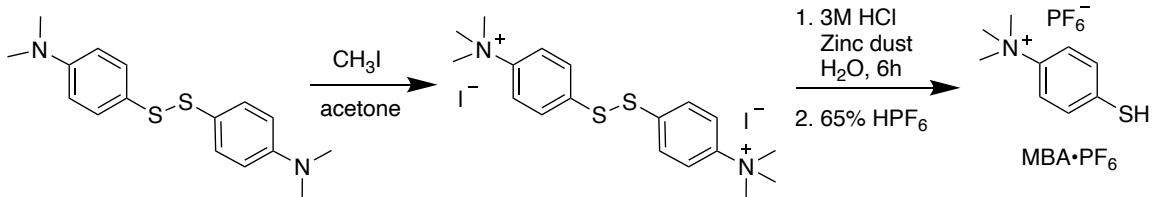
Scheme 2.2. Syntheses of MBA.
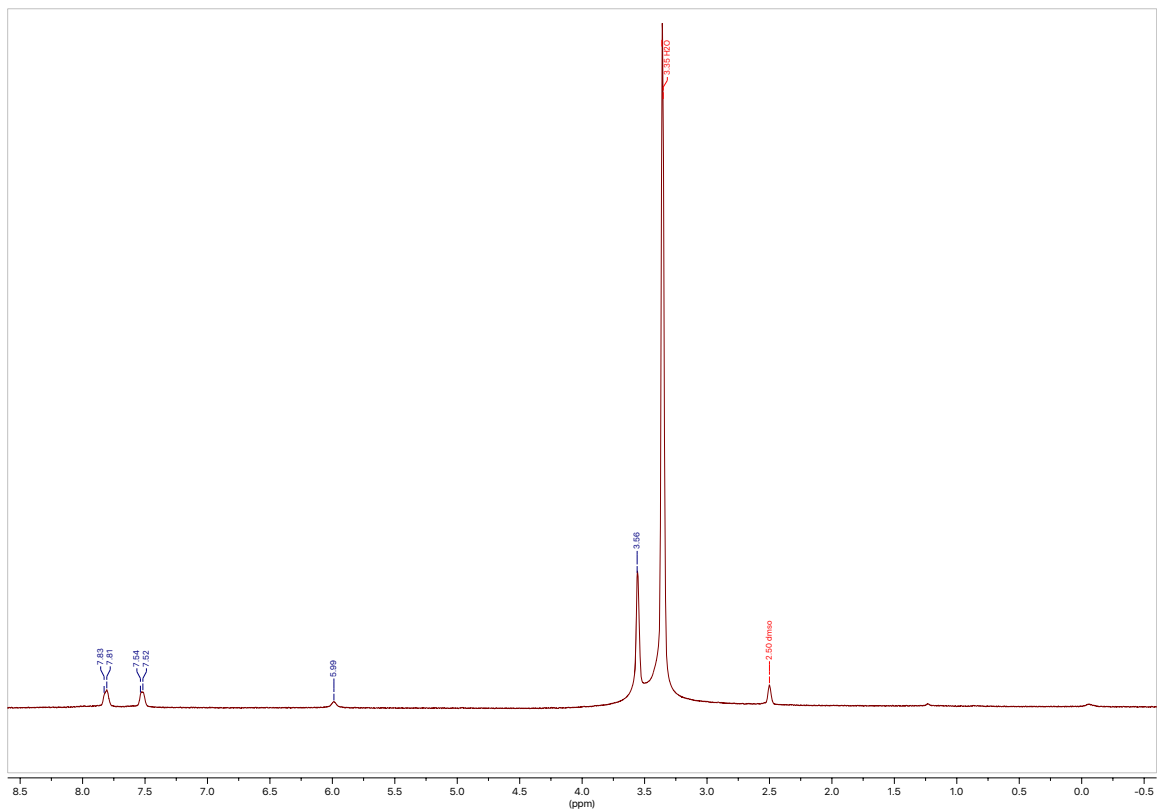
Figure 2.3. ^{1}H NMR spectrum. (DMSO, 400 MHz) of structure MBA.

To prepare MTA we used a similar strategy, starting with commercially available acetylthiocholine iodide. 2-Mercapto-*N,N,N*-trimethylethan-1-ammonium chloride (MTA) was prepared by refluxing acetylthiocholine with methanolic HCl (Scheme 2.3). Similar to MBA, MTA displays a prominent 9H singlet attributed to the trimethylammonium moiety at d 3.10 ppm and a thiol proton at d 5.29 ppm (Figure 2.4) support the structural assignment of MTA.
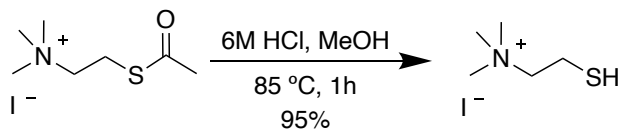
Scheme 2.3. Synthesis of MTA.
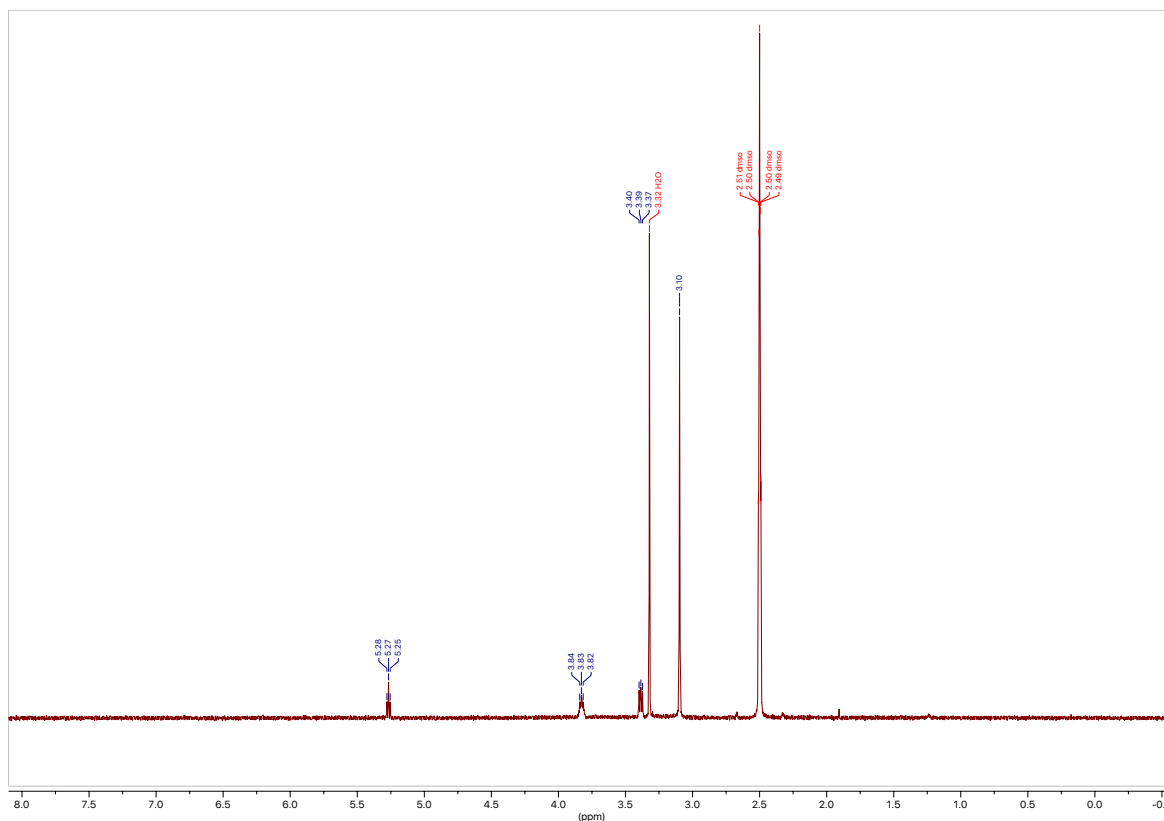
Figure 2.4. ¹H NMR spectrum. (DMSO, 400 MHz) of structure MTA.

MBA was tested first using the bubbler apparatus because Gopal *et al.* reported both efficient solvent free thiol reactions with α,β-unsaturated aldehydes and faster reactions with aryl thiols.[24]

2.3   Investigation of the Thiol-Michael Approach Using MBA

The setup of the pump driven dispersion apparatus required the purchase of commercially available equipment. After considering potential pump flow rates, the adjustable flow rate peristaltic pump seen in Figure 2.6A was purchased from Harvard Apparatus. In the search for gas dispersion tubes there were two requirements, small tube diameter to fit into capture reagent test tube and fine frit porosity of dispersion tube. Three dispersion tubes were purchased, all having dispersion tube frit porosity of 4.5-5 μm. Two dispersion tubes purchased from Ace Glass were pencil like in shape but had different outer diameters of 5 and 7 mm. The other gas dispersion tube purchased from Safety Emporium had a similar outer diameter of 6 mm, however the frit end has a bell like shape. The image in Figure 2.5 shows the two dispersion tube shapes.

Figure 2.5. Image of gas dispersion tubes.

Initial testing demonstrated vial size was another variable to consider. The vial diameter could not be too large, because the larger the vial diameter, the more shallow the capture reagent solution.

Bubbler solvent was the next variable considered, as there is a need for the solvent to readily solubilize organic compounds, allowing for easy VOC gas to liquid phase transfer, but also needed to be rather polar to solubilize the cationic capture reagent. A predecessor of mine in the Nantz group, Dr. Stephanie Mattingly, published a study involving a cationic derivatizing agent to extract carbonyls from a complex mixture. [27] The process from Dr. Mattingly's study required an extraction solvent for the cationic (quaternary ammonium) adducts.[27] She examined chloroform, ethyl acetate and n-butanol as extraction solvents and found that n-butanol was the most efficient solvent.[27]Consequently, we selected n-butanol as the solvent for our bubbler apparatus investigation.

The peristaltic pump purchased had an adjustable flow rate allowing Tedlar bag evacuation at rates ranging from 3.5 to 17.5 mL/min. Inspired by established protocols using the ATM silicon microreactor breath analysis method,[18] and in order to be able to compare new thiol bubbler method results with those from a microreactor, a flow rate of 7 mL/min for the bubbler apparatus was set.

A test tube was charged with a solution of MBA iodide in *n*-butanol (0.5 mL). To the solution was added ~5 mg of $KHSO_4 \bullet SiO_2$, (Das *et al.* reported that catalytic $NaHSO_4 \bullet SiO_2$ improved the 1,4-addition of thiols to $\alpha\beta$-unsaturated carbonyls). [28] The tube was then sealed with a rubber septum, a gas dispersion tube and outlet needle were

introduced according to the set-up depicted in Figure 2.6A. A 500 mL Tedlar bag

containing argon was spiked with crotonaldehyde (12 mmol), with a resulting

concentration of 24 mM. The bag was then connected to the peristaltic pump as shown

in Figure 2.6A. The gas sample was passed through the reaction suspension at a flow rate

of roughly 7 mL/min. NOTE: For this experiment, only one pass through the *n*-butanol

solution was conducted. Figure 2.6A shows the actual laboratory set-up of the apparatus

and testing.
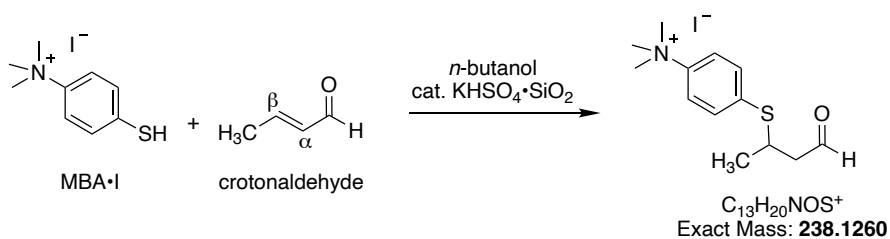
Scheme 2.4. Initial thiol-Michael attempt using the bubbler set-up with MBA.

Figure 2.6A. Image of laboratory set-up for the reaction of MBA with crotonaldehyde.
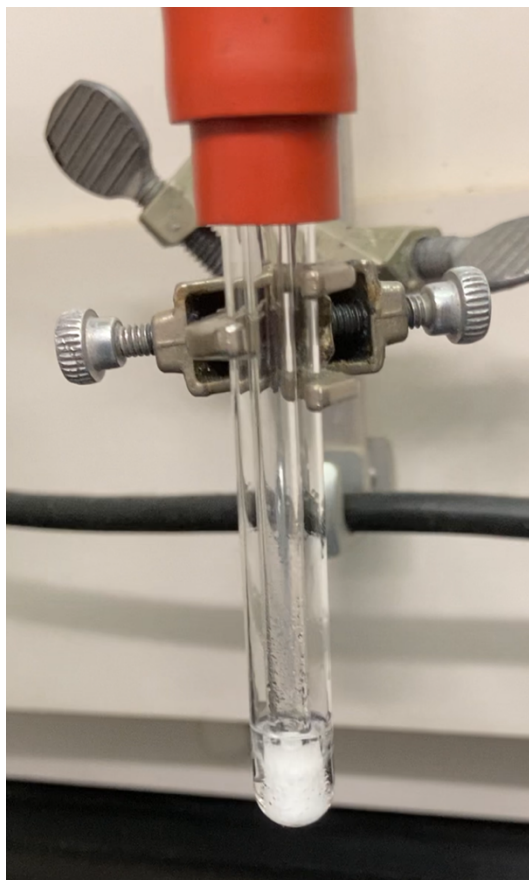
Figure 2.6B. Close up image of gas dispersion into capture reagent solvent in test tube.

To analyze for the expected thiol Michael adduct (Scheme 2.4), the reaction suspension was filtered (cotton plug in pipette) and then an aliquot was directly analyzed by HRMS. The adduct was observed at the expected m/z (Figure 2.4C). Prominent signals from the mass spectrum at m/z 154 and 224 were determined to be due to an impurity in the early synthesis stages of MBA. The m/z signal at 154 is due to protonated starting material 4-(dimethylamino)benzenethiol with an expect m/z of 154.0685. The corresponding 4-(dimethylamino)benzenethiol–crotonaldehyde adduct is responsible for the m/z signal at 224.
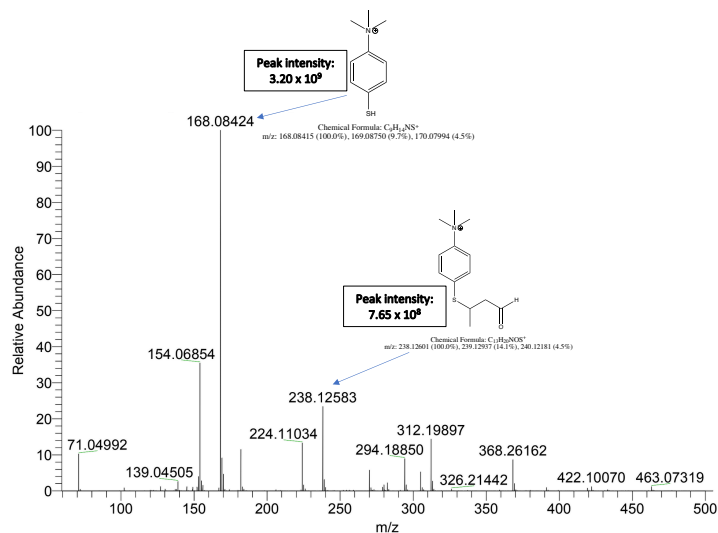
Figure 2.6C. HRMS data of the crude MBA-crotonaldehyde reaction in *n*-butanol using the bubbler set-up shows that the thiol-Michael addition occurred.

Subsequent research and development of this approach focused on many different factors that affect interaction between the gas to liquid phases, as described in Table 2.2. Initially considered were the optimization of the gas dispersion tube and the solvent vial, and how each effected the other. Different factors effect gas dispersion, such as dispersion tube shape, or diameter. The size and shape of the sample vial also effects how long the solution volume is exposed to gas bubbles, for example too narrow a vial or too wide a tube would cause the solvent/gas foam that is sometimes created to rise and leak from the top of the vial or needle outlet. If there is too large a gap between the vial walls and the dispersion tube, the bubbles quickly exit solution, minimizing gas to liquid phase exposure. We quickly moved away from the bell-shaped dispersion tube because the gas seemed to bubble out into solution in larger bubbles possibly due to a slight gap between the frit and glass dispersion tube. The gas dispersion tubes from Ace Glass

46

worked well, distributing gas as the desired fine bubbles seen in Figure 2.6B. Also tested

were different solvents, as there is a need to balance the desire for more viscous solvents

and the need for polarity to dissolve the ionic capture reagents such as isopropanol or t-

butanol. A mixture of n-butanol and methanol was found to be best, encouraged by Dr.

Mattingly's findings with a minimal addition of methanol to increase capture reagent

solubility.[27] The addition of potential acid catalysts was considered, adding silica

impregnated potassium hydrogen bisulfate, encouraged by Das et al. that reported silica

supported acid catalyst increased complete reaction time to the order of minutes.[28] The

pKa of bisulfate is approximately 2. Also, the catalytic acid adherence to silica allows for

easy removal by filtration. Flow rate was another variable considered. We found,

however, that at flow rates faster than 10 mL/min resulted in rapid solvent loss. Captures

efficiencies were attempted with a model α,β-unsaturated aldehyde, crotonaldehyde.

The thiol reagents MBA•I and MTA•I were tested by spiking crotonaldehyde in the

nanomolar range to Tedlar bags filled with Argon.

Table 2.2. Variables examined for bubble apparatus method.

Item	Issue	Decision	Ref.
Gas dispersion tube	length, diameter, bubble volume	5 mm diameter tube commercially available and no loss of solution loss	–
Sample vial size	length, diameter	8 mm diameter test tube commercially available narrow to maximize solvent depth without solution loss	–
Solvent	solubility of reagent and target VOCs	n-butanol:methanol (90:10)	27
Catalyst	acid to help catalyze rxn	$KHSO_4$•SiO_2 being on silica is easy to remove	28
Flow rate	a desire for rapid tests calls for faster flow rates	flow rate of 7 mL/min to minimize solvent loss	

While there was capture of crotonaldehyde when it was in the millimolar range, no crotonaldehyde was captured by MBA or MTA using the novel technique when the α,β-unsaturated aldehyde was in the nanomolar range, the range needed for breath analysis. Exhaled breath α,β-unsaturated aldehydes reports have been in the picomolar or low nanomolar range. Table 2.3 is a summary of the trials, attempts that were made with different thiol reagents and aldehyde concentrations.

Table 2.3. Bubbler apparatus trial results. (All experiments were carried out in 90:10 n-butanol:methanol and flow rate of 7 mL/min unless indicated otherwise.) [a] Trials 1-9 were run with MBA•I and trials 10-12 were run with MTA•I.

Trial	Crotonaldehyde nmol in 500 mL Tedlar bag	Experiment details	Capture efficiency (%)
1	0.182	one pass; no catalyst	0
2	0.182	one pass; with catalyst	0
3	0.182	multiple passes (3.5 hrs.); with catalyst	0
4	18.2	one pass; no catalyst	0
5	18.2	one pass; with catalyst	0
6	18.2	multiple passes (3.5 hrs.); with catalyst	0
7	181.5	one pass; no catalyst	<1
8	181.5	one pass; with catalyst	<1
9	181.5	one pass; with catalyst; flow rate 3.5 mL/min	<1
10	181.5	one pass; no catalyst	0
11	181.5	one pass; with catalyst	0
12	181.5	one pass; with catalyst; flow rate 3.5 mL/min	0

2.4 Summary

A few conclusions can be drawn. First, due to the need that capture solution volume remain small, to maximize the concentration for better instrument analysis, vial shape and size must be narrow allowing solution to pool and create sufficient submersion of dispersion tube into solution. The vial must also be long enough to avoid the foam of dispersion from climbing vial walls and leaking over the sides. Additionally, we speculate

that the kinetics of the 1,4-Michael addition are not fast enough at the gas/liquid

interface, and/or there is minimal transfer of VOC from gas to liquid phase for sufficient

VOC capture. Finally, the largest issue with aryl thiols is their tendency to form disulfides

when in solution, and as a disulfide it is incapable of fulfilling a nucleophilic addition in

the given conditions. Further research can be done in a few different directions. The

introduction of sonication to the process may enhance the VOC transfer from gas to liquid

phase. Perhaps a cooling of the solution could help with the transition of VOCs from the

gaseous to liquid phase. Another possibility is to use a larger apparatus, larger solvent

volume, and concentrate after capture, before analysis. To solve the disulfide problem,

there is a need for a reducing agent that will not react with target VOCs or interfere in the

analysis process. Ongoing work concurrent to this approach became more promising, so

a decision was made to cease work on this route in favor of pursuing the other route,

which is discussed in Chapter 3.

CHAPTER 3

UV SPECTROSCOPY OF CHEMOSELECTIVELY PRECONCENTRATED EXHALED BREATH AS NOVEL COVID-19 SCREENING METHOD

3.0 Introduction

Electronic Transitions. The measure of absorption or emission of light by molecules is referred to as spectroscopy.[1] Within the broad range of electromagnetic radiation are the adjacent ultraviolet (200-400nm) and visible (400-800nm) light spectra, which can be used for quantitative chemical analysis called ultraviolet-visible (UV-Vis) spectroscopy.[1] Organic molecules have discrete energy levels associated with orbitals that electrons may occupy. The occupied and most stable, lowest energy level of a molecule is called the ground state. With the absorption of quantized energy, electrons move to a higher energy level called the excited state (Figure 3.1).[1] These transitions, or absorptions, can be measured using a spectrophotometer. A spectrophotometer is an instrument that measures the amount of photons (the intensity of light) absorbed by a sample solution after a beam of light passes through it.
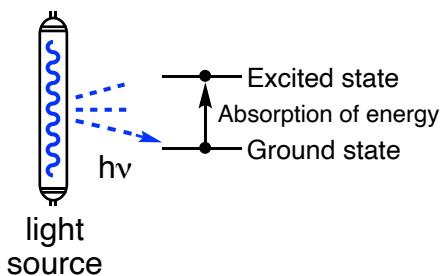
Figure 3.1. Illustration of electron excitation from ground state due to absorption of light.

Some organic molecules have electrons in nonbonding or π-bonding orbitals, which are often the highest occupied molecular orbitals (HOMO) of these molecules. As electrons in a HOMO absorb light, they are excited to the lowest unoccupied molecular orbital (LUMO) of the molecule.[1] The energy gap between the HOMO and LUMO

determines the wavelength of light that can be absorbed. As molecular structure and bonding can be quite complex and diverse, multiple types of absorptions from a single molecule are possible. Using a spectrophotometer, a sample is irradiated with different wavelengths of light from the UV-Vis spectrum, the instrument measures the percent transmittance of each wavelength of light that passes through the sample solution relative to a reference blank where most or all light was transmitted.[1] The sample's percent transmittance is often converted and reported as sample absorbance.

Carbonyls are a good example of organic molecules with multiple absorptions, because they have non- and π-bonded electrons. When considering the absorption of UV-Vis light by a carbonyl compound, two principal electron transitions are observed in the UV-Vis spectrum, nonbonded electrons moving to the $\pi*$ orbital and π-bonded electrons moving to the $\pi*$ orbital (see Figure 3.2 for a simplistic representation of relative orbital energies and these transitions).[1]
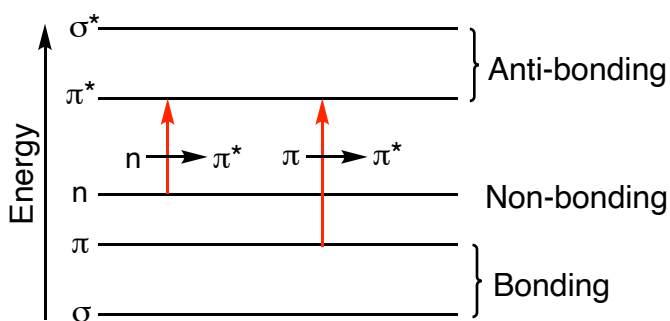
Figure 3.2. Relative orbital enegy levels and electron transitions from HOMOs n and π to LUMO $\pi*$.

In the case of the nonbonded electrons (i.e., carbonyl lone pair electrons), the electrons are excited from the HOMO to the LUMO, which in this example is the $\pi*$

antibonding orbital. In the case of the pi-bonded electrons, higher energy is required to excite the electrons to the LUMO relative to the energy required for n→π*. The relationship between energy and light is the higher the energy the shorter the wavelength, meaning higher energy transitions like π→π* will absorb shorter wavelengths of light. UV light-induced excitation of carbonyl non- and pi-bonded electrons to pi* orbitals is far more complex than depicted in Fig. 2 in that there are two sets of lone pair electrons in a carbonyl group, and these are not degenerate due to differences in oxygen hybridization.[1,2,3]

3.1 Example Carbonyl Absorbances

Comparison of Saturated and α,β-Unsaturated Aldehyde Absorbances. Shown in Figures 3.3 and 3.4 are plots of the UV absorption spectra of pentanal and 2-pentenal to illustrate some key differences to note when comparing UV light-induced transitions of a saturated carbonyl compound to an α,β-unsaturated carbonyl compound. First, the λ_{max} (maximum absorption for each type of absorption) observed for these compounds differ. The pentanal π→π* λ_{max} is 207.5 nm, whereas the 2-pentenal π→π* λ_{max} is 216.5 nm (Fig. 3.3). The pentanal n→π* λ_{max} is 282.5 nm, whereas the 2-pentenal n→π* λ_{max} is 309 nm (Fig. 3.4).   2-Pentenal absorptions are shifted to longer wavelengths, or a bathochromic shift, because the α,β-unsaturation is in conjugation with the carbonyl π bond. Conjugation narrows the energy differences between HOMO and LUMO, thus requiring less energy for electron excitation in a conjugated system relative to a saturated system. Less energy corresponds to longer wavelengths. Another major difference is the

intensity of absorbance. Note that the solutions of the two compounds being compared are at different concentrations, with the solution of 2-pentenal being 4,500-fold less concentrated, yet still absorbing more light than the solution of pentanal. Unsaturated compounds absorb more light relative to saturated compounds at the same concentration; a phenomenon that is explained by the Beer-Lambert Law. [1]
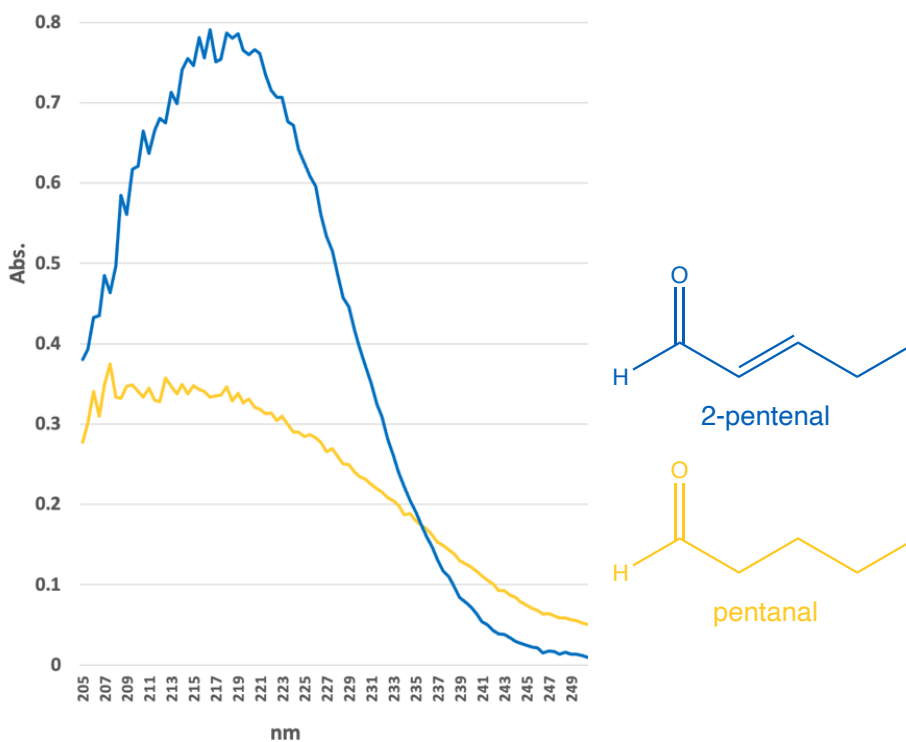
Figure 3.3. Comparison of pentanal and 2-pentenal $\pi \rightarrow \pi^*$ UV absorbance spectra, and their molecular structures. 2-pentenal and pentanal were dissolved in separate solutions with methanol at concentrations of 22.5 mM and 0.005 mM, respectively.

54
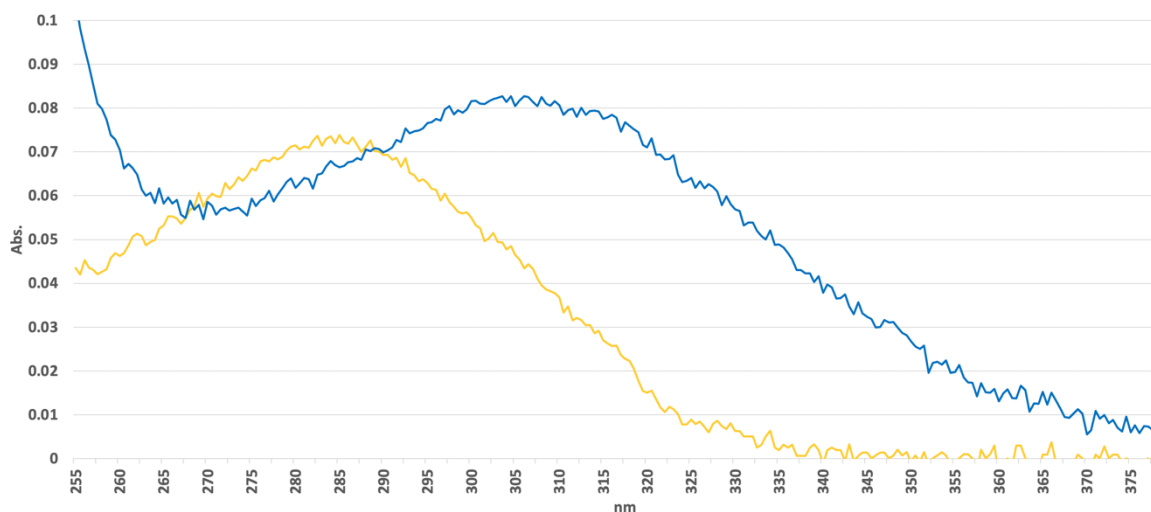
Figure 3.4. Comparison of pentanal (blue line) and 2-pentenal (yellow line) n→π* UV absorbance spectra. Pentanal and 2-pentenal were dissolved in separate solutions with methanol at concentrations of 22.5 mM and 0.1 mM, respectively.

The Beer-Lambert Law can be represented by the equation A=εlC, where A is absorbance, ε is molar absorptivity (sometimes referred to as the molar extinction coefficient, is directly related to probability of the electronic transition), l is length of sample cell and C is concentration of sample solution. As the equation implies, absorbance and concentration are directly proportional; an increase in concentration will cause an increase in absorbance. While organic functional groups have a common range of molar absorptivity, every compound will have a unique ε as it is an inherent property. Although saturated and conjugated unsaturated aldehydes may have n→π* molar absorptivities in a similar range, the π→π* molar absorptivities of conjugated unsaturated aldehydes tend to be approximately eight to ten times larger than those of the corresponding saturated aldehydes (hence the greater absorbance difference in Fig. 3.3

55

vs. Fig. 3.4). Finally, the bathochromic shift due to conjugation results in absorption at wavelengths where a saturated counterpart has no absorption. In this case, pentanal absorption at 335 nm is near zero whereas 2-pentenal still has measurable absorption at this wavelength. This feature suggests that screening mixtures of aldehydes for absorptions at these higher wavelengths may be a rapid means of discerning whether unsaturated compounds are present in the mixture.

3.2 Breath analysis

Background. In 1971, Pauling *et al.* first reported quantitative determination of nearly 250 volatile organic compounds (VOCs) in exhaled breath by gas chromatography (GC).[4] Technological and instrumentation advances since then have shown that breath contains a complex mixture of metabolites.[5] In 1999, Phillips *et al.* reported more than 3,400 different VOCs in exhaled breath.[6] The presence of, or an increased or decreased concentration of certain VOCs, in exhaled breath can be an indicator of disease.[7,8,9] Breath analysis for disease screening has long been of interest, with various exhaled VOCs being reported as biomarkers.[10,11] Reviews of breast cancer VOC markers by Leemans *et al.*[12] and of lung cancer markers by Sutaria *et al.*[13] list many examples of biomarkers in breath and point toward the potential of breath analysis for diagnosis of disease.

Many spectroscopic techniques have been used for breath analysis. Selvaraj *et al.* recently reviewed mid-infrared sensing techniques for exhaled breath diagnostics of a wide range of diseases and detection of potential biomarkers.[14] Nuclear magnetic resonance spectroscopy has been used to analyze exhaled breath condensate and was

able to differentiate between asthmatic and healthy patients.[15] UV-Vis spectroscopy also has been applied to breath analysis. Kudo *et al.* demonstrate a method to measure the acetone concentration in exhaled breath using UV-Vis measurements.[16] In the Kudo *et al.* protocol, breath was collected using an optical fiber glass cell coated with aluminum.[16] One way the method was validated was by comparing a breath sample UV absorbance spectrum to that of an acetone-spiked breath sample (Figure 3.5) to highlight the absorbances attributed to acetone.[16]
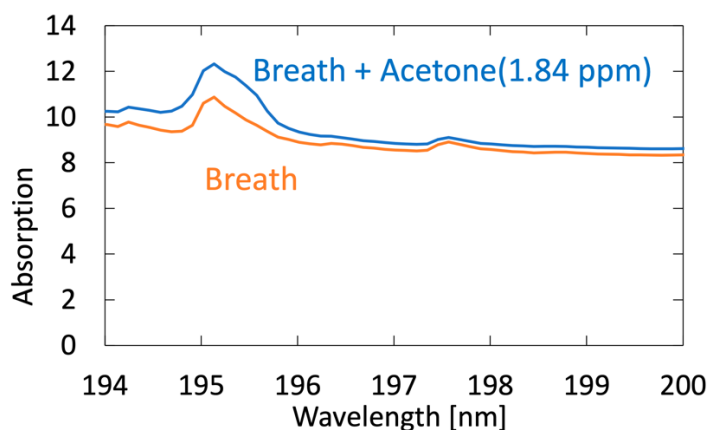
Figure 3.5. UV absorbance spectra of breath sample vs acetone-spiked breath sample.[16]

In another example using UV-Vis spectroscopy, Iwata *et al.* report development of a method to measure the concentration of isoprene in exhaled breath.[17] The authors state that UV measurements of exhaled breath have an advantage over that of mid-infrared spectroscopy because water has a strong absorption in the mid-infrared spectrum, and much less in the UV spectrum.[17] In fact desiccants are often used with mid-infrared spectroscopy to remove water due to its interference, but the desiccant may also remove potential marker VOCs from exhaled breath in the drying process. Considering my

experience from both reading the literature and experimentation with exhaled breath, I cannot rule out the possibility other exhaled carbonyls could contribute to the principal absorbance seen by the Kudo *et al.* method.

Established breath analysis protocol. Nantz and Fu have reported exhaled breath analysis using a silicon microreactor approach.[19] The microreactor consists of 1000s of micro-pillars of silica oxide coated with 2-aminooxy-*N,N,N*-trimethylethan-1-ammonium iodide (ATM) for chemoselective preconcentration of carbonyl VOCs (Scheme 1).[18] The chemoselectivity of this approach allows for the analysis of carbonyl biomarkers with far less interference from the many VOCs in exhaled breath samples, while the preconcentration allows for the accurate measure of carbonyl biomarkers in the nano- to pico-molar range. Volatile carbonyl capture depends on the click chemistry reaction between an aldehyde or ketone carbonyl and the ATM aminooxy group, an oximation reaction. The ATM derivatization also serves the purpose of converting the carbonyl VOC to a charged (cationic) non-volatile salt, which makes the preconcentration process more efficient. The ATM-VOC adducts are collected from the microreactor by elution with methanol. The methanol solutions are then analyzed by liquid chromatography and mass spectrometry (e.g., UHPLC-MS). The cationic derivatization allows for easier analysis and quantification by MS, with little to no fragmentation. These authors have reported biomarkers that predict lung cancer; specifically, butan-2-one, 2-hydroxyacetaldehyde, 3-hydroxybutan-2-one, 4-hydroxyhex-2-enal, and 4-hydroxynon-2-enal.[19,20,21,22,23,24,25] In the present work, we use the same silicon microreactor technology (Figure 3.6) to obtain methanol solutions for direct analysis by UV-Vis spectroscopy. This new breath analysis

approach circumvents the need for adduct separation via chromatography as well as analysis by MS.
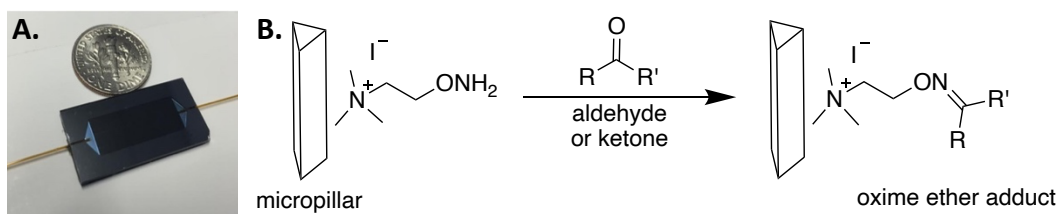
Figure 3.6. **A.** Silicon micropreconcentrator featuring 1000s of micropillars. **B.** Oximation reaction on silica micropillars in microreactor.

New UV-Vis breath analysis approach. The underlying principle of our new approach to breath analysis is to use UV-Vis spectroscopy to determine the presence of conjugated carbonyl compounds in breath. We have previously reported that α,β-unsaturated aldehydes are mechanistically expected in exhaled breath from lipid peroxidation.[13] An increase in cellular oxidative stress, as happens in diseased cells, will result in even higher levels of aldehydes, both saturated and unsaturated, in exhaled breath.[26] Indeed, increases in the levels of saturated aldehydes in breath as a consequence of lung cancer, for example, have been well documented.[13] However, there is severe lack of detection and reporting of α,β-unsaturated aldehydes in the exhaled breath of lung cancer patients.[13] Thus, a method to detect this expected class of metabolites within a complex mixture might prove useful as a tool for diagnosis of certain diseases.

Coupling the established carbonyl breath capture technology with UV-Vis spectroscopy could result in a fast, inexpensive, and noninvasive analysis of disease. For

the technique to succeed, however, the collective absorption of the unsaturated carbonyl VOC adducts, which can be expected to have a higher molar absorptivity relative to the saturated analogs, must exceed limits of detection thresholds. While acetone has been reported to have exhaled breath concentrations in the nanomolar range,[27] other saturated and specifically α,β-unsaturated aldehydes are reported to be in the picomolar concentration range.[28] Corradi *et al*. searched for potential biomarkers in exhaled breath of non-small cell lung cancer patients, and reported 2-hexenal, 2-heptenal and 2-nonenal in exhaled breath ranging from 1.2 to 9.9 picomolar.[28] An increase in the concentration of UV active compounds in a solution is reflected by an increase in UV absorbance, and if any of those are α,β-unsaturated, their contribution to the overall absorbance will be significant due to their much larger molar absorptivity values. Because UV spectroscopy absorbance is additive, the overall absorbance should increase. Given below is an initial demonstration how UV detection of the fraction of α,β-unsaturated aldehydes in breath can be used to diagnose disease, in this case an infection by the SARS-CoV-2, a coronavirus that is known to cause COVID-19 illness.[29]

Method Validation. All UV-Vis spectra were taken in LC-grade methanol ($\geq$99.9%, VWR Chemicals BDH) using a VWR Cell Quartz 100 uL Z8.5mm cuvette and a Beckman Coulter DU 800 spectrophotometer. Aldehydes and ketones were purchased from Millipore Sigma and Tokyo Chemical Industry.

Figure 3.7 depicts the comparison of UV absorbances for a panel of saturated ATM-carbonyl adducts with one unsaturated ATM-carbonyl adduct, namely that of 4-hydroxy-2-hexenal (4-HHE). The carbonyls on the panel were chosen for a few different

reasons. First acetone was chosen because it is one of the most abundant exhaled breath carbonyls, with healthy breath concentrations ranging from 19.8 nmol/L to 79.4 nmol/L.[27] Other ketones and hydroxyacetaldehyde were chosen because they were reported as lung cancer markers in exhaled breath using the previously mentioned breath carbonyl collection protocol.[24] Finally, 4-HHE was not only a reported a lung cancer marker in exhaled breath by Li *et al.*,[24] but it is also identified in Table 1.2 as one of the mechanistically expected aldehyde metabolites of lipid peroxidation along with 2-hydroxyheptanal. The ATM-4-HHE adduct (red line, Figure 3.7) clearly has a greater molar absorptivity relative to those of the saturated ATM-carbonyl adducts.
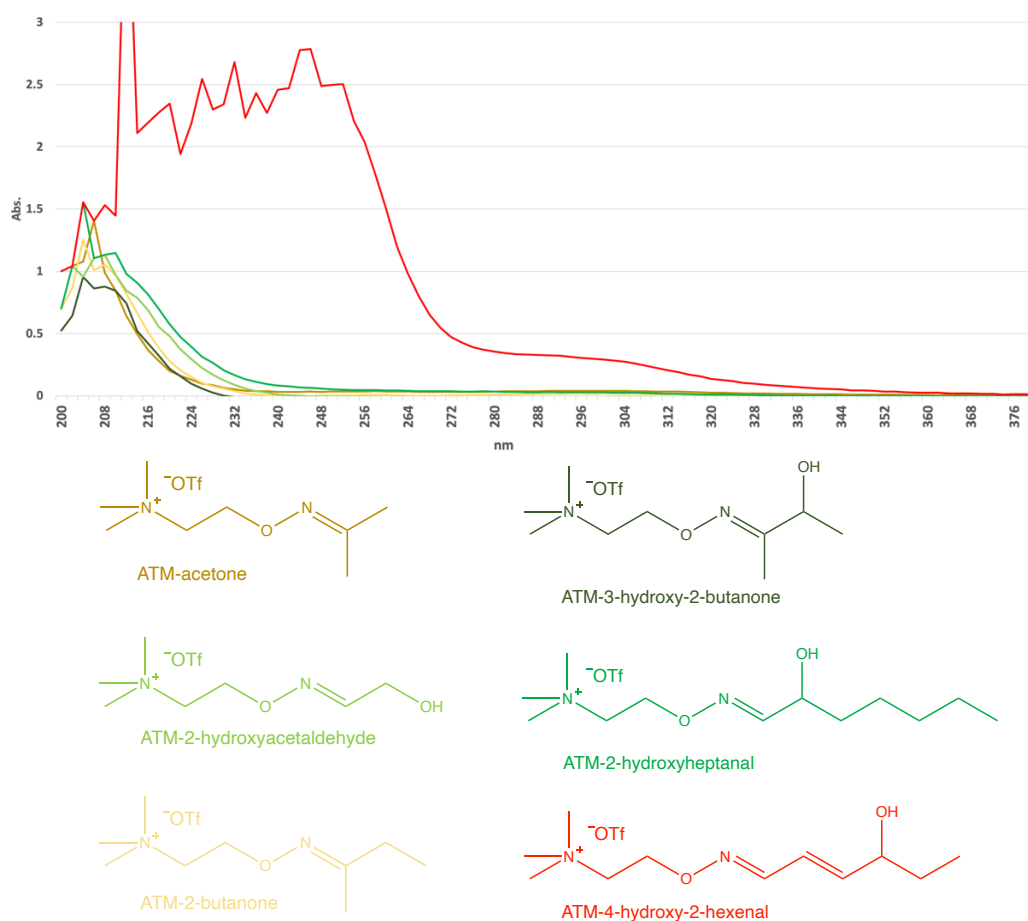
Figure 3.7. Molecular structures and UV absorbance spectra of select ATM-carbonyl adducts. All spectra were acquired from 1 mM solutions in methanol.

Importantly, the UV absorbance of the ATM-4-HHE adduct extends well beyond the λ_{max} absorbances of any of the saturated analogs (i.e., 205 nm).

With regard to the use of ATM in the carbonyl derivatization step, other reagents can be used for chemoselective carbonyl derivatization to obtain adducts that have similar molar absorptivity distinctions as the ATM adducts. 4-(2-Aminooxyethyl)-morpholin-4-ium chloride (AMAH) was developed by Dr. Ralph Knipp, a previous group member, for gas chromatography-mass spectrometry purposes.[23] For example, AMAH was prepared using the published protocol and then reacted with hexanal and 2-hexenal to obtain the corresponding oxime ether adducts. Two separate 1 mM solutions of these AMAH adducts were then examined by UV-Vis spectroscopy (Figures 3.8). The α,β-unsaturated AMAH adduct absorbance is similar to that of the closely related ATM adduct; conjugation causes a bathochromic shift in wavelengths absorbed as well as an increase in the molar absorptivity.
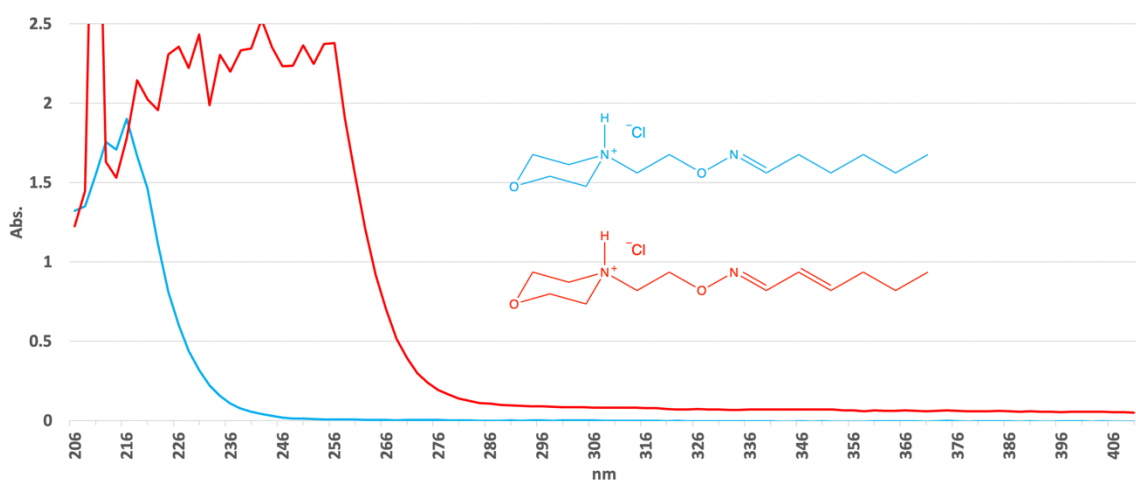
Figure 3.8. Molecular structures and UV absorbance spectra of AMAH-aldehyde adducts. All spectra were acquired from 1 mM solutions in methanol.

Figure 3.9. Molecular structures and UV absorbance spectra of AMP-aldehyde adducts. All spectra were acquired from 1 mM solutions in methanol.

Carbonyl adducts of a commercially available hydrazine similar to AMAH, 1-amino-4-methylpiperazine (AMP), were also briefly examined by UV-Vis measurements. In this case, AMP was of interest because the hydrazine functionality, unlike the aminooxy functionality of both ATM and AMAH, reacts with unsaturated aldehydes at a faster rate to form adducts called hydrazones.[30] AMP was commercially available and purchased from Millipore Sigma. The AMP was then reacted with hexanal and 2-hexenal to obtain the corresponding hydrazone adducts. Two separate 1 mM solutions of these AMP adducts were then examined by UV-Vis spectroscopy (Figures 3.9). The α,β-unsaturated AMP adduct has a bathochromic shift in absorbance relative to the saturated AMP adduct due to its conjugation. However, there does not seem to be as pronounced of a difference in molar absorptivity between the AMP saturated and α,β-unsaturated adducts. In comparing UV-Vis spectra of saturated and unsaturated adducts, the difference between ATM-pentanal and ATM-2-pentenal were relatively more pronounced than with any other adduct pair examined, so we pursued development of our method using this reagent.

Trace α,β-unsaturated aldehyde effect on UV spectrum. Most exhaled aldehydes tend to be lower in concentration; specifically, α,β-unsaturated aldehydes are present at the pmol/L range.[24] To better understand the relationship between an increase in the concentration of an α,β-unsaturated aldehyde and the effect on the resultant UV spectrum, the UV absorbance of six solutions with a constant concentration of a saturated aldehyde and decreasing concentrations of an α,β-unsaturated aldehyde were examined (Figure 3.10). For these experiments, two ATM-aldehyde adducts were chosen, ATM-pentanal to represent the saturated fraction of aldehydes in breath and ATM-2-pentenal to represent the α,β-unsaturated fraction. The solutions were constituted to be same volume (200 μL) as the silicon microreactor elution volume. Each of the six solutions had ATM-pentanal concentrations of 50 nmol/200μL, to represent the larger saturated fraction of exhaled breath aldehydes.
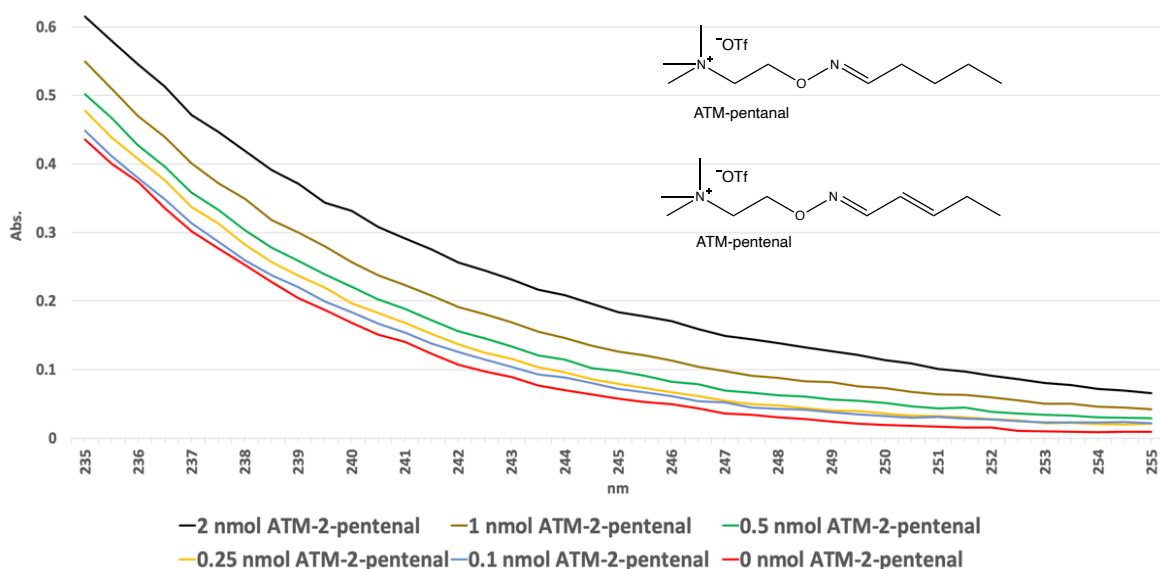
Figure 3.10. Molecular structures and each absorbance spectrum shown has 50 nmol ATM–pentanal and X nmol ATM-2-pentenal, dissolved in 200 μL methanol.

In order to mimic a slight increase of α,β-unsaturated aldehydes in exhaled breath concentration due to LPO and disease and determine a limit of detection relative to the ever-present larger concentration of saturated aldehydes, to each solution was added an increasing amount of ATM-2-pentenal, ranging from zero to 2 nmol, as indicated by the colors of the traces from Figure 3.10.

While absorbances were recorded in the range 205-350 nm (not shown in Figure 3.10), the absorbances at wavelengths between 237-252 nm show a linear relationship between an increase in the α,β-unsaturated ATM-2-pentenal adduct concentration and absorbance. Additionally, the increased absorbance due to 0.1 nmol of the α,β-unsaturated ATM-2-pentenal adduct can be observed in the presence of 50 nmol of saturated ATM-pentanal adduct. These experiments suggest trace levels of unsaturated carbonyls in a mixture produce measurable differences in absorption spectra. Thus, we set out to test the method in a pilot study involving patient breath.

Protocol Development. Lung cancer is not the only respiratory disease to be associated with oxidative stress. SARS-CoV-2 infection, or COVID-19, is also a respiratory disease and there have been many reports linking COVID-19 with oxidative stress.[31,32,33] As discussed in Chapter 1, oxidative stress will lead to a greater amount of lipid peroxidation-derived aldehyde metabolites in exhaled breath, including α,β-unsaturated aldehydes. Due to the global pandemic, COVID-19 has put a spotlight on the dire need for an accurate, rapid, and noninvasive test because of the contagious nature and potential health effects of the disease. For these reasons and all of those previously mentioned, we launched a pilot study to examine the UV absorptions of the ATM-carbonyl adduct

mixtures obtained from the exhaled breath of healthy vs. symptomatic COVID-19-positive subjects.

Collecting breath samples from human subjects, especially COVID-19 positive subjects, required that certain steps involving the ATM-coated silicon microreactor (e.g., elution of ATM-carbonyl adducts from the microreactor) be performed off-site and by others. To ensure consistent sample handling, we first explored the development of an UV-active internal reference to serve as an indicator of proper sample collection. The ability to compare samples requires protocol consistency, and the UV-Vis approach provided the opportunity to integrate quality assurance procedure. Coating the microreactor with a reference compound (along with ATM) in a known, consistent amount could allow its use as an internal reference (IR) standard, as long as the λ_{max} for this reference compound does not overlap with the ATM-adduct absorbance wavelength range of interest from 235-350 nm (Figure 3.13). Of course, the reference compound also must not interfere with the oximation chemistry that is central to carbonyl capture by the microreactor. After considering commercially available UV-Vis IR standards for those that were stable and unlikely to react with ATM, silica, or any breath component, 3-(2-benzothiazolyl)-7-(diethylamino)coumarin was purchased from Chemodex. While the purchased UV-Vis IR standard has a λ_{max} at 458 nm, other absorptions needed to be considered. Figure 3.11 shows the results of a necessary UV-Vis study to determine if the UV-Vis IR standard has an absorbance that would interfere with ATM-carbonyl adduct absorbances, by obtaining the absorbances at different known concentrations. The determination was that if the UV-Vis IR has a concentration less than 0.0001 mM then

there is no absorbance interference in the absorbance wavelength range of interest, 205-350 nm. At the concentration of 0.0001 mM the benzothiazole UV-Vis IR absorbs from 385 to 500 nm, with λ_{max} at 458 nm. As shown in Figure 3.12, the R^2 value indicates the absorbance response variable is well correlated to concentration.
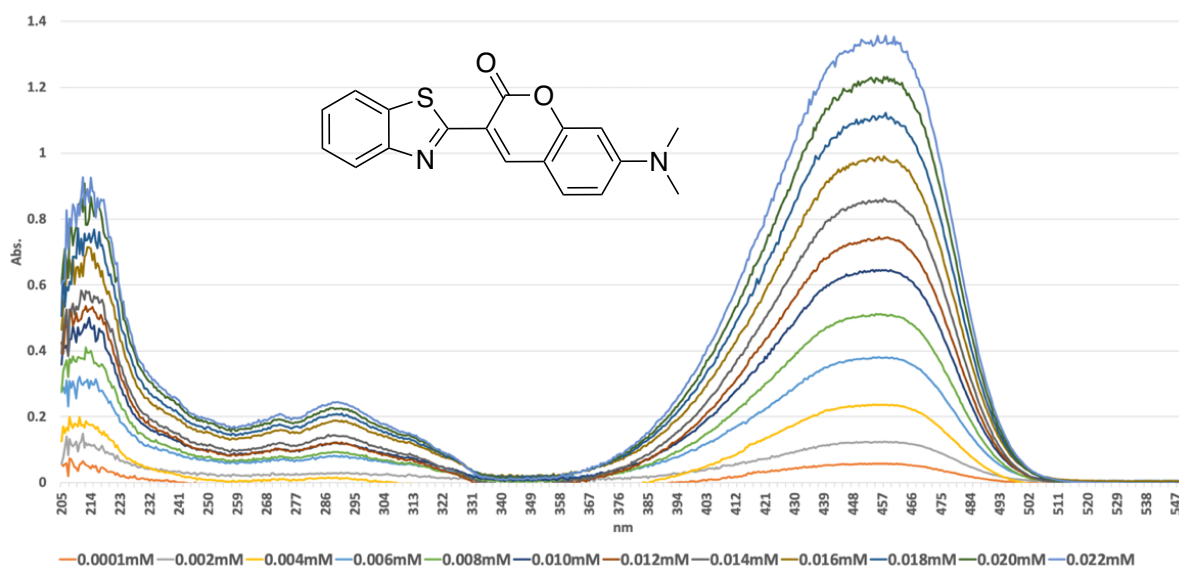
Figure 3.11. Benzothiazole UV-Vis IR standard structure and absorbance spectra at different concentrations.
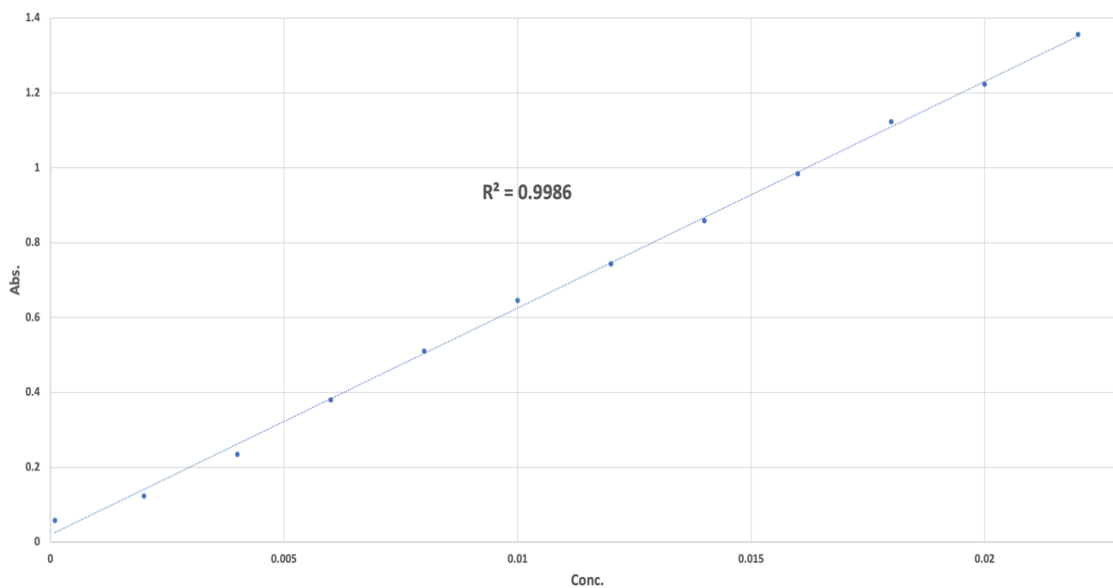
Figure 3.12. Benzothiazole UV-Vis IR standard λ_{max} 458nm absorbance linearity.
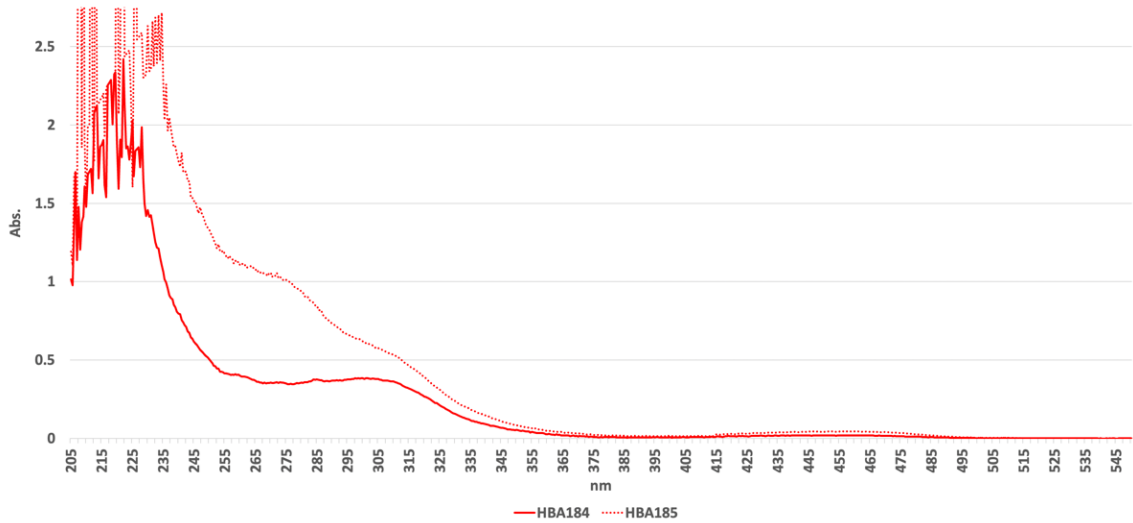
Figure 3.13. UV-Vis spectral data from symptomatic COVID-19 positive samples HBA184 and HBA 185.

Shown in Figure 3.13 are the UV-Vis spectra from exhaled breath samples of symptomatic COVID-19 positive patients, samples HBA184 and HBA185. The ATM-carbonyl UV absorption range of interest as previously stated is 235-350nm. There is no interference from the benzothiazole UV-Vis IR standard absorptions from 390-500 nm with that of ATM-carbonyls from breath sample absorbance range of interest.
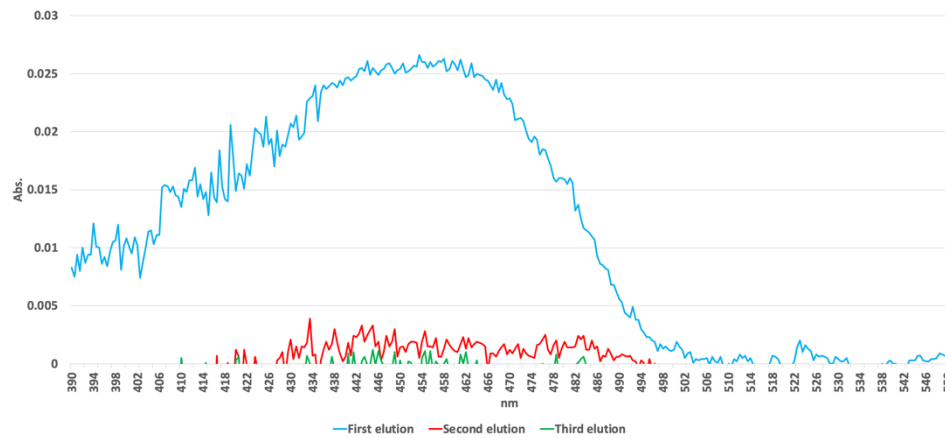
Figure 3.14. UV-Vis spectral data from elution of silicon micro-reactor loaded with benzothiazole UV-Vis IR standard.

To ensure UV-Vis IR can be used with existing ATM carbonyl derivatization and preconcentration protocols, an elution study was carried out in duplicate. The microreactors were loaded with UV-Vis IR and subjected to normal drying procedures. The microreactors were eluted three separate times with a volume of 200μL of methanol to mimic typical microreactor elution protocol. The absorbance spectra of the three elutions from one microreactor are shown in Figure 3.14, other trials had similar results. The data from Figure 3.14 demonstrates nearly all the UV-Vis IR is eluted from the microreactor by the first elution of 200μL methanol. Shown in Figure 3.15 is the first elution of benzothiazole UV-Vis IR standard absorptions compared to symptomatic COVID-19 positive samples HBA184 and HBA185. The focus of Figure 3.15 is the nanometer range the IR standards λ_{max} falls within. HBA184 absorbance value around λ_{max} 458 nm that is similar to the first elution test sample, indicating each were similarly loaded
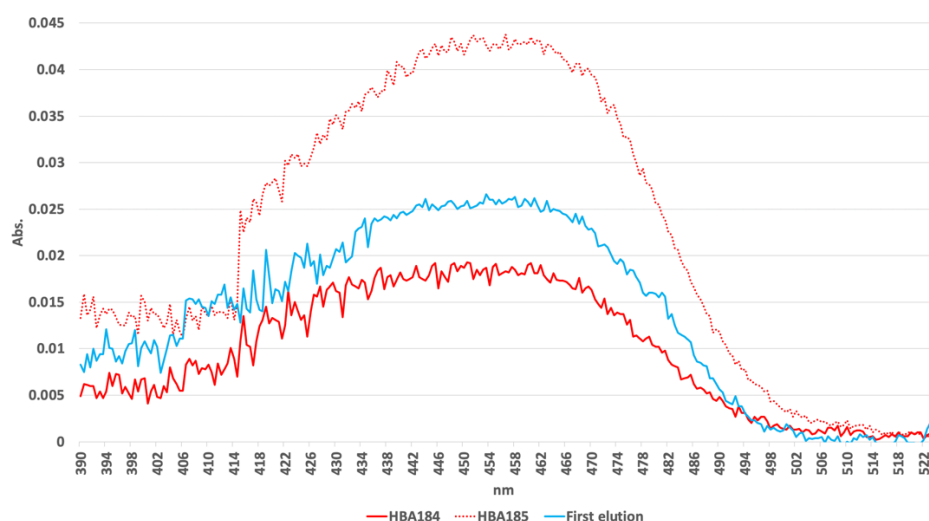
Figure 3.15. UV-Vis spectral data from first elution of silicon micro-reactor loaded with benzothiazole UV-Vis IR standard, and data from symptomatic COVID-19 positive samples HBA184 and HBA185.

and eluted. However, the same comparison between the first elution test sample and HBA185, the UV-Vis IR standard λ_{max} absorbance of sample HBA 185 is demonstrably higher and indicates there was an issue with microreactor loading, microreactor elution or sample handling.

Pilot study. Institutional Review Board 20.1154 was approved by the University of Louisville to recruit subjects and process exhaled breath samples. The IRB was approved under Co-Principal Investigators Dr. Xiao-An Fu, PhD, and Dr. Jiapeng Huang, MD, PhD, Department of Anesthesiology, University of Louisville School of Medicine. With IRB approval, one-liter breath samples were collected from 10 symptomatic COVID-19 patients in the clinic at the University of Louisville Hospital. The breath samples were passed through the IR- and ATM-coated microreactors to preconcentrate the carbonyl fraction through ATM derivatization.[19] The COVID-positive samples were collected, processed, and then transported to our labs by either Elizabeth Cooke, Subathra Marimuthu, Holly Aliesky, James D. Morris, or Zhenzhen Xie. One-liter breath samples from 10 healthy control volunteers were obtained and subjected to the same protocol. Volunteer breath samples were taken between June 16th, 2022 and July 25th, 2022. According to SARS-CoV-2 variant tracking data from the Centers for Disease Control and Prevention, throughout the period that breath samples were taken, 99.9% of subvariants circulating in Health and Human Services Region 4 are the Omicron variant.[34] At the beginning of the period the Omicron subvariant BA.2.12.1 was dominant, by the end of the period the Omicron subvariants BA.4 and BA.5 were dominant.[34]

Pilot study data is shown in Figure 3.16 where healthy patient data are plotted as green lines and symptomatic COVID-19 patient data are the red lines. Before discussing the data further, the corresponding UV-Vis IR data must first be evaluated to ensure each sample was properly eluted from the microreactor, as shown in Figure 3.17.
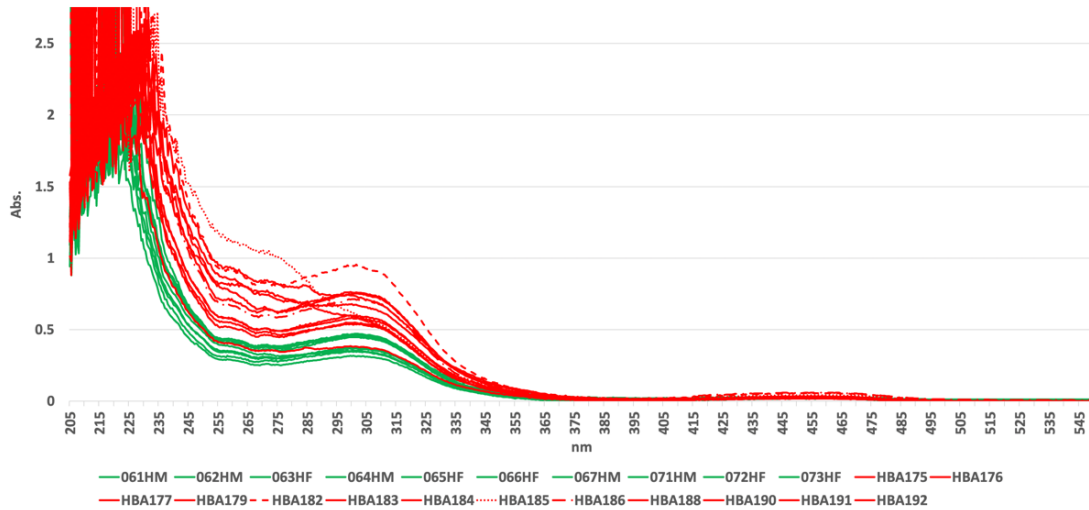
Figure 3.16. Pilot study samples full absorbance spectra.

There are three COVID-19 positive traces in Figure 3.16 that are not solid lines. This is because upon looking are the UV-Vis IR wavelength region closely in Figure 3.17, there are three traces that are higher and not well grouped with the others at the UV-Vis IR λ_{max} wavelength.
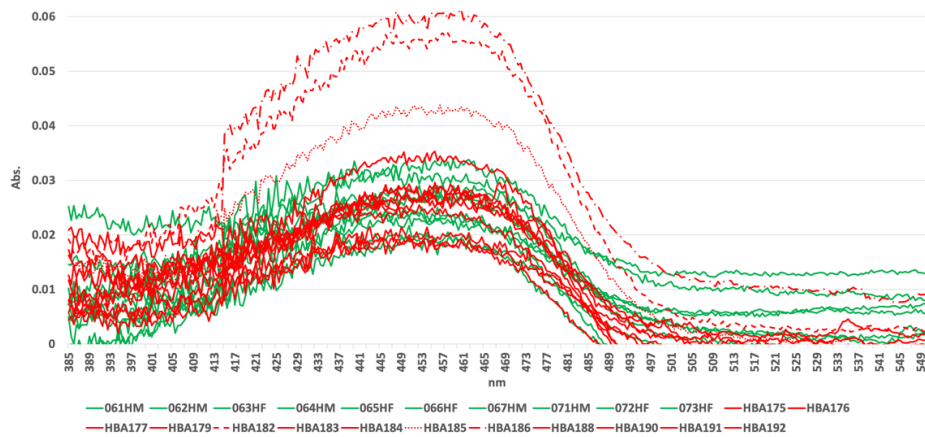
Figure 3.17. Pilot study data UV-Vis IR Standard absorbance spectra. The dotted line traces were outside the range of one standard deviation of the mean absorption at λ_{max} 458 nm.

The mean absorbance of all pilot study samples at λ_{max} 458 nm is 0.03 with a standard deviation of 0.01, and plus or minus 1σ about the mean is an absorbance range from 0.02 to 0.04. There are three samples from the pilot study that have a UV-Vis IR Standard λ_{max} absorbance outside the plus or minus one standard deviation range, the three non-solid red traces in Figure 3.17. These are COVID-19 positive samples HBA182POS5, HBA185POS8 and HBA186POS9. There are several possible reasons for an increase in the UV-Vis IR λ_{max} absorbance above the expected mean absorbance, such as the sample could have been eluted with a smaller volume than the standard 200 μL or perhaps the eluted sample was not properly sealed and there was some solvent evaporation. Whatever the reason, these three samples were removed from the data set because they were out of range. Figure 3.18 shows the pilot study data of 10 healthy
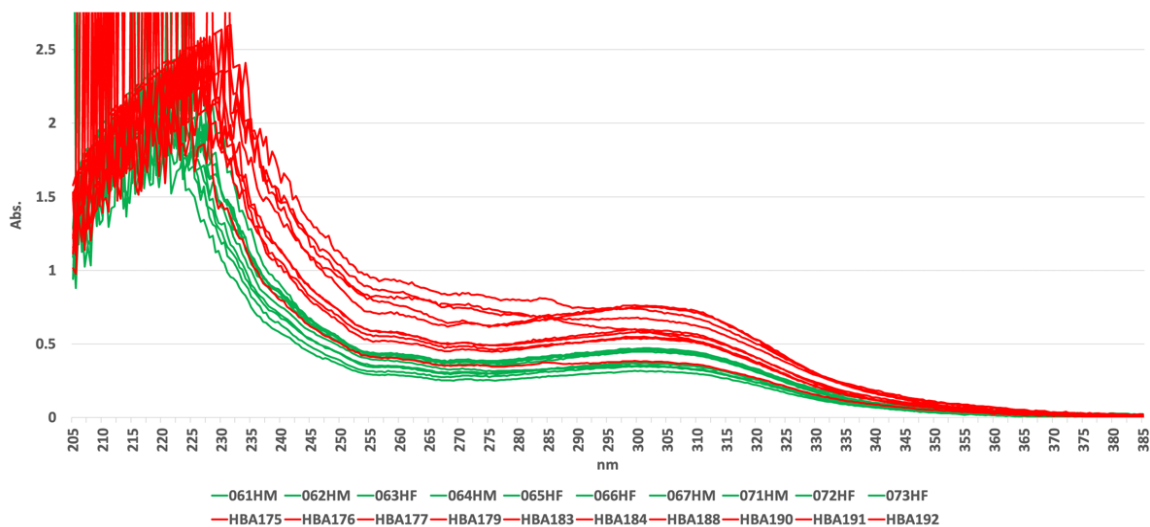
Figure 3.18. Absorbance spectra of final data set from pilot study on IR- and ATM-loaded microreactors for analysis of exhaled breath from healthy (green) vs. COVID-19 positive subjects (red).

patients and 10 symptomatic COVID-19 positive patients; the healthy and symptomatic

COVID-19 positive data seem well grouped.   There is one overlapping COVID-19 positive

trace in the range of the healthy subjects. These preliminary data groupings yield initial

healthy and COVID-19 positive absorbance ranges, which were determined by plotting

the mean traces for each group and using plus and minus standard deviations as error

bars (Figure 3.19).
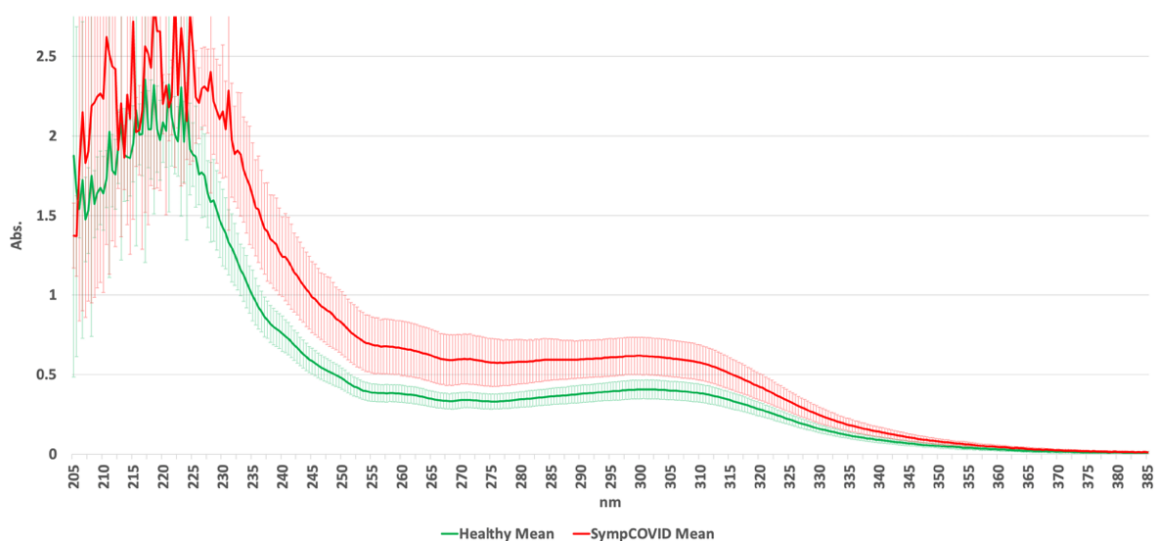
Figure 3.19. Pilot study ATM-carbonyl healthy vs symptomatic COVID-19 positive absorbance means with plus and minus 1σ error bars.

While there is some variation, there are many candidate wavelengths to select for

prospective studies, from 235 nm to 305 nm, where there is clear separation between the

two groups and potential threshold absorbance intensities at certain wavelengths

indicative of COVID-19. One of the largest gaps between the two means was at 240 nm.

To compare the healthy and COVID positive means at 240 nm a two-tailed Welch's *t*-test

was performed. The mean of the absorbance of 10 healthy patients at 240 nm is 0.8 with

a standard deviation of 0.1. The mean of the absorbance of 10 COVID positive patients at

240 nm is 1.2 with a standard deviation of 0.2. There is a significant difference between the healthy and COVID positive mean at 240 nm, $t(12) = 5.6$, $p < 0.01$.

We also examined the data using the IR to normalize the data. All absorbance values from each patients' spectra were divided by the 458 nm λ_{max} absorbance of the IR from the same spectrum. In using the IR to normalize measurements, we no longer needed to disqualify the three samples that were originally removed. Again, to compare the healthy and COVID positive means at 240 nm a two tailed Welch's t-test was performed because of the different variances between the two group. The mean of the absorbance of 10 healthy patients at 240 nm is 31 with a standard deviation of 8. The mean of the absorbance of 13 COVID positive patients at 240 nm is 47 with a standard deviation of 16. Once again, there is a significant difference between the healthy and COVID positive mean at 240 nm, $t(18) = 3.21$, $p < 0.005$.

We noted an interesting detail from one of the healthy volunteers, a current cigarette smoker, whose exhaled breath sample absorbance fell within the one standard deviation of the healthy mean. This is interesting because smoking has been reported to contribute to exhaled breath VOC concentrations, aldehydes among them, so higher carbonyl levels would have been expected.[35] Though smoking in the United States has declined from 21% in 2005 to 12.5% of the population in 2020,[36] smoking status must be considered when conducting breath analysis, putting together a sample set and determining disease threshold.

Other COVID-19 breath tests are being developed, like Chen *et al.*, who combined chromatography, spectroscopy and machine learning for analyses.[37] Grassin-Delyle *et al.*

carried out breath analysis of COVID-19 patients using Proton Transfer Reaction Mass Spectrometry (PTR-MS), and reported the aldehyde nonanal as significantly elevated in Acute Respiratory Distress Syndrome (ARDS) patients with COVID-19 relative to ARDS patients without COVID-19.[38] Ruszkiewicz *et al.* using the common combination of chromatography and mass spectrometry, observed aldehydes propanal, heptanal, octanal and ketones acetone and butan-2-one all elevated in breath of COVID positive patients, and went on to use heptanal and octanal in their COVID-19 classification model.[39] Also using PTR-MS, Liangou *et al.* identified heptanal as important to identification of COVID-19 from breath analysis.[40]

Though promising that many attempts are being made to develop a rapid COVID-19 breath test, none of these studies observed or reported any unbranched α,β-unsaturated aldehydes, which are likely to be present in diseased breath. The mentioned studies have a few drawbacks as well. None of them used preconcentration techniques, leaving their sample analysis susceptible to signal to noise ratio issues and lack accuracy, or potential interference from the thousands of other VOCs present in exhaled breath with potential higher and/or unresolved signals. Also, each of these reported techniques use separation science, requiring expensive laboratory based chromatographic and analytical chemistry instruments.

The use of UV-Vis spectrometry does not require extensive use of elution solvents or bulky tanks of inert gas, it only requires a sample and electricity to power the instrument. There are many portable UV-Vis spectrophotometers commercially available to easily integrate with the silicon microreactor methodology. The combination of silicon

micro-preconcentrator with ATM aminooxy derivatization and UV spectroscopy for breath analysis has not been examined prior to this work. Further clinical studies are necessary with large sample sets to properly determine the threshold above which a result is truly indicative of COVID-19. Research and development is ongoing by the Nantz and Fu groups to devise a method to reduce breath derivatization and preconcentration time from greater than two hours down to minutes. There is great potential that this novel approach, outlined in step-by-step detail below, could be used for a variety of diseases, given proper clinical trials are completed to determine UV-Vis absorbance disease thresholds of exhaled breath.

Protocol for Breath Analysis Using UV-Vis Spectroscopy to Diagnose COVID-19
- Breath Collection (subject breathes into 1-L Tedlar bag)
- Breath Derivatization and Preconcentration (exhaled breath passed through IR-loaded ATM-microreactor)
- Elution (microreactor is eluted using 200 μL methanol to afford sample solution)
- Sample Preparation (microcuvette is charged with 100 μL of sample solution)
- UV Measurement (absorbance measurement is recorded from 200-550 nm)
- Algorithm Application (value is checked to see if in range (1 std. dev.) of positive)
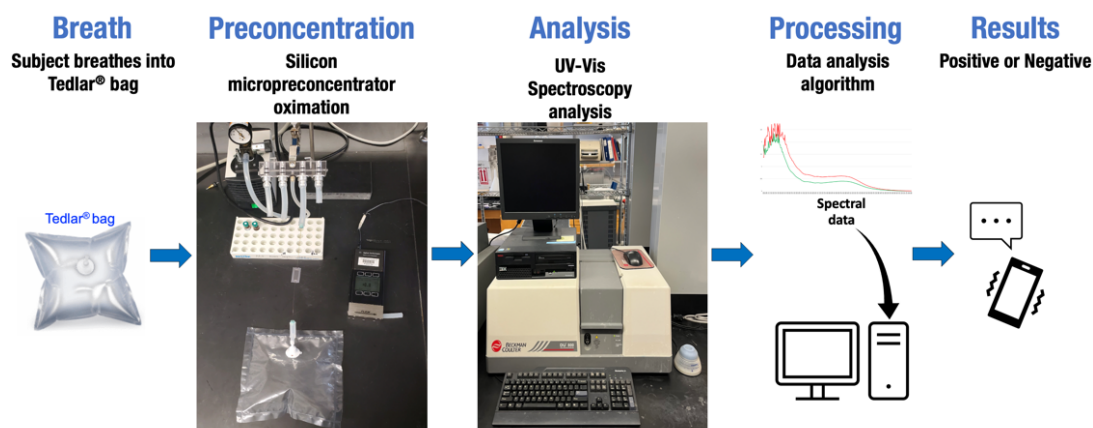
Figure 3.20. Breath analysis protocol using IR-ATM-microreactor, UV-Vis spectroscopy protocol.

CHAPTER 4

SYNTHESIS OF (*E,E*)-MUCONALDEHYDE

4.0 Introduction

As α,β-unsaturated aldehydes are known to elicit harmful effects through alkylation of DNA, proteins and other biomacromolecule, we explored the toxic effects of a well-known metabolite of benzene, muconaldehyde. Working with the University of Louisville Superfund Research Center,[1] which focuses on the effects of harmful volatile organic compounds in the environment, led us to collaborate on a project involving (*E*, *E*)-muconaldehyde (**1**, Figure 4.1). Muconaldehyde (also known as muconic dialdehyde or (*2E*, *4E*)-hexa-2,4-dienedial) is an open-ring metabolite of benzene[2] that has become the subject of numerous investigations into the toxic effects of exposure to benzene.[3,4,5] The presumed formation of muconaldehyde as a result of tropospheric oxidation of benzene in photochemical smog also has stimulated investigations on its formation in the atmosphere and resultant effects on pollution.[6,7,8] Finally, muconaldehyde is of interest to synthetic chemists, particularly as a linking substrate for polyene synthesis[9,10,11] and as a diene reactant for inverse electron-demand Diels-Alder reactions.[12] Muconaldehyde is not commercially available. Our interest in the toxicological studies of this widely investigated dialdehyde led us to examine its synthesis from the corresponding diacid, muconic acid (**2**).

muconaldehyde (**1**)   muconic acid (**2**)
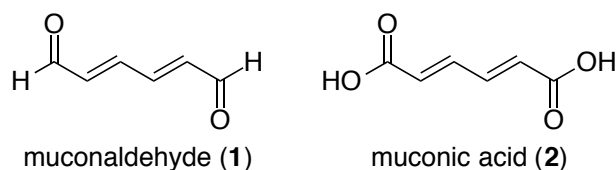
Figure 4.1. Muconaldehyde and commercially available muconic acid.

Described below are the results of our studies on a new method for preparation of muconaldehyde.

4.1 Prior Syntheses of Muconaldehyde

Several syntheses of muconaldehyde have been reported (Figure 4.2),[13,14,15,16,17,18] spanning a wide variety of approaches from the first synthesis in 1949 by Karrer *et al.*[13] (3 steps, 32% overall yield) to the more recent reports in 2005 by Kurteva and Afonso[17] (4 steps, 27%) and in 2016 by Chen *et al.*[18] (2 steps, 24%). The double Wittig-Horner approach to the title compound by Kossmehl and Bohn[14] appears most expeditious; however, while they reported a crude yield of 77%, a recent application of this route reports isolation of muconaldehyde in 22% yield.[19] Murray *et al*. made the minor change of starting with glyoxal trimeric hydrate, instead of glyoxal as Kossmehl and Bohn did. Yet Murray *et al*. were not able to achieve the high crude yield reported by Kossmehl and Bohn, perhaps due to four column chromatography attempts at purification as opposed to the sublimation method originally reported. Given the uncertainty involved in using the double Wittig-Horner approach, we opted to explore a different route to prepare muconaldehyde.

ref. 13

1. pyridine
60 °C, 5 min

2. p-ONC$_6$H$_4$NMe$_2$
NaOH, H$_2$O, EtOH

3. HCl, H$_2$O
Et$_2$O

1

ref. 14

OHC−CHO + 2 OHC=PPh$_3$

DMF
80 °C

crude
(77%)

sublimation

1

ref. 15

2 steps
51%

NaOMe
Et$_2$O, reflux
80%

NBS
DMSO, H$_2$O
72%

1

ref. 16

microbial
oxidation

NaIO$_4$
H$_2$O, 0 °C
68%

Et$_3$N, CH$_3$CN
reflux, 3h
54%

1

ref. 17

2 steps
44%

(COCl)$_2$, Et$_3$N
CH$_2$Cl$_2$, 0 °C
100%

a. O$_3$
CH$_2$Cl$_2$, −78 °C

b. Me$_2$S
c. piperidinium·OAc
62%

1

ref. 18

OH + OHC=PPh$_3$

CH$_2$Cl$_2$
reflux
35%

diphenyl-
prolinol (cat.)

IBX (2.5 eq)
DMSO, CH$_3$CN
68%

1

Figure 4.2. Reported syntheses of muconaldehyde.

4.2 Synthesis of (2E,4E)-N^1,N^6-diisopropyl-N^1,N^6-bis(isopropylcarbamoyl)hexa-2,4-dienediamide

Given that (E,E)-muconic acid is commercially available from Millipore Sigma and that there are multiple options for the reduction of carboxylic acid derivatives to aldehydes,[20] such as the mono-reduction of acid chlorides,[21] derived carboxymethyleniminium salts,[22] or corresponding Weinreb amides,[23] we postulated that the conversion of muconic acid to a bis-activated intermediate might provide an efficient route to **1**. We were motivated by the separate but synthetically connected reports of N,

N'-diisopropylcarbodiimide (DIC) mediated coupling of carboxylic acids to oxazolidinones,[24] and selective mono-reduction of a platform intermediate *N*-acyl oxazolidinone to aldehyde.[25]
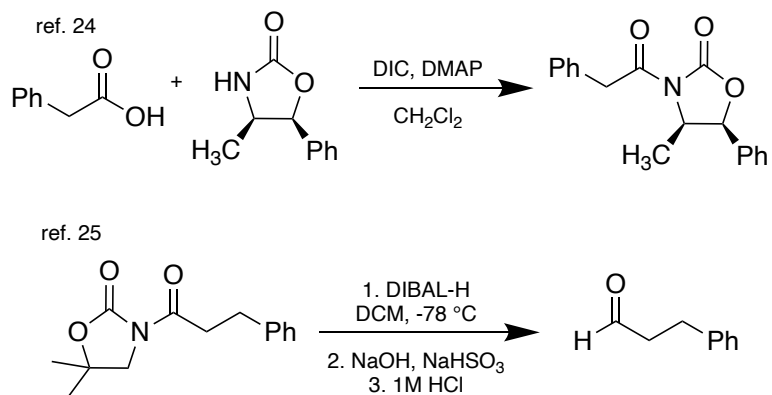
Figure 4.3. DIC assisted coupling of carboxylic acid and oxazolidinone.[24] (DMAP is 4-dimethylaminopyridine). Mono-reduction of *N*-acyl oxazolidinone to aldehyde.[25]

Graham *et al.* showed that known stable intermediate *N*-acyl oxazolidinones can be formed in good yields without an additional step by using DIC activated carboxylic acids formed *in situ*.[24] Though Bach *et al.* made their *N*-acyl oxazolidinone by acylation with an acid chloride, the subsequent mono-reduction to the corresponding aldehyde was achieved in high yield (Figure 4.4).[25] This chemistry pointed us to consider preparing bis-N-acyl oxazolidinone (2*E*,4*E*)-1,6-bis(5,5-dimethyl-2-oxooxazolidin-3-yl)hexa-2,4-diene-1,6-dione as our proximal target for a new route to muconaldehyde (**3**, Scheme 4.1).
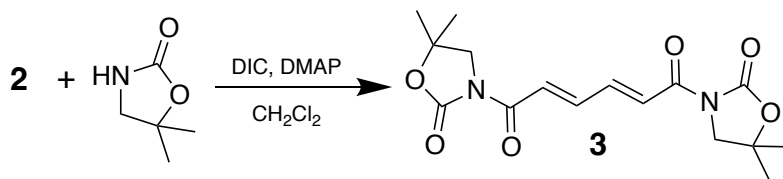
Scheme 4.1. Proposed *N*-acyl oxazolidinone strategy.

The initial synthetic strategy was to prepare bis *N*-acyl oxazolidinone intermediate 3 from muconic acid, then selectively mono-reduce each N-acyloxazolidinone using a hydride reagent, such as DIBAL-H as described in the work by Bach.[25] However, we discovered that the reaction of muconic acid and DIC formed a high yielding, stable adduct, assigned initially as structure **4**, (Scheme 4.2). The ^{13}C NMR spectrum (Figure 4.4) and infrared spectroscopy data of the isolated adduct suggests the well-known rearrangement of bis-(*O*-acyl-*N, N'*-diisopropyl isourea) (**4**) to (2*E*,4*E*)-*N*[1],*N*[6]-diisopropyl-*N*[1],*N*[6]-bis(isopropylcarbamoyl)hexa-2,4-dienediamide (**5**) had occurred.
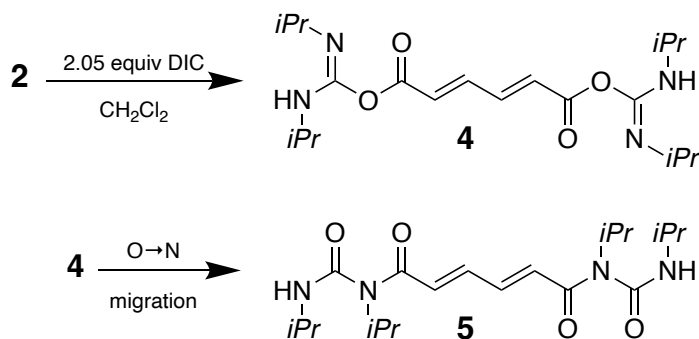
Scheme 4.2. Synthesis of *O*-acylisourea **4** and subsequent rearrangement to *N*-acylurea (**5**).

Analogous *N*-acylurea structures found and characterized in the literature support the O→N migration products bis-*N*-acylurea **5**, (Scheme 4.3 and Table 4.1).[26,27]
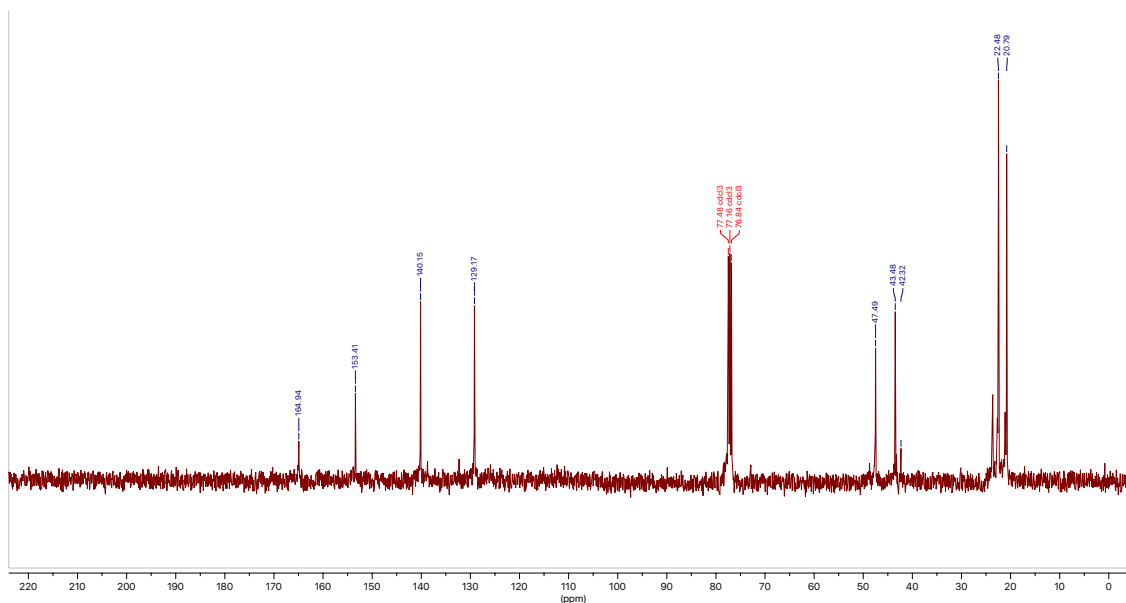
Figure 4.4. ^{13}C NMR spectrum. (CDCl$_3$, 100 MHz) of structure **5**.
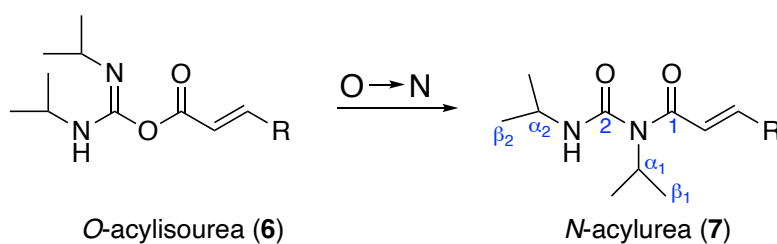
Scheme 4.3. *O*-acylisourea O→N migration forming *N*-acylurea

Table 4.1. Comparison of ^1H and ^{13}C NMR shifts of bis *N*-acylurea **5** to literature values.[a,26,27]

Entry	^{13}C: C_1, C_2	^{13}C: α_1, α_2	^{13}C: β_1, β_2	^1H: α_1, α_2	^1H: β_1, β_2
5 [b]	165.0, 153.4	47.5, 43.5	22.5, 20.8	4.48, 4.01	1.34, 1.27
7 R = 3-ClC$_6$H$_4$ [c]	167.4, 154.2	48.5, 42.9	22.6, 21.0	4.51, 4.04	1.44, 1.23
7 R = 4-ClC$_6$H$_4$ [c]	167.2, 153.9	48.3, 42.9	22.6, 21.0	4.54, 4.09	1.43, 1.23
7 R = C$_6$H$_5$ [c]	173.1, 154.5	48.5, 42.8	22.6, 21.2	4.54, 4.03	1.46, 1.23
7 R = CH$_3$ [d]	167.7, 153.9	48.2, 42.6	22.5, 20.8	4.35, 3.95	1.3, 1.1
7 R = H [d]	167.3, 153.7	48.3, 42.8	22.3, 20.8	4.35, 3.95	1.4, 1.2
6 R = CH$_3$ [d]	158.1, 139.0	48.6, 42.6	22.6, 20.9	4.45, 3.95	1.4, 1.2

[a] Chemical shifts (δ, ppm) reported in CDCl$_3$; [b] ^{13}C NMR 100 MHz, ^1H NMR 400 MHz; [c] ^{13}C NMR 62.5 MHz, ^1H NMR 250 MHz; [d] ^{13}C NMR 50.3 or 75 MHz, ^1H NMR 200 MHz.

Table 4.1 provides a comparison of ^{1}H and ^{13}C NMR shifts of *N*-acylurea **5** to literature values of analogous *N*-acylurea*s* and one *O*-acylisourea. Ramazani *et al.* reported α,β-unsaturated carboxylic acid with varying β-aryl substitutions as adducts with DIC, forming *N*-acylureas.[27] The ^{1}H NMR shifts of the two *N*-isopropyl groups and ^{13}C NMR shifts of the two Csp^2 carbons bonded to heteroatoms are quite like those of structure **5**. Anglada *et al.* reported of *N*-acylurea acrolein and crotonaldehyde DIC adducts, as well as the crotonaldehyde DIC *O*-acylisourea.[26] While there is some variation when comparing the ^{1}H NMR shifts of the *N*-isopropyl groups, the ^{13}C NMR shifts indicate structure **5** is the *N*-acylurea as its C_1 and C_2 signals align with the *N*-acylurea crotonaldehyde–DIC adduct and not the *O*-acylisourea crotonaldehyde–DIC adduct. Finally, the IR data of analogs **7** also support the determination that structure **5** is the *N*-acylurea. Anglada *et al.* reported the IR signal due to the carbonyl of *O*-acylisourea of crotonaldehyde–DIC to be at 1790 cm^{-1}, while the *N*-acylurea crotonaldehyde–DIC adduct carbonyl signal is at 1700 cm^{-1}.[26] All the IR data from Ramazani *et al.* report *N*-acylurea carbonyls to be around 1700 cm^{-1} as well, agreeing with that of structure **5**.[27] The proposed mechanism of the *O* to *N* transfer was reported by Eyley *et al.* (Scheme 4.4).[28]
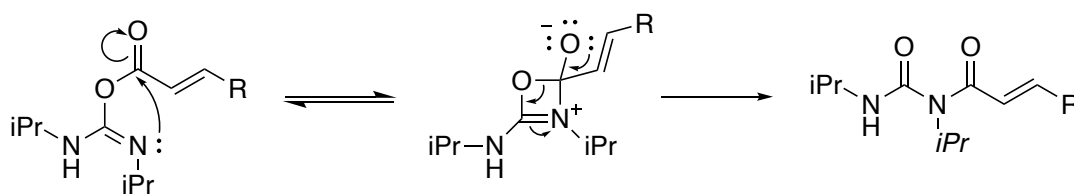
Scheme 4.4. Proposed mechanism of *O*-acyl to *N*-acyl migration.[28]

Having confirmed the structure of our *N*-acyl urea intermediate, we began to consider that its similarity to a bis *N*-acyl oxazolidinone (e.g., our original proximal target **3**) might circumvent the need to actually prepare a bis *N*-acyl oxazolidinone. Why not examine bis mono-reduction of *N*-acyl urea **5** directly? Although there are no reports of selective mono-reduction of *N*-acyl ureas, this consideration led us to explore the route that eventually led to a muconaldehyde synthesis.

4.3   Selective Mono-Reduction of (2*E*,4*E*)-*N*^{1},*N*^{6}-diisopropyl-*N*^{1},*N*^{6}-bis(isopropylcarbamoyl)hexa-2,4-dienediamide (5)

To a stirring solution of compound **5**, slow addition of diisobutylaluminum hydride (DIBAL-H) at low temperature followed by quenching the putative bis(mono-reduced) aluminum chelate [**8**] to yield muconaldehyde. Scheme 4.5 shows the full one-pot reaction forming muconaldehyde. The reaction is quenched by addition of acetic acid, followed by Rochelle's salt work up, and extraction with diethyl ether to isolate muconaldehyde in 71% yield after chromatography. Attempts were made using a few different reagents for reaction quenching including addition of ethyl acetate, ethanol, and ammonium chloride, but all gave low yields. The extraction solvent was also a variable as DCM, THF or chloroform all led to hard-to-separate emulsions and low yields as well. The specific combination of acetic acid quench and diethyl ether was key.
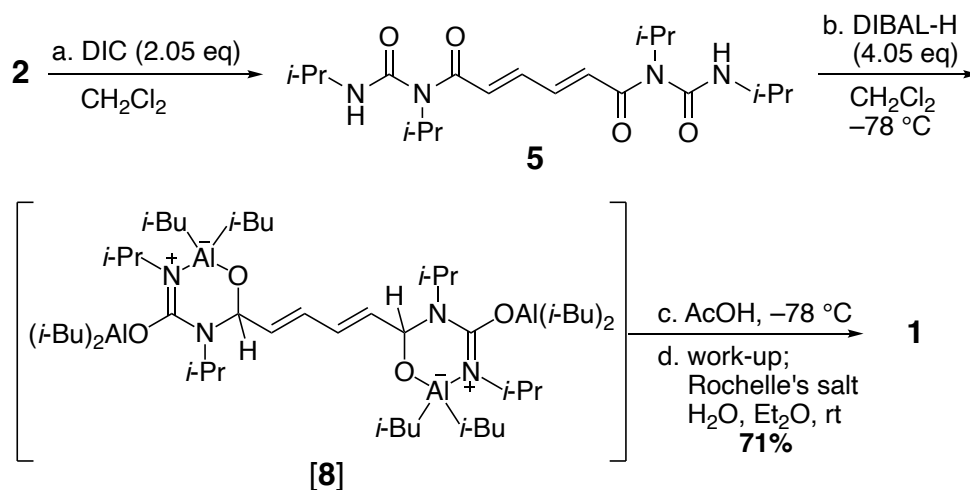
Scheme 4.5. Hydride reduction of the bis *N*-acyl urea derivative of muconic acid. DIC = *N, N′*-diisopropylcarbodiimide

The characteristic ^{1}H NMR vinyl signals at δ 7.57 and 6.63 ppm coupled to the aldehydic proton at δ 9.68 ppm clearly show the isolated product to be muconaldehyde (Figure 4.5). All characterization data for isolated compound **1** agree with reports from the literature.[16,17]
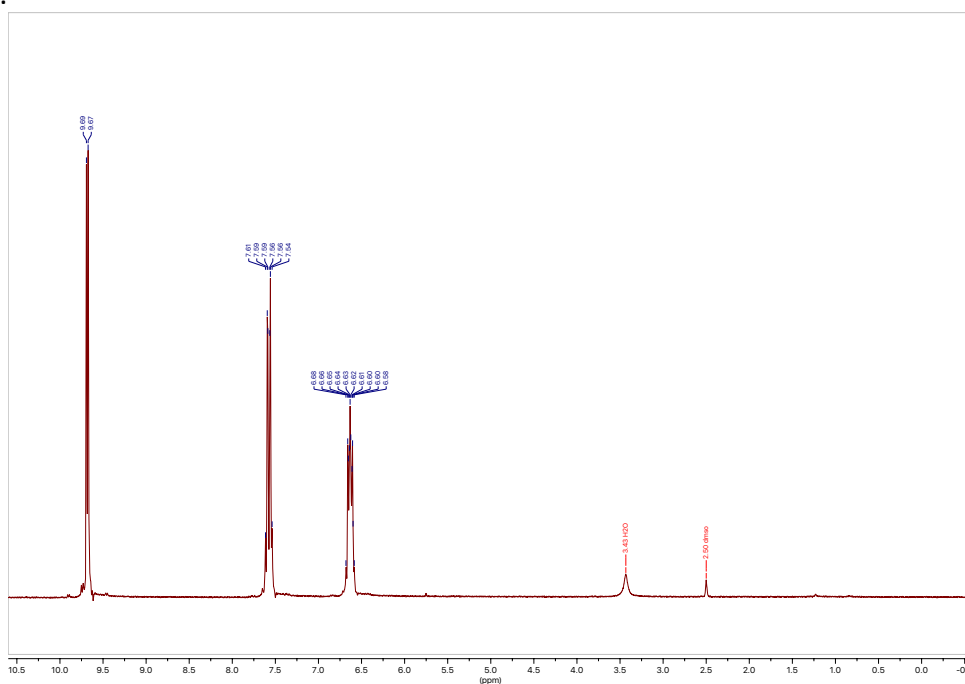
Figure 4.5. ^{1}H NMR spectrum. (DMSO, 400 MHz) of structure **1**.

86

We briefly examined other coupling agents and reducing agents but were unable to improve upon these results. For example, the use of *N*, *N'*-dicyclohexyl-carbodiimide or sodium bis(2-methoxyethoxy)aluminum hydride failed to deliver **1** as effectively as the one-pot DIC/DIBAL-H procedure.

4.4 Extrapolation of the Method to Reduction of Other Carboxylic Acids

Given that there have been no reports on selective mono-reduction of *N*-acyl ureas as a means for aldehyde synthesis, we wanted to explore if the DIC/DIBAL-H procedure could be extrapolated to transformation of other carboxylic acids to aldehydes. Initially attempts were made using citraconic acid (Figure 4.6). Over the course of multiple attempts using different reaction solvents only over-reduced alcohol and some carboxylic acid starting material were recovered (Table 4.2).

citraconic acid (**9**)   cyclohexane-
                                carboxylic
                                acid (**10**)   benzoic acid (**11**)
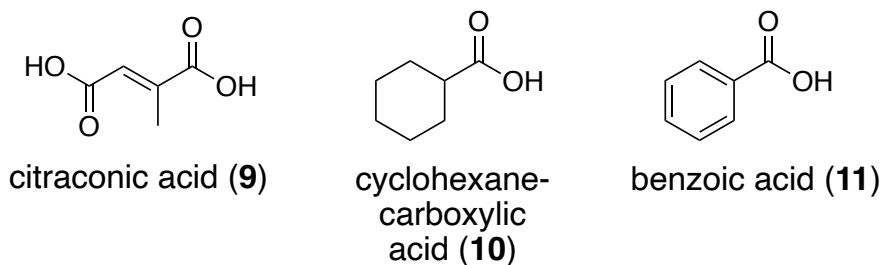
Figure 4.6. Molecular structures of select carboxylic acids.

Table 4.2. Reduction protocol trails on other carboxylic acid substrates.

Trial	Acid substrate	DIC rxn solvent	Yield/comments
1	**9**	DCM	over reduction
2	**9**	chloroform	over reduction
3	**9**	THF	over reduction
4	**10**	DCM	<5%
5	**10**	chloroform	<5%
6	**10**	THF	<5%
7	**11**	DCM	<5%
8	**11**	chloroform	<5%
9	**11**	THF	<5%

After the failures with substrate 9, the reduction protocol was attempted with aryl and alkyl carboxylic acids, benzoic acid, and cyclohexane carboxylic acid (Figure 4.6) Though aldehyde product was observed using substrates 10 and 11, yields were very low. Crude ^{1}H NMR spectrum of benzoic acid reaction is shown in Figure 4.7, the labeled peaks are of the benzaldehyde product.
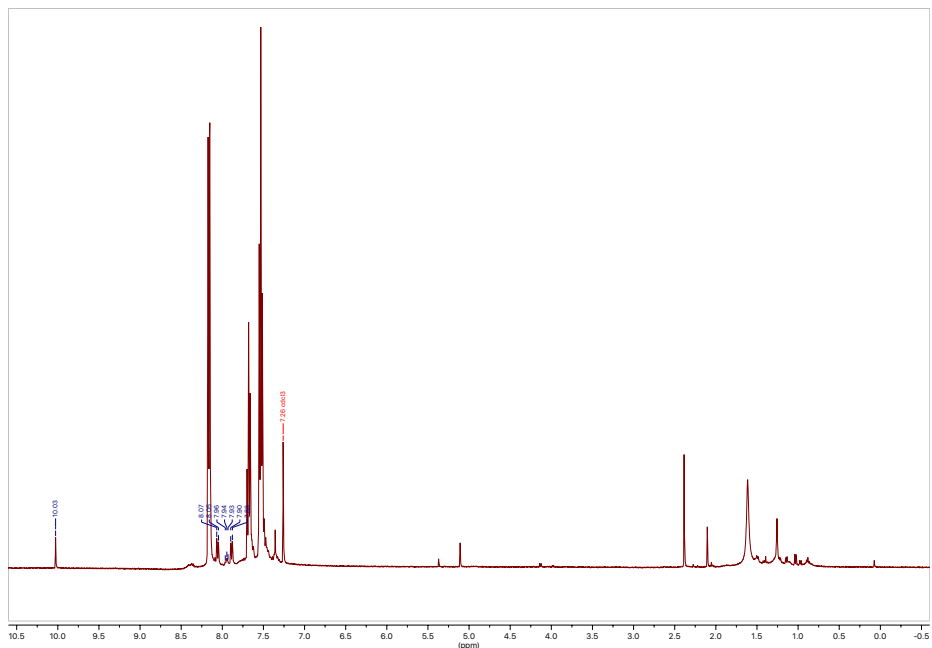
Figure 4.7. ^{1}H NMR spectrum. (CDCl$_3$, 400 MHz) and molecular structure of benzaldehyde.

With the lack of success of the reduction protocol on more than one substrate we decided to examine the DIC carboxylic acid precursor by looking at the benzoic acid reaction with DIC. When TLC analysis showed two major products, a column chromatography was carried out to separate and identify them. ^{1}H NMR showed the two major products to be benzoic anhydride (Figure 4.8), and byproduct diisopropylurea.
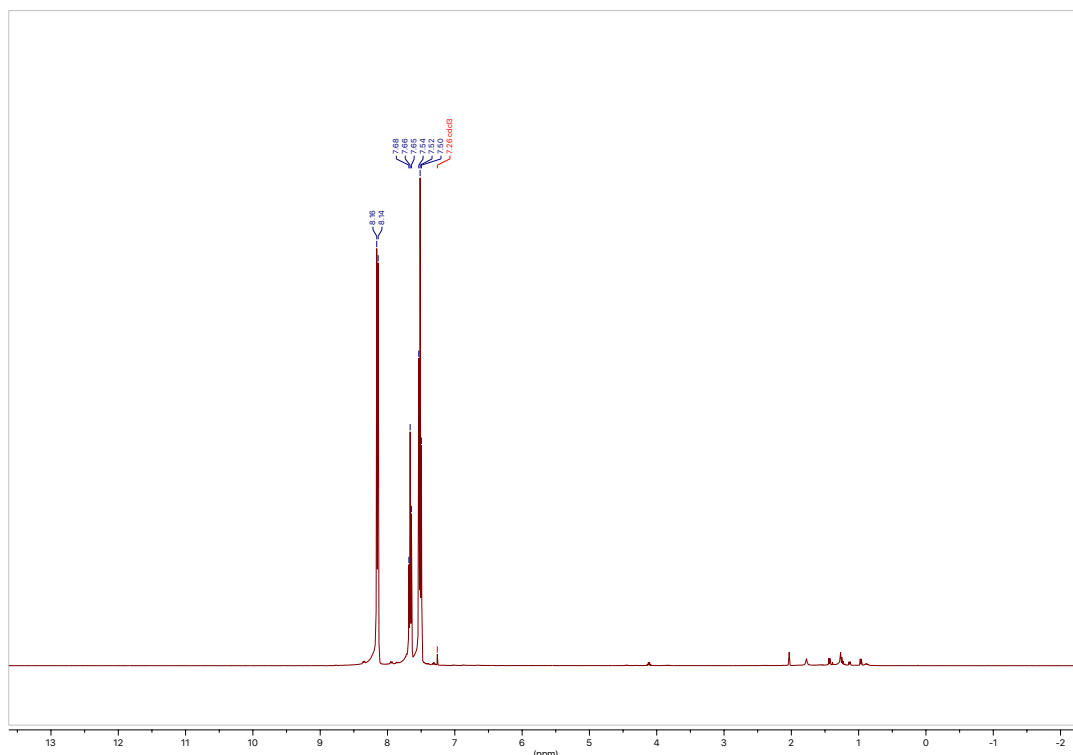
Figure 4.8. ^{1}H NMR spectrum. (CDCl$_3$, 400 MHz) of structure **16**, benzoic anhydride.

The isolation of the anhydride helped our understanding of why the method is not generally applicable to soluble carboxylic acids: As the acid-DIC adduct is formed (the expected *O*-acyl isourea, intermediate **12**, Scheme 4.6 below), it is susceptible to nucleophilic attack by neighboring unreacted benzoic acid (or carboxylate anion, since the initial mechanistic step in the reaction between benzoic acid and DIC (**13**) is deprotonation of the acid). The *O*-acyl isourea adduct generally is formed next by nucleophilic attack of carboxylate anion onto DIC (e.g., **14** → **15**). While this step occurs to form adduct **12**, **14** can also react with **12** to form the undesired product anhydride **16**. This is undesirable for a few reasons. First, this reduces potential reaction yield by nearly half, as the carboxylate leaving group from an anhydride reduction cannot be selectivity reduced because it has no ability to form an aluminum chelate to prevent over-reduction. Second, the anhydride
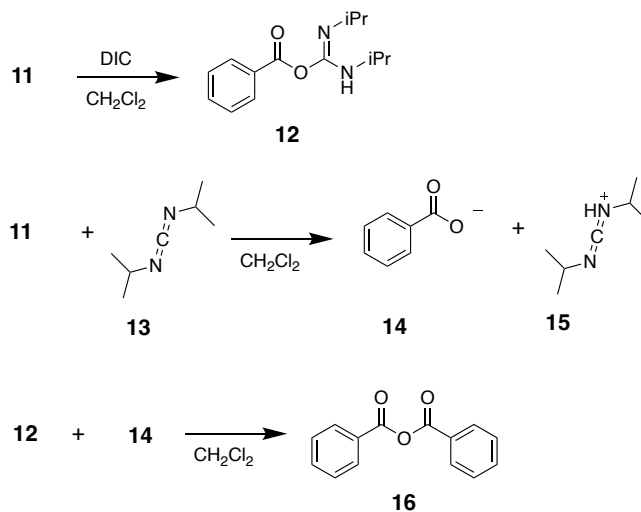
Scheme 4.6. Reaction taking place in a mixture of benzoic acid (**11**) and DIC (**13**).

itself may not form a strong chelate, and results in over-reduction to the benzyl alcohol.

To avoid the formation of side product anhydride we tried many different conditions, slow addition of the carboxylic acid, cold temperatures, and different solvents. Looking to our successful model with selective reduction of muconic acid, the key to this protocol becomes apparent, it comes down to carboxylic acid substrate solubility. Muconic acid required overnight stirring with DIC to form adduct because muconic acid is insoluble in DCM and remains insoluble until both acid functionalities have reacted with DIC. This unique circumstance allowed for the bis-DIC activated carboxylic acid (**5**) to be in solution without the presence of a nucleophile (i.e., unreacted carboxylic acid or carboxylate anion) until we introduce DIBAL-H. Figure 4.9 is a breakdown of muconic acid, mono- and bis-adducts and their solubility in DCM.

DCM solubility

insoluble

insoluble

soluble
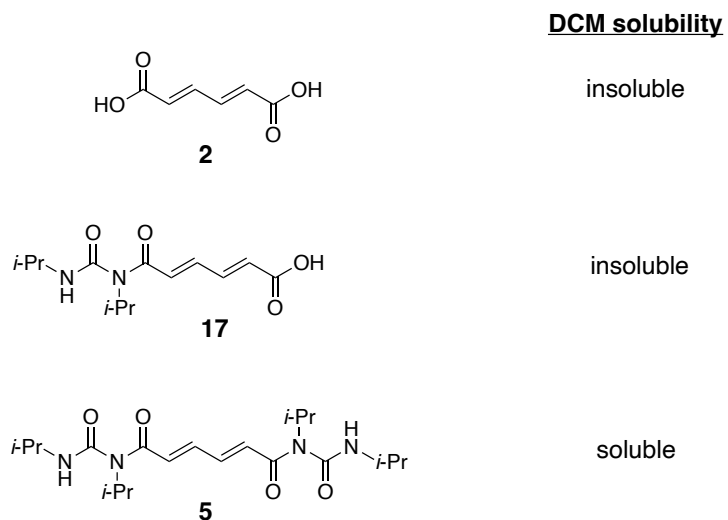
Figure 4.9. Muconic acid, mono- and bis-muconic acid DIC adduct structures and their DCM solubility.

4.5 Benzene Cardiovascular Toxicity Study

When considering cardiovascular health, the endothelium is important for the health of the entire cardiovascular system.[29] Disruptions of endothelium can lead to initiation and exacerbation of atherosclerosis and may result in thrombotic and cardiovascular events such as stroke or acute myocardial infarction. The Superfund Research Center is studying how benzene metabolite muconaldehyde affects the endothelium utilizing well controlled animal models.[1] A study determined that mice exposed to benzene inhalation had a significant endothelial injury response relative to controls exposed to HEPA-filtered air.[30] In the same work, Malovichko *et al.* exposed human aortic endothelial cells to benzene metabolites, like hydroquinone, catechol and muconaldehyde; and found muconaldhyde to be most toxic, having the greatest endothelial microparticle response indicating cardiovascular damage.[30] As the Superfund

Research Center continues their studies on benzene toxicity, I have continued to provide

muconaldehyde. In May of 2022, I successfully carried out the synthesis of

muconaldehyde on gram scale, producing 1.14g in 65% yield, using the newly developed

approach.

CHAPTER 5

EXPERIMENTAL PROCEDURES

5.1 General Statement

All chemicals (reagents, starting materials, and solvents) were purchased either from VWR Chemicals BDH, Beantown Chemical, Tokyo Chemical Industry, or MilliporeSigma. CH_2Cl_2 was dried over activated molecular sieves. All purchased starting materials were used as delivered. Melting point data was determined on an SRS MPA160 apparatus and is uncorrected. ^1H and ^{13}C NMR spectra were recorded at 400 MHz and 100 MHz, respectively, using a Varian 400-MR spectrometer. DMSO-d_6, CD_3OD, CD_3CN and $CDCl_3$ were used as solvents for NMR spectra acquisition and their residual protonated solvent peak as the internal reference. The chemical shifts are reported in ppm values relative to the residual protonated solvent peak: DMSO (2.50 ppm for ^1H NMR and 39.5 ppm for ^{13}C NMR), CH_3OH (3.31 ppm for ^1H NMR and 49.0 ppm for ^{13}C NMR), CD_3CN (1.94 ppm for ^1H NMR and 1.32 and 118.3 ppm for ^{13}C NMR), $CHCl_3$ (7.26 ppm for ^1H NMR and 77.2 ppm for ^{13}C NMR). Coupling constants are reported in hertz (Hz). A Q Exactive™ Hybrid Quadrupole-Orbitrap™ MS instruments was used for direct injection mass spectrometry of samples dissolved in methanol or n-butanol. A FreeZone 4.5 Liter Freeze Dry System was used to lyophilize frozen samples dissolved in water under a vacuum pressure of 0.285 mbar.

The progress of reactions was monitored by thin-layer chromatography (TLC). TLC was performed using glass plates coated with Merck Silica gel 60G F254. TLC spots were examined using UV light (254 nm), then visualized by a *p*-anisaldehyde stain (2.5% p-anisaldehyde acid/ethanol solution). Column chromatography was conducted using RediSep Silica 40-60μ, 60Å or RediSep R_f Gold C_{18} aq. columns inserted in a Teledyne Isco

combiflash system. Fraction collection was managed by combiflash UV measurements. Samples were dissolved in water and loaded onto a combiflash loading column packed with celite. Instrument method used for separation started 100% H_2O with an increasing gradient until 100% methanol.

Ultra high performance liquid chromatography-mass spectrometry (UHPLC-MS) was carried out using Thermo Fisher Vanquish™ UHPLC and Q Exactive™ Hybrid Quadrupole-Orbitrap™ MS instruments. The UHPLC was fitted with a BEH phenyl Waters column and elutions generally were conducted using a mixed solvent system of acetonitrile and 0.1% formic acid. UV-Vis data were collected using a Beckman Coulter DU 800 spectrophotometer. UV-Vis method parameters were as follows: Abs. scan of 200-550 nm, scan speed of 600 nm/min, and a wavelength interval of 0.5 nm.

5.2 Experimental Procedures of Chapter 2

5.2.1 Synthesis of MBA
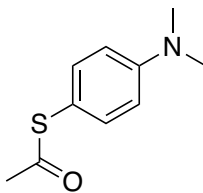
***S*-(4-(Dimethylamino)phenyl)ethanethioate**. Acetyl chloride (0.256 mL, 3.59 mmol) was added dropwise to a stirred solution of 4-(dimethylamino)benzenethiol (0.510 g, 3.33 mmol) and triethylamine (0.500 mL, 3.60 mmol) in dry DCM (16 mL) at 0 °C under nitrogen. The solution was allowed to warm to room temperature and stirring was continued. After 4 h, the reaction mixture was transferred to a separatory funnel, the reaction flask was rinsed with 10 mL DCM and added to separatory funnel, then washed

with NaHCO$_3$ (2 x 15 mL) and cold water (1 x 15 mL). The organic phase was dried with Na$_2$SO$_4$ and then filtered. The remaining organic solvent was removed *in vacuo*. The resulting yellow solid (0.598 g) was used directly in the next step without further purification; mp, 78-80 °C; ^{1}HNMR (CDCl$_3$) δ 2.20 (s, 3H), 2.82 (s, 6H),6.55 (m, 2H), 7.08 (m, 2H) ppm; ^{13}C NMR (CDCl$_3$) δ 29.9, 40.4, 112.9, 135.9, 151.2, 196.7 ppm.
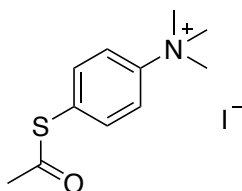
4-(Acetylthio)-*N,N,N*-trimethylbenzenammonium iodide. Methyl iodide (214 μL, 3.44 mmol) was added to a stirred solution of crude *S*-(4-(dimethylamino)phenyl)ethane-thioate (0.598 g, 3.06 mmol) in dry DCM (5 mL) at 0 °C overnight. DCM and unreacted methyl iodide then were removed *in vacuo*. The resultant crude yellow solid was purified by reverse phase column chromatography (C$_{18}$, H$_2$O/MeOH). The MeOH was removed from collected fractions *in vacuo*. The remaining aqueous solution was frozen, then lyophilized to remove H$_2$O *in vacuo* to yield 4-(acetylthio)-*N,N,N*-trimethylbenzen-ammonium iodide (0.619 g, 60%) as a white solid; ^{1}H NMR (CD$_3$CN) δ 2.54 (s, 3H), 3.57 (s, 9H), 7.68 (d, *J* = 8.0 Hz, 2H), 7.8 (d, *J* = 8.0 Hz, 2H) ppm; ^{13}C NMR (CD$_3$CN) δ 40.4, 58.1, 122.2, 129.2, 132.4, 136.8, 193.5 ppm; HRMS calcd for C$_{11}$H$_{16}$NOS$^+$ [M]$^+$ *m/z* 210.0947, found 210.0944.
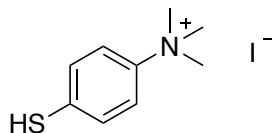
4-Mercapto-*N,N,N*-trimethylbenzenammonium   iodide.   4-(Acetylthio)-*N,N,N*-trimethylbenzenammonium iodide (0.750 g, 2.22 mmol) was added to a stirred solution of conc. HCl (0.85 mL, 10.3 mmol) in MeOH (10 mL). The solution was heated to reflux for 1h. The solution was then allowed to cool and then put on ice and neutralized by slow addition of NaHCO3. The MeOH was removed *in vacuo* and the remaining aqueous solution was frozen, then lyophilized to remove H_2O *in vacuo*. The crude white solid was purified by reverse phase column chromatography (C_{18}, H_2O/MeOH). The MeOH was removed from collected fractions *in vacuo*. The remaining aqueous solution was frozen, then lyophilized to remove H_2O *in vacuo* to yield 4-mercapto-*N,N,N*-trimethylbenzenammonium iodide (MBA, 0.615 g, 94%); mp, 165-167 °C; (lit. 167-168 °C);[1] ^{1}H NMR (DMSO) δ 3.56 (s, 9H), 5.99 (bs, 1H), 7.53 (d, *J* = 8.0 Hz, 2H), 7.82 (d, *J* = 8.0 Hz, 2H) ppm; HRMS calcd for $C_9H_{14}NS^+$ [M]$^+$ *m/z* 168.0842, found 168.0840.

5.2.2 Synthesis of MTA
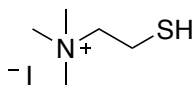
MTA. Acetylthiocholine iodide (0.201 g, 0.695 mmol) was added to a stirred solution of conc. HCl (0.30 mL, 3.63 mmol) in MeOH (3.5 mL). The solution was heated to reflux for 1h. The solution was then allowed to cool, then put on ice and neutralized by slow addition of NaHCO3. The MeOH was removed *in vacuo*. The remaining aqueous solution was frozen, then lyophilized to remove H_2O *in vacuo*. The crude white solid was purified

by reverse phase column chromatography (C_{18}, H_2O/MeOH). The MeOH was removed from collected fractions *in vacuo*. The remaining aqueous solution was frozen, then lyophilized to remove H_2O *in vacuo* to yield 2-mercapto-*N,N,N*-trimethylethan-1-ammonium (MTA, 0.168 g, 98%) a white solid; ^{1}H NMR (DMSO) δ 3.10 (s, 9H), 3.39 (t, *J* = 6.0 Hz, 2H), 3.83 (m, 2H), 5.27 (t, *J* = 6.0 Hz, 1H) ppm; HRMS calcd for $C_5H_{14}NS^+$ [M]$^+$ *m/z* 120.0842, found 120.0844.

5.2.3 Gas-Solution Carbonyl Capture Experimentation
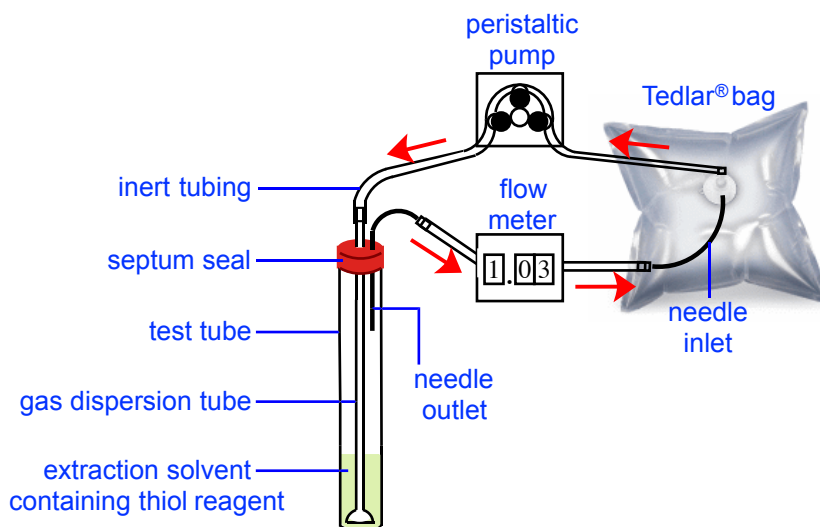
General Protocol for Carbonyl Capture using Bubbler Apparatus. A test tube was charged with a solution of thiol capture reagent (3.5 mM) in *n*-butanol (0.5 mL). To the solution was added ~5 mg of $KHSO_4 \bullet SiO_2$ ($KHSO_4 \bullet SiO_2$ was prepared according to reported synthesis of the analogous $NaHSO_4 \bullet SiO_2$).[2] The tube was then sealed with a rubber septum. A gas dispersion tube and outlet needle were introduced according to the set-up diagram depicted above. A 500 mL Tedlar bag containing inert air spiked with

carbonyl compounds (to mimic a breath sample) was attached by silicone pump tubing to the peristaltic pump. The gas sample was passed through the reaction suspension at a flow rate of roughly 7 mL/min. After one hour and fifteen minutes the pump was stopped, and the reaction suspension was filtered (cotton plug in pipette) and then an aliquot was directly analyzed by HRMS. To the filtrate *N,N,N*-trimethylhexan-1-ammonium iodide was added as an internal reference (IR) (the IR was prepared by Dr. Tirtha Sibakoti).[3] The IR was added in an amount equal to the amount of mmoles of α,β-unsaturated aldehyde used in experiment. The sample was analyzed by HRMS, from the mass spectrum, adduct parent ion signal intensity can be used as a ratio to that of the IR parent ion signal intensity for quantification.

5.3   Experimental Procedures of Chapter 3

5.3.1 Silicon Microreactor Fabrication

Silicon Microreactor Fabrication. All microreactor fabrications were completed in the Micro Nano Technology Center at the University of Louisville by James. D. Morris. The fabrication steps to generate the '3x' silicon microreactor followed the procedure published by the by Fu group at University of Louisville for generation of the '1x' microreactor with the following exceptions.[4] Two modifications were made: (a) microreactor length was increased — this change allowed for a faster flow rate (i.e., faster breath sample evacuation through the microreactor) to minimize breath carbonyl reactions within the Tedlar bag; (b) the micropillar shape was changed from circular columns to triangular pillars, also allowing for better flow through the microreactor.

5.3.2 ATM•OTf
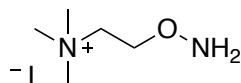
2-(Aminooxy)-*N,N,N*-trimethylethan-1-ammonium iodide. ATM•I was prepared as reported by Biswas *et al.*[5]
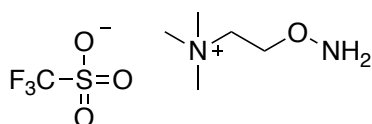
2-(Aminooxy)-*N,N,N*-trimethylethan-1-ammonium trifluoromethanesulfonate. To a stirred solution of ATM•I (0.575 g, 2.34 mmol) dissolved in methanol (11.5 mL) in a 50 mL round bottom flask was added a solution of silver triflate (0.600 g, 2.34 mmol) dissolved in methanol (11.5 mL) under argon at room temperature. A methanol (2 mL) rinse of the silver triflate solution vial was added to the 50 mL round bottom flask. The reaction flask was wrapped with foil to protect from light and the stirring was continued. After 14 h, the grey, off-white precipitate was allowed to settle and then filtered inside an Atmos bag filled with argon using a long-stem fritted glass funnel to remove the AgI precipitate. The filtrate was collected and the methanol was removed *in vacuo* followed by drying the solid under vacuum overnight to afford 2-(aminooxy)-*N,N,N*-trimethylethan-1-ammonium trifluoromethanesulfonate (ATM•OTf, 0.614 g, 98%) as a white powder; ^{1}H NMR (CD$_3$OD) δ 3.19 (s, 9H), 3.62 (m, 2H), 4.07 (m, 2H) ppm; ^{13}C NMR (CD$_3$OD) δ 54.6, 65.6, 70.0 ppm; ^{19}F NMR (CD$_3$OD) 80.3 ppm.

### 5.3.3 Breath Preconcentration and Derivatization

Silicon microreactor loading protocol. 3-(2-Benzothiazolyl)-7-(diethylamino)-coumarin (IR) (2.7 mg, 0.008 mmol) was added to a 250 mL volumetric flask wrapped with foil to protect from light, which then was charged with methanol (220 mL) and stirred for 2h. The stir bar was removed, and methanol (~30 mL) added to fill the flask to its volumetric marking. Finally, the volumetric flask was stoppered, vortexed for 2 minutes then inverted and shaken (x3) to insure uniform mixing. A 333 μL aliquot of the IR solution (1.03 x $10^{-3}\mu$mol) was then added to a stirred solution of ATM•OTf (13.4 mg, 0.050 mmol) in MeOH (667 μL). A 35 μL aliquot of the resultant methanolic IR-ATM solution was subsequently introduced into the silicon microreactor via borosilicated tubing that is affixed to each of the two ports of the microreactor. The microreactor was placed in a vacuum oven at 50 °C and dried overnight under vacuum. The borosilicate glass ends of the microreactor were then capped and sealed in a vacuum seal bag for storage until the microreactor was used for breath preconcentration.

Preconcentration protocol. Breath preconcentration was accomplished by attaching the IR- and ATM•OTf-loaded microreactor to a vacuum pump and setting the flow rate expected through the microreactor to 7 mL/minute. A 1L-Tedlar bag containing a breath sample was connected to microreactor and allowed to evacuate for approximately two hours and twenty-five minutes. The microreactor was then disconnected from the vacuum and Tedlar bag and eluted with 200 μL methanol to collect all ATM-carbonyl adducts and IR.

5.3.4 UV-Vis Absorbance Measurements

UV-Vis spectral collection protocol. The deuterium and tungsten lamps of the Beckman Coulter DU 800 Spectrophotometer were turned on a minimum of thirty minutes before measuring any absorbance data. The sample data are measured using a VWR Cell Quartz 100 μL Z8.5mm cuvette. 100 μL of sample was transferred to quartz cuvette with a pipette. The instrument is reference blanked using LC-grade methanol. The cuvette is rinsed with methanol (x3) between each sample. Samples are subjected to the UV-Vis method described in General Statement.

5.3.5 AMAH•Cl
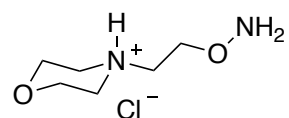
4-(2-Aminooxyethyl)-morpholin-4-ium chloride. AMAH•Cl was prepared as reported by Knipp *et al*.[6]

5.3.6 AMAH Derivatives
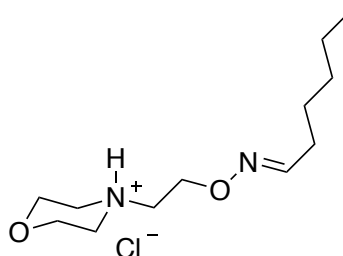
AMAH-hexanal chloride. Hexanal (67 μL, 0.5445 mmol) was added to a 20 mL glass scintillation vial charged with AMAH (82.9 mg, 0.4538 mmol) in methanol (2 mL) under argon. The reaction was stirred overnight, then methanol solvent was removed *in vacuo*. The crude oil was purified by reverse phase column chromatography (C$_{18}$,

H₂O/MeOH). The MeOH was removed from collected fractions *in vacuo*. The remaining aqueous solution was frozen, then lyophilized to remove H_2O *in vacuo* to yield AMAH-hexanal (97.3 mg, 81%) as a mixture of *E*- and *Z*-isomers. Characterization data for the major isomer is given: ¹HNMR (CD₃OD) δ 0.92 (t, 3H), 1.34 (m, 4H), 1.49 (m, 2H), 2.17 (m, 2H), 2.55 (t, 4H), 2.66 (t, 2H), 3.70 (t, 4H), 4.14 (t, 2H), 7.40 (t, 1H) ppm; ¹³CNMR (CD₃OD) δ 14.3, 23.4, 27.4, 30.3, 32.4, 55.1, 58.4, 67.5, 71.4, 152.7 ppm; HRMS calcd for $C_{12}H_{25}N_2O_2^+$ [M+H]⁺ *m/z* 229.1911, found 229.1905.
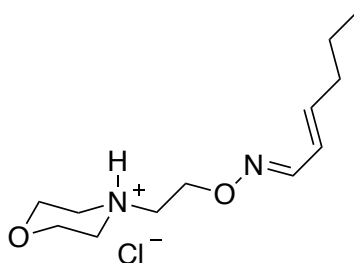
AMAH-2-hexenal chloride. 2-Hexenal (65 μL, 0.5461 mmol) was added to a 20 mL glass scintillation vial charged with AMAH (83.1 mg, 0.4551 mmol) in methanol (2 mL) under argon. The reaction was stirred overnight, then methanol solvent was removed *in vacuo*. The crude oil was purified by reverse phase column chromatography (C₁₈, H₂O/MeOH). The MeOH was removed from collected fractions *in vacuo*. The remaining aqueous solution was frozen, then lyophilized to remove H_2O *in vacuo* to yield AMA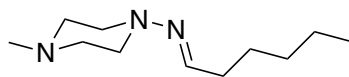H-2-hexenal (94.5 mg, 79%) as a mixture of *E*- and *Z*-isomers. Characterization data for the major isomer is given: ¹HNMR (CD₃OD) δ 0.94 (t, 3H), 1.48 (m, 2H), 2.17 (m, 2H), 2.53 (t, 4H), 2.67 (t, 2H), 3.70 (t, 4H), 4.17 (t, 2H), 6.10 (m, 2H), 7.73 (d, 1H) ppm; ¹³CNMR (CD₃OD) δ 14.0, 23.0, 35.9, 55.1, 58.4, 67.5, 72.0, 125.1, 143.9, 152.1 ppm; HRMS calcd for $C_{12}H_{23}N_2O_2^+$ [M+H]⁺ *m/z* 227.1754, found 227.1749.

5.3.7 AMP Derivatives

AMP-hexanal. Hexanal (67 μL, 0.545 mmol) was added to a 20 mL glass scintillation vial charged with AMP (57.6 mg, 0.500 mmol) in methanol (2 mL) under argon. The reaction was stirred overnight, then the solvent was removed *in vacuo*. The crude oil was purified by normal phase column chromatography (DCM/MeOH). The solvent was removed from collected fractions *in vacuo* to yield AMP-hexanal (87.8 mg, 89%) as a mixture of *E*- and *Z*-isomers. Characterization data for the major isomer is given: ^{1}HNMR (CD$_3$OD) δ 0.92 (t, 3H), 1.35 (m, 4H), 1.50 (m, 2H), 2.24 (m, 2H), 2.32 (s, 3H), 2.61 (t, 4H), 2.97 (t, 4H), 7.06 (t, 1H) ppm; ^{13}CNMR (CD$_3$OD) δ 14.3, 23.5, 28.0, 32.5, 33.7, 45.8, 52.4, 55.3, 145.9 ppm.
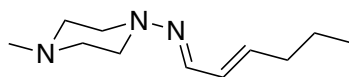

AMP-2-hexenal. 2-Hexenal (65 μL, 0.546 mmol) was added to a 20 mL glass scintillation vial charged with AMP (57.6 mg, 0.500 mmol) in methanol (2 mL) under argon. The reaction was stirred overnight, then methanol solvent was removed *in vacuo*. The crude oil was purified by normal phase column chromatography (DCM/MeOH). The solvent was removed from collected fractions *in vacuo* to yield AMP-2-hexenal (81.1 mg, 83%) as a mixture of *E*- and *Z*-isomers. Characterization data for the major isomer is given: ^{1}HNMR (CD$_3$OD) δ 0.94 (t, 3H), 1.47 (m, 2H), 2.16 (m, 2H), 2.33 (s, 3H), 2.61 (t, 4H), 3.04 (t, 4H), 6.03 (m, 1H), 6.16 (m, 1H), 7.41 (d, 1H) ppm; ^{13}CNMR (CD$_3$OD) δ 14.0, 23.2, 35.8, 45.8, 51.9, 55.2, 129.4, 140.6, 143.0 ppm.

5.3.8 ATM Derivative Panel

$$F_3C-\underset{\underset{O}{\overset{O}{\|}}}{\overset{O^-}{S}}=O \qquad \underset{|}{\overset{|}{N^+}}\diagup\diagdown O\diagup N=$$
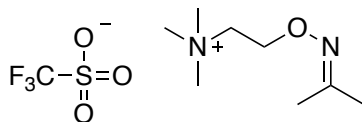
ATM-acetone triflate. Acetone (1 mL, 13.51 mmol) was added to a 20 mL glass scintillation vial charged with ATM (48.7 mg, 0.1815 mmol) under argon. The reaction was stirred overnight, then excess acetone was removed *in vacuo*. The crude oil was purified by reverse phase column chromatography (C_{18}, H_2O/MeOH). The MeOH was removed from collected fractions *in vacuo*. The remaining aqueous solution was frozen, then lyophilized to remove H_2O *in vacuo* to yield ATM-acetone triflate (49.8 mg, 89%); ^{1}H (CD$_3$OD) NMR (CD$_3$OD) δ 1.89 (s, 6H), 3.69 (m, 2H), 4.45 (m, 2H) ppm; ^{13}CNMR (CD$_3$OD) δ 21.8, 54.9, 66.3, 67.9, 158.7 ppm.

$$F_3C-\underset{\underset{O}{\overset{O}{\|}}}{\overset{O^-}{S}}=O \qquad \underset{|}{\overset{|}{N^+}}\diagup\diagdown O\diagup N=$$
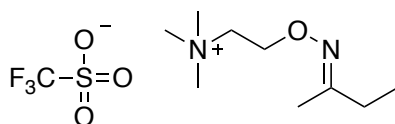
ATM-butan-2-one triflate. Butan-2-one (22.5 μL, 0.2516 mmol) was added to a 20 mL glass scintillation vial charged with ATM•OTf (56.2 mg, 0.210 mmol) in methanol (1 mL) under argon. The reaction was stirred overnight, then the solvent was removed *in vacuo*. The crude oil was purified by reverse phase column chromatography (C_{18}, H_2O/MeOH). The MeOH was removed from collected fractions *in vacuo*. The remaining aqueous solution was frozen, then lyophilized to remove H_2O *in vacuo* to yield ATM-butan-2-one (60.8 mg, 90%); ^{1}H NMR (CD$_3$OD) δ minor isomer: 1.07 (t, *J* = 8.0, 3H), major isomer: 1.10 (d, *J* = 8.0, 3H), major isomer: 1.87 (s, 3H), minor isomer: 1.88 (s, 3H), major

isomer: 2.23 (q, *J* = 7.0 2H), minor isomer: 2.36 (q, *J* = 7.5 2H), 3.20 (s, 9H), 3.69 (m, 2H), 4.46 (m, 2H); ^{13}CNMR (CD$_3$OD) δ 10.3, 14.3, 19.1, 23.5, 54.5, 66.3, 67.9, 162.5 ppm; HRMS calcd for $C_9H_{21}N_2O^+$ [M]$^+$ *m/z* 173.1648, found 173.1646.
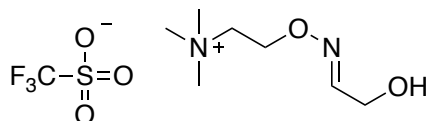
ATM-2-hydroxyacetaldehyde triflate. Glycolaldehyde dimer (23.67 mg, 0.1971 mmol) was added to a 20 mL glass scintillation vial charged with ATM (105.7 mg, 0.3940 mmol) in methanol (2 mL) under argon. The reaction was stirred overnight, then methanol solvent was removed *in vacuo*. The crude oil was purified by reverse phase column chromatography (C$_{18}$, H$_2$O/MeOH). The MeOH was removed from collected fractions *in vacuo*. The remaining aqueous solution was frozen, then lyophilized to remove H$_2$O *in vacuo* to yield ATM-2-hydroxyacetaldehyde (100.3 mg, 82%); ^{1}H (CD$_3$OD) NMR (CD$_3$OD) δ 3.20 (s, 9H), 3.70 (m, 2H), major isomer: 4.16 (d, *J* = 5.5, 2H), minor isomer: 4.35 (d, *J* = 4.0, 2H), 4.51 (m, 2H), minor isomer: 6.95 (t, *J* = 3.5, 1H), major isomer: 7.55 (t, *J* = 5.5, 1H) ppm; ^{13}CNMR (CD$_3$OD) δ 54.6, 60.0, 68.4, 120.5, 153.0 ppm; HRMS calcd for $C_7H_{17}N_2O_2^+$ [M]$^+$ *m/z* 161.1284, found 161.1281.
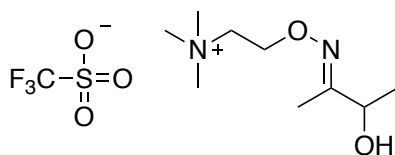
ATM-3-hydroxybutan-2-one. 3-hydroxybutan-2-one (40.4 μL, 0.453 mmol) was added to a 20 mL glass scintillation vial charged with ATM (101.3 mg, 0.378 mmol) in methanol (2

mL) under argon. The reaction was stirred overnight, then methanol solvent was removed *in vacuo*. The crude oil was purified by reverse phase column chromatography (C_{18}, H_2O/MeOH). The MeOH was removed from collected fractions *in vacuo*. The remaining aqueous solution was frozen, then lyophilized to remove H_2O *in vacuo* to yield ATM-3-hydroxybutan-2-one (102 mg, 0.323 mmol, 80%); ^{1}H NMR (CD_3OD) δ minor isomer: 1.25 (d, *J* = 6.5, 3H), major isomer: 1.30 (d, *J* = 6.5, 3H), major isomer: 1.87 (s, 3H), minor isomer: 1.88 (s, 3H), 3.21 (s, 9H), 3.71 (m, 2H), major isomer: 4.30 (q, *J* = 6.5, 1H), minor isomer: 4.98 (q, *J* = 6.5, 1H), 4.49 (m, 2H); ^{13}CNMR (CD_3OD) δ 10.2, 20.7, 54.6, 66.1, 68.2, 69.7, 163.2 ppm; HRMS calcd for $C_9H_{21}N_2O_2^+$ [M]$^+$ *m/z* 189.1598, found 189.1594.
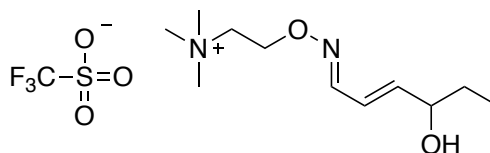
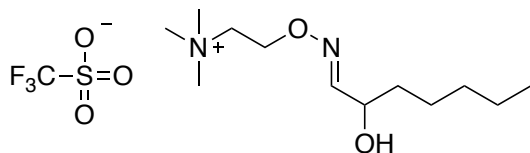**ATM-4-hydroxyhex-2-enal triflate**. 4-hydroxyhex-2-enal (50 mg, 0.44 mmol) was added to a 20 mL glass scintillation vial charged with ATM (141.0 mg, 0.5256 mmol) in methanol (2 mL) under argon. The reaction was stirred overnight, then methanol solvent was removed *in vacuo*. The crude oil was purified by reverse phase column chromatography (C_{18}, H_2O/MeOH). The MeOH was removed from collected fractions *in vacuo*. The remaining aqueous solution was frozen, then lyophilized to remove H_2O *in vacuo* to yield ATM-4-hydroxyhex-2-enal (129.7 mg, 81%); ^{1}H NMR (CD_3OD) δ 0.941 (t, *J* = 5.8 Hz, 3H), 1.57 (m, 2H), 3.20 (s, 9H), 3.71 (m, 2H), 4.12 (m, 1H), major isomer: 4.51 (m, 2H), minor isomer: 4.55 (m, 2H), major isomer: 6.18 (dd, *J* = 5.5, 15.5 Hz, 1H), minor isomer: 6.28 (m, 1H), major isomer: 6.31 (m, 1H), minor isomer: 6.81 (m, 1H), minor isomer: 7.23 (d, *J* = 8.0

Hz, 1H), major isomer: 7.88 (d, J = 8.0 Hz, 1H) ppm; ^{13}CNMR (CD$_3$OD) δ 10.0, 30.8, 54.7, 66.2, 68.6, 73.6, 123.3, 147.1, 153.5 ppm; HRMS calcd for $C_{11}H_{23}N_2O_2^+$ [M]$^+$ *m/z* 215.1754, found 215.1751.

ATM-2-hydroxyheptanal triflate. Selective deprotection of primary silyl ether with HF•pyridine was carried out on 1,2-(di-((*tert*-Butyldimethylsilyl)oxy))heptane as reported by Baker *et al.*[7] The primary alcohol was oxidized to with pyridinium chlorochromate to yield 2-((tert-Butyldimethylsilyl)oxy)heptanal as reported in literature.[8]

2-((*tert*-Butyldimethylsilyl)oxy)heptanal (30.9 g, 0.126 mmol) was added to a 20 mL glass scintillation vial charged with ATM (41.0 mg, 0.153 mmol) in methanol (1 mL) under argon. The reaction was stirred overnight, then methanol solvent was removed *in vacuo*. The crude oil was dissolved in THF (1 mL), cooled to 0 °C. To the stirring cooled solution was added 1 M tetrabutylammonium fluoride solution (130μL). The THF solvent was removed *in vacuo*, and the crude oil purified by reverse phase column chromatography (C$_{18}$, H$_2$O/MeOH). The MeOH was removed from collected fractions *in vacuo*. The remaining aqueous solution was frozen, then lyophilized to remove H$_2$O *in vacuo* to yield ATM-2-hydroxybutanal (33.6 mg, 70%); ^{1}H NMR (CD$_3$OD) δ 0.94 (t, J = 8.0 Hz, 3H), 1.37 (m, 6H), 1.62 (m, 2H), 3.23 (s, 9H), 3.74 (m, 2H), major isomer: 4.17 (m, 1H), minor isomer: 4.73 (m, 1H), 4.53 (m, 2H), minor isomer: 6.82 (d, J = 8.0 Hz, 1H), major isomer: 7.45 (d, J

= 4 Hz, 1H) ppm; ^{13}CNMR (CD$_3$OD) δ 14.3, 23.5, 25.7, 32.7, 36.0, 54.7, 66.0, 68.3, 70.0, 156.0 ppm; HRMS calcd for C$_9$H$_{21}$N$_2$O$_2^+$ [M]$^+$ *m/z* 189.1598, found 189.1594.
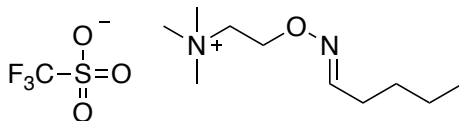
ATM-pentanal triflate. Pentanal (54 μL, 0.50 mmol) was added to a 20 mL glass scintillation vial charged with ATM (111.8 mg, 0.4167 mmol) in methanol (2 mL) under argon. The reaction was stirred overnight, then methanol solvent was removed *in vacuo*. The crude oil was purified by reverse phase column chromatography (C$_{18}$, H$_2$O/MeOH). The MeOH was removed from collected fractions *in vacuo*. The remaining aqueous solution was frozen, then lyophilized to remove H$_2$O *in vacuo* to yield ATM-pentanal (121.9 mg, 87%); ^{1}H NMR (CD$_3$OD) δ 0.94 (t, *J* = 6.0 Hz, 3H), 1.36 (m, 2H), 1.49 (m, 2H), minor isomer: 2.22 (q, *J* = 6.7 Hz, 1H), major isomer: 2.35 (q, *J* = 6.7 Hz, 1H), 3.21 (s, 9H), 3.76 (m, 2H), major isomer: 4.46 (m, 2H), minor isomer: 4.52 (m, 2H), minor isomer: 6.83 (t, *J* = 4.0 Hz, 1H), major isomer: 7.52 (t, *J* = 4.0 Hz, 1H) ppm; ^{13}CNMR (CD$_3$OD) δ 14.1, 23.2, 26.7, 29.6, 54.7, 66.1, 68.0, 155.3 ppm; HRMS calcd for C$_{10}$H$_{23}$N$_2$O$^+$ [M]$^+$ *m/z* 187.1805, found 187.1801.
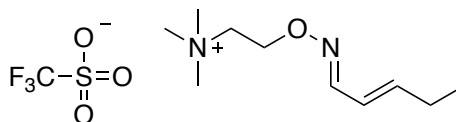

ATM-2-pentenal triflate. 2-Pentenal (52 μL, 0.50 mmol) was added to a 20 mL glass scintillation vial charged with ATM (106 mg, 0.394 mmol) in methanol (2 mL) under argon. The reaction was stirred overnight, then the solvent was removed *in vacuo*. The crude oil

was purified by reverse phase column chromatography (C_{18}, H_2O/MeOH). The MeOH was removed from collected fractions *in vacuo*. The remaining aqueous solution was frozen, then lyophilized to remove H_2O *in vacuo* to yield ATM-2-pentanal (107.9 mg, 82%); ^{1}H NMR (CD$_3$OD) δ 1.06 (t, *J* = 8.0 Hz, 3H), 2.22 (m, 2H), 3.21 (s, 9H), 3.72 (m, 2H), major isomer: 4.49 (m, 2H), minor isomer: 4.54 (m, 2H), major isomer: 6.24 (m, 1H), minor isomer: 6.34 (m, 1H), major isomer: 6.13 (m, 1H), minor isomer: 6.63 (m, 1H), minor isomer: 7.17 (d, *J* = 12.0 Hz, 1H), major isomer: 7.83 (d, *J* = 8.0 Hz, 1H) ppm; ^{13}CNMR (CD$_3$OD) δ 13.1, 26.9, 54.7, 66.1, 68.4, 123.5, 147.1, 153.9 ppm; HRMS calcd for $C_{10}H_{21}N_2O^+$ [M]$^+$ *m/z* 185.1648, found 185.1647.

5.4 Experimental Procedures of Chapter 4

5.4.1 (*2E,4E*)-hexa-2,4-dienedial
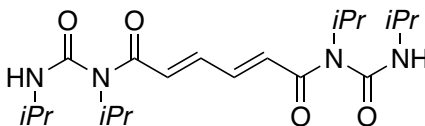
(2*E*,4*E*)-*N*[1],*N*[6]-diisopropyl-*N*[1],*N*[6]-bis(isopropylcarbamoyl)hexa-2,4-dienediamide.

To a stirred suspension of *trans*, *trans*-muconic acid (0.285 g, 2.01 mmol) in dry DCM (10 mL) was added diisopropylcarbodiimide (0.519 g, 4.11 mmol) dropwise. The reaction mixture was gradually warmed to room temperature and stirred overnight. The organic solvent from the resulting clear brown solution was removed *in vacuo*. The pale brown solid was recrystallized in EtOH to yield the title compound (0.666 g, 84%) as a while solid; IR (neat) 3266, 1705, 1635 cm^{-1}; ^{1}H NMR (CDCl$_3$): δ 7.41 (2H, brs), 7.12 (2H, m), 6.36 (2H,

m), 4.48 (2H, m), 4.01 (2H, m), 1.34 (12H, d, J = 4.0Hz), 1.28 (12H, d, J = 4.0Hz) ppm; ^{13}C

NMR (CDCl$_3$) δ 165.0, 153.4, 140.1, 129.2, 47.5, 43.5, 22.5, 20.8 ppm.
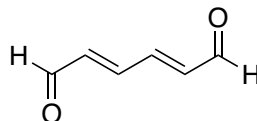
(2*E*, 4*E*)-hexa-2,4-dienedial. To a stirred suspension of *trans*, *trans*-muconic acid

(0.285 g, 2.01 mmol) in dry CH$_2$Cl$_2$ (10 mL) at 0 °C was added diisopropylcarbodiimide

(0.519 g, 4.11 mmol) dropwise. The reaction mixture was gradually warmed to room

temperature and stirred overnight. The resulting clear brown solution was diluted by

addition of CH$_2$Cl$_2$ (10 mL) and then cooled to *ca.* −78 °C. Diisobutylaluminum hydride

(8.14 mL of a 1 M solution in CH$_2$Cl$_2$, 8.14 mmol) was added dropwise over 10 minutes via

syringe. The reaction was stirred 1 hour while maintaining the temperature near −78 °C.

The reaction was quenched by slow addition of acetic acid (0.505 mL, 0.530 g, 8.83 mmol)

via syringe. The solution was diluted with Et$_2$O (60 mL) and added to a stirred solution of

saturated potassium sodium tartrate tetrahydrate (30 mL) and water (30 mL). After

vigorous stirring for 30 min., the organic layer was separated, and the aqueous layer was

extracted with Et$_2$O (45 mL x 3). The combined organic extract was dried (MgSO$_4$), filtered

and concentrated by rotary evaporation. The crude product was purified by silica gel

column chromatography, eluting with 3:7 v/v ethyl acetate:hexane, to afford (2*E*, 4*E*)-

hexa-2,4-dienedial (muconaldehyde, 0.157 g, 71%) as a pale-yellow solid; mp. 120–121

°C, (lit. 120–121 °C)[9]; ^{1}H NMR (DMSO) δ 9.68 (2H, d, J = 7.6 Hz), δ 7.56 (2H, m), δ 6.62 (2H,

m) ppm; ^{13}C NMR (DMSO) δ 194.19, δ 147.82, δ 137.80 ppm.

REFERENCES

R.1   CHAPTER 1 REFERENCES

1.   Bargagli, E.; Olivieri, C.; Bennett, D.; Prasse, A.; Muller-Quernheim, J.; Rottoli, P. Oxidative stress in the pathogenesis of diffuse lung diseases: A review. *Respir. Med.* **2009**, *103*, 1245–1256.

2.   Rahman, T.H., I; Islam, M.M.T.; Shekhar, H.U. Oxidative stress and human health. *J. Avd. Biol. Biotechnol.* **2012**, *3*, 997–1019.

3.   Klaunig, J.E.; Wang, Z.; Pu, X.; Zhou, S. Oxidative stress and oxidative damage in chemical carcinogenesis. *Toxicol. Appl. Pharmacol.* **2011**, *254*, 86–99.

4.   Hauck, A.K.; Bernlohr, D.A. Oxidative stress and lipotoxicity. *J. Lipid Res.* **2016**, *57*, 1976–1986.

5.   Gueraud, F.; Atalay, M.; Bresgen, N.; Cipak, A.; Eckl, P.M.; Huc, L.; Jouanin, I.; Siems, W.; Uchida, K. Chemistry and biochemistry of lipid peroxidation products. *Free Radic. Res.* **2010**, *44*, 1098–1124.

6.   Hakim, M.; Broza, Y.Y.; Barash, O.; Peled, N.; Phillips, M.; Amann, A.; Haick, H. Volatile organic compounds of lung cancer and possible biochemical pathways. *Chem. Rev.* **2012**, *112*, 5949–5966.

7.   Hu, C.; Wang, M.; Han, X. Shotgun lipidomics in substantiating lipid peroxidation in redox biology: Methods and applications. *Redox Biol.* **2017**, *12*, 946–955.

8.   Poli, D.; Goldoni, M.; Corradi, M.; Acampa, O.; Carbognani, P.; Internullo, E.; Casalini, A.; Mutti, A. Determination of aldehydes in exhaled breath of patients with lung cancer by means of on-fiber-derivatization SPME–GC/MS. *J. Chromatogr. B Anal. Technol. Biomed. Life Sci.* **2010**, *878*, 2643–2651.

9.   United States Cancer Statistics Lung Cancer Stat Bite. Available online: https://www.cdc.gov/cancer/uscs/about/stat-bites/stat-bite-lung.htm (accessed on 24 May 2022).

10.   Aberle, D.R.; Adams, A.M.; Berg, C.D.; Black, W.C.; Clapp, J.D.; Fagerstrom, R.M.; Gareen, I.F.; Gatsonis, C.; Marcus, P.M.; Sicks, J.D. Reduced lung-cancer mortality with low-dose computed tomographic screening. *N. Engl. J. Med.* **2011**, *365*, 395–409.

11.   Krilaviciute, A.; Heiss, J.A.; Leja, M.; Kupcinskas, J.; Haick, H.; Brenner, H. Detection of cancer through exhaled breath: A systematic review. *Oncotarget* **2015**, *6*, 38643–38657.

12.   Pauling, L.; Robinson, A.B.; Teranishi, R.; Cary, P. Quantitative analysis of urine vapor and breath by gas-liquid partition chromatography. *Proc. Natl. Acad. Sci. USA* **1971**, *68*, 2374–2376.

13.   Gentile, F.; Arcaro, A.; Pizzimenti, S.; Daga, M.; Cetrangolo, G.P.; Dianzani, C.; Lepore, A.; Graf, M.; Ames, P.R.J.; Barrera, G. DNA damage by lipid peroxidation products: Implications in cancer, inflammation and autoimmunity. *AIMS Genet.* **2017**, *4*, 103–137.

14.   Ratcliffe, N.; Wieczorek, T.; Drabinska, N.; Gould, O.; Osborne, A.; De Lacy Costello, B. A mechanistic study and review of volatile products from peroxidation of

unsaturated fatty acids: An aid to understanding the origins of volatile organic compounds from the human body. *J. Breath Res.* **2020**, *14*, 34001.

15. Van Gossum, A.; Decuyper, J. Breath alkanes as an index of lipid peroxidation. *Eur. Respir. J.* **1989**, *2*, 787–791.

16. Fisher, A.B. Chapter 22—Lung Lipid Composition and Surfactant Biology. In *Comparative Biology of the Normal Lung*, 2nd ed.; Parent, R.A., Ed.; Academic Press: San Diego, CA, USA, 2015; pp. 423–466.

17. Kyle, J.E.; Clair, G.; Bandyopadhyay, G.; Misra, R.S.; Zink, E.M.; Bloodsworth, K.J.; Shukla, A.K.; Du, Y.; Lillis, J.; Myers, J.R.; et al. Cell type-resolved human lung lipidome reveals cellular cooperation in lung function. *Sci. Rep.* **2018**, *8*, 13455.

18. Zemski Berry, K.A.; Murphy, R.C.; Kosmider, B.; Mason, R.J. Lipidomic characterization and localization of phospholipids in the human lung. *J. Lipid Res.* **2017**, *58*, 926–933.

19. Veldhuizen, R.; Nag, K.; Orgeig, S.; Possmayer, F. The role of lipids in pulmonary surfactant. *Biochim. Biophys. Acta* **1998**, *1408*, 90–108.

20. Stachowicz-Kusnierz, A.; Cwiklik, L.; Korchowiec, J.; Rogalska, E.; Korchowiec, B. The impact of lipid oxidation on the functioning of a lung surfactant model. *Phys. Chem. Chem. Phys.* **2018**, *20*, 24968–24978.

21. Schmidt, R.; Meier, U.; Markart, P.; Grimminger, F.; Velcovsky, H.G.; Morr, H.; Seeger, W.; Gunther, A. Altered fatty acid composition of lung surfactant phospholipids in interstitial lung disease. *Am. J. Physiol. Lung Cell. Mol. Physiol.* **2002**, *283*, L1079–L1085.

22. Yin, H.; Xu, L.; Porter, N.A. Free radical lipid peroxidation: Mechanisms and analysis. *Chem. Rev.* **2011**, *111*, 5944–5972.

23. Harlan, W.R., Jr.; Margraf, J.H.; Said, S.I. Pulmonary lipid composition of species with and without surfactant. *Am. J. Physiol.* **1966**, *211*, 855–861.

24. Zhang, M.; He, J.; Li, T.; Hu, H.; Li, X.; Xing, H.; Wang, J.; Yang, F.; Ma, Q.; Liu, B.; et al. Accurate Classification of Non-small Cell Lung Cancer (NSCLC) Pathology and Mapping of EGFR Mutation Spatial Distribution by Ambient Mass Spectrometry Imaging. *Front. Oncol.* **2019**, *9*, 804.

25. Tang, B.; Zhao, J.; Xu, J.-F.; Zhang, X. Tuning the stability of organic radicals: From covalent approaches to non-covalent approaches. *Chem. Sci.* **2020**, *11*, 1192–1204.

26. Tallman, K.A.; Roschek, B., Jr.; Porter, N.A. Factors influencing the autoxidation of fatty acids: Effect of olefin geometry of the nonconjugated diene. *J. Am. Chem. Soc.* **2004**, *126*, 9240–9247.

27. Xu, L.; Davis, T.A.; Porter, N.A. Rate constants for peroxidation of polyunsaturated fatty acids and sterols in solution and in liposomes. *J. Am. Chem. Soc.* **2009**, *131*, 13037–13044.

28. Porter, N.A.; Lehman, L.S.; Weber, B.A.; Smith, K.J. Unified mechanism for polyunsaturated fatty acid autoxidation. Competition of peroxy radical hydrogen atom abstraction, beta-scission, and cyclization. *J. Am. Chem. Soc.* **1981**, *103*, 6447–6455.

29. Yin, H.; Havrilla, C.M.; Gao, L.; Morrow, J.D.; Porter, N.A. Mechanisms for the formation of isoprostane endoperoxides from arachidonic acid. "Dioxetane" intermediate versus beta-fragmentation of peroxyl radicals. *J. Biol. Chem.* **2003**, *278*, 16720–16725.

30. Gu, X.; Zhang, W.; Salomon, R.G. Fe2+ catalyzes vitamin E-induced fragmentation of hydroperoxy and hydroxy endoperoxides that generates gamma-hydroxy alkenals. *J. Am. Chem. Soc.* **2007**, *129*, 6088–6089.

31. Scibior, A.; Kurus, J. Vanadium and Oxidative Stress Markers—In Vivo Model: A Review. *Curr. Med. Chem.* **2019**, *26*, 5456–5500.

32. Jomova, K.; Baros, S.; Valko, M. Redox active metal-induced oxidative stress in biological systems. *Transit. Met. Chem.* **2012**, *37*, 127–134.

33. Aust, S.D.; Morehouse, L.A.; Thomas, C.E. Role of metals in oxygen radical reactions. *J. Free Radic. Biol. Med.* **1985**, *1*, 3–25.

34. Schaich, K.M. Metals and lipid oxidation. Contemporary issues. *Lipids* **1992**, *27*, 209–218.

35. Posner, G.H.; O'Neill, P.M. Knowledge of the proposed chemical mechanism of action and cytochrome p450 metabolism of antimalarial trioxanes like artemisinin allows rational design of new antimalarial peroxides. *Acc. Chem. Res.* **2004**, *37*, 397–404.

36. Vieira, S.A.; Zhang, G.; Decker, E.A. Biological Implications of Lipid Oxidation Products. *J. Am. Oil Chem. Soc.* **2017**, *94*, 339–351.

37. Imai, H.; Nakagawa, Y. Biological significance of phospholipid hydroperoxide glutathione peroxidase (PHGPx, GPx4) in mammalian cells. *Free Radic. Biol. Med.* **2003**, *34*, 145–169.

38. Toppo, S.; Flohe, L.; Ursini, F.; Vanin, S.; Maiorino, M. Catalytic mechanisms and specificities of glutathione peroxidases: Variations of a basic scheme. *Biochim. Biophys. Acta* **2009**, *1790*, 1486–1500.

39. Bui, P.H.; Hsu, E.L.; Hankinson, O. Fatty acid hydroperoxides support cytochrome P450 2S1-mediated bioactivation of benzo[a]pyrene-7,8-dihydrodiol. *Mol. Pharmacol.* **2009**, *76*, 1044–1052.

40. Frankel, E.N.; Neff, W.E. Formation of malonaldehyde from lipid oxidation products. *Biochim. Biophys. Acta* **1983**, *754*, 264–270.

41. Yaremenko, I.A.; Vil, V.A.; Demchuk, D.V.; Terent'ev, A.O. Rearrangements of organic peroxides and related processes. *Beilstein J. Org. Chem.* **2016**, *12*, 1647–1748.

42. Hazen, S.L. Oxidized phospholipids as endogenous pattern recognition ligands in innate immunity. *J. Biol. Chem.* **2008**, *283*, 15527–15531.

43. Loidl-Stahlhofen, A.; Hannemann, K.; Spiteller, G. Generation of α-hydroxyaldehydic compounds in the course of lipid peroxidation. *Biochim. Biophys. Acta* **1994**, *1213*, 140–148.

44. Hölzel, C.; Spiteller, G. Zellschädigung als Ursache für die Bildung von Hydroperoxiden ungesättigter Fettsäuren. *Naturwissenschaften* **1995**, *82*, 452–460.

45. Miakar, A.; Spiteller, G. Reinvestigation of lipid peroxidation of linolenic acid. *Biochim. Biophys. Acta* **1994**, *1214*, 209–220.
46. Kern, W.; Spiteller, G. Synthesis and properties of natural occurring α-hydroxyaldehydes. *Tetrahedron* **1996**, *52*, 4347–4362.
47. Muzio, G.; Ricci, M.; Traverso, N.; Monacelli, F.; Oraldi, M.; Maggiora, M.; Canuto, R.A. 4-Hydroxyhexenal and 4-hydroxynonenal are mediators of the anti-cachectic effect of n-3 and n-6 polyunsaturated fatty acids on human lung cancer cells. *Free Radic. Biol. Med.* **2016**, *99*, 63–70.
48. Vander Jagt, D.L.; Hunsaker, L.A.; Vander Jagt, T.J.; Gomez, M.S.; Gonzales, D.M.; Deck, L.M.; Royer, R.E. Inactivation of glutathione reductase by 4-hydroxynonenal and other endogenous aldehydes. *Biochem. Pharma.* **1997**, *53*, 1133–1140.
49. Uchida, K. 4-Hydroxy-2-nonenal: A product and mediator of oxidative stress. *Prog. Lipid Res.* **2003**, *42*, 318–343.
50. Barrera, G.; Pizzimenti, S.; Ciamporcero, E.S.; Daga, M.; Ullio, C.; Arcaro, A.; Cetrangolo, G.P.; Ferretti, C.; Dianzani, C.; Lepore, A.; et al. Role of 4-hydroxynonenal-protein adducts in human diseases. *Antioxid. Redox Signal.* **2015**, *22*, 1681–1702.
51. Tamura, H.; Kitta, K.; Shibamoto, T. Formation of reactive aldehydes from fatty acids in an iron(2+)/hydrogen peroxide oxidation system. *J. Agric. Food Chem.* **1991**, *39*, 439–442.
52. Kawai, Y.; Takeda, S.; Terao, J. Lipidomic analysis for lipid peroxidation-derived aldehydes using gas chromatography-mass spectrometry. *Chem. Res. Toxicol.* **2007**, *20*, 99–107.
53. Jones, A.W. Measuring and reporting the concentration of acetaldehyde in human breath. *Alcohol Alcohol.* **1995**, *30*, 271–285.
54. Filipiak, W.; Ruzsanyi, V.; Mochalski, P.; Filipiak, A.; Bajtarevic, A.; Ager, C.; Denz, H.; Hilbe, W.; Jamnig, H.; Hackl, M.; et al. Dependence of exhaled breath composition on exogenous factors, smoking habits and exposure to air pollutants. *J. Breath Res.* **2012**, *6*, 36008.
55. Del Rio, D.; Stewart, A.J.; Pellegrini, N. A review of recent studies on malondialdehyde as toxic molecule and biological marker of oxidative stress. *Nutr. Metab. Cardiovasc. Dis.* **2005**, *15*, 316–328.
56. Fu, X.-A.; Li, M.; Knipp, R.J.; Nantz, M.H.; Bousamra, M. Noninvasive detection of lung cancer using exhaled breath. *Cancer Med.* **2014**, *3*, 174–181.
57. Anderson, M.M.; Hazen, S.L.; Hsu, F.F.; Heinecke, J.W. Human neutrophils employ the myeloperoxidase-hydrogen peroxide-chloride system to convert hydroxy-amino acids into glycolaldehyde, 2-hydroxypropanal, and acrolein. A mechanism for the generation of highly reactive alpha-hydroxy and alpha,beta-unsaturated aldehydes by phagocytes at sites of inflammation. *J. Clin. Investig.* **1997**, *99*, 424–432.
58. Lorenzi, R.; Andrades, M.E.; Bortolin, R.C.; Nagai, R.; Dal-Pizzol, F.; Moreira, J.C.F. Circulating glycolaldehyde induces oxidative damage in the kidney of rats. *Diabetes Res. Clin. Pract.* **2010**, *89*, 262–267.

59. O'Neill, H.J.; Gordon, S.M.; O'Neill, M.H.; Gibbons, R.D.; Szidon, J.P. A computerized classification technique for screening for the presence of breath biomarkers in lung cancer. *Clin. Chem.* **1988**, *34*, 1613–1618.

60. Phillips, M.; Gleeson, K.; Hughes, J.M.B.; Greenberg, J.; Cataneo, R.N.; Baker, L.; McVay, W.P. Volatile organic compounds in breath as markers of lung cancer: A cross-sectional study. *Lancet* **1999**, *353*, 1930–1933.

61. Deng, C.; Zhang, X.; Li, N. Investigation of volatile biomarkers in lung cancer blood using solid-phase microextraction and capillary gas chromatography-mass spectrometry. *J. Chromatogr. B* **2004**, *808*, 269–277.

62. Chen, X.; Cao, M.; Hao, Y.; Li, Y.; Wang, P.; Ying, K.; Pan, H. A Non-invasive detection of lung cancer combined virtual gas sensors array with imaging recognition technique. *Conf. Proc. IEEE Eng. Med. Biol. Soc.* **2005**, *2005*, 5873–5876.

63. Chen, X.; Xu, F.; Wang, Y.; Pan, Y.; Lu, D.; Wang, P.; Ying, K.; Chen, E.; Zhang, W. A study of the volatile organic compounds exhaled by lung cancer cells in vitro for breath diagnosis. *Cancer* **2007**, *110*, 835–844.

64. Bajtarevic, A.; Ager, C.; Pienz, M.; Klieber, M.; Schwarz, K.; Ligor, M.; Ligor, T.; Filipiak, W.; Denz, H.; Fiegl, M.; et al. Noninvasive detection of lung cancer by analysis of exhaled breath. *BMC Cancer* **2009**, *9*, 348.

65. Gaspar, E.M.; Lucena, A.F.; Duro da Costa, J.; Chaves das Neves, H. Organic metabolites in exhaled human breath--a multivariate approach for identification of biomarkers in lung disorders. *J. Chromatogr. A* **2009**, *1216*, 2749–2756.

66. Ligor, M.; Ligor, T.; Bajtarevic, A.; Ager, C.; Pienz, M.; Klieber, M.; Denz, H.; Fiegl, M.; Hilbe, W.; Weiss, W.; et al. Determination of volatile organic compounds in exhaled breath of patients with lung cancer using solid phase microextraction and gas chromatography mass spectrometry. *Clin. Chem. Lab. Med.* **2009**, *47*, 550–560.

67. Fuchs, P.; Loeseken, C.; Schubert, J.K.; Miekisch, W. Breath gas aldehydes as biomarkers of lung cancer. *Int. J. Cancer* **2010**, *126*, 2663–2670.

68. Kischkel, S.; Miekisch, W.; Sawacki, A.; Straker, E.M.; Trefz, P.; Amann, A.; Schubert, J.K. Breath biomarkers for lung cancer detection and assessment of smoking related effects--confounding variables, influence of normalization and statistical algorithms. *Clin. Chim. Acta* **2010**, *411*, 1637–1644.

69. Rudnicka, J.; Kowalkowski, T.; Ligor, T.; Buszewski, B. Determination of volatile organic compounds as biomarkers of lung cancer by SPME-GC-TOF/MS and chemometrics. *J. Chromatogr. B* **2011**, *879*, 3360–3366.

70. Ulanowska, A.; Kowalkowski, T.; Trawinska, E.; Buszewski, B. The application of statistical methods using VOCs to identify patients with lung cancer. *J. Breath Res.* **2011**, *5*, 46008.

71. Buszewski, B.; Ulanowska, A.; Kowalkowski, T.; Cieslinski, K. Investigation of lung cancer biomarkers by hyphenated separation techniques and chemometrics. *Clin. Chem. Lab. Med.* **2011**, *50*, 573–581.

72. Buszewski, B.; Ligor, T.; Jezierski, T.; Wenda-Piesik, A.; Walczak, M.; Rudnicka, J. Identification of volatile lung cancer markers by gas chromatography-mass

spectrometry: Comparison with discrimination by canines. *Anal. Bioanal. Chem.* **2012**, *404*, 141–146.

73. Peled, N.; Hakim, M.; Bunn, P.A., Jr.; Miller, Y.E.; Kennedy, T.C.; Mattei, J.; Mitchell, J.D.; Hirsch, F.R.; Haick, H. Non-invasive breath analysis of pulmonary nodules. *J. Thorac. Oncol.* **2012**, *7*, 1528–1533.

74. Bousamra, M., 2nd; Schumer, E.; Li, M.; Knipp, R.J.; Nantz, M.H.; van Berkel, V.; Fu, X.A. Quantitative analysis of exhaled carbonyl compounds distinguishes benign from malignant pulmonary disease. *J. Thorac. Cardiovasc. Surg.* **2014**, *148*, 1074–1080; discussion 1080-1071.

75. Filipiak, W.; Filipiak, A.; Sponring, A.; Schmid, T.; Zelger, B.; Ager, C.; Klodzinska, E.; Denz, H.; Pizzini, A.; Lucciarini, P.; et al. Comparative analyses of volatile organic compounds (VOCs) from patients, tumors and transformed cell lines for the validation of lung cancer-derived breath markers. *J. Breath Res.* **2014**, *8*, 27111.

76. Handa, H.; Usuba, A.; Maddula, S.; Baumbach, J.I.; Mineshita, M.; Miyazawa, T. Exhaled breath analysis for lung cancer detection using ion mobility spectrometry. *PLoS ONE* **2014**, *9*, e114555.

77. Rudnicka, J.; Walczak, M.; Kowalkowski, T.; Jezierski, T.; Buszewski, B. Determination of volatile organic compounds as potential markers of lung cancer by gas chromatography–mass spectrometry versus trained dogs. *Sens. Actuators B Chem.* **2014**, *202*, 615–621.

78. Corradi, M.; Poli, D.; Banda, I.; Bonini, S.; Mozzoni, P.; Pinelli, S.; Alinovi, R.; Andreoli, R.; Ampollini, L.; Casalini, A.; et al. Exhaled breath analysis in suspected cases of non-small-cell lung cancer: A cross-sectional study. *J. Breath Res.* **2015**, *9*, 27101.

79. Li, M.; Yang, D.; Brock, G.; Knipp, R.J.; Bousamra, M.; Nantz, M.H.; Fu, X.A. Breath carbonyl compounds as biomarkers of lung cancer. *Lung Cancer* **2015**, *90*, 92–97.

80. Ligor, T.; Pater, Ł.; Buszewski, B. Application of an artificial neural network model for selection of potential lung cancer biomarkers. *J. Breath Res.* **2015**, *9*, 27106.

81. Schumer, E.M.; Trivedi, J.R.; van Berkel, V.; Black, M.C.; Li, M.; Fu, X.-A.; Bousamra, M. High sensitivity for lung cancer detection using analysis of exhaled carbonyl compounds. *J. Thorac. Cardiovasc. Surg.* **2015**, *150*, 1517–1524.

82. Feinberg, T.; Alkoby-Meshulam, L.; Herbig, J.; Cancilla, J.C.; Torrecilla, J.S.; Gai Mor, N.; Bar, J.; Ilouze, M.; Haick, H.; Peled, N. Cancerous glucose metabolism in lung cancer-evidence from exhaled breath analysis. *J. Breath Res.* **2016**, *10*, 26012.

83. Schallschmidt, K.; Becker, R.; Jung, C.; Bremser, W.; Walles, T.; Neudecker, J.; Leschber, G.; Frese, S.; Nehls, I. Comparison of volatile organic compounds from lung cancer patients and healthy controls-challenges and limitations of an observational study. *J. Breath Res.* **2016**, *10*, 46007.

84. Schumer, E.M.; Black, M.C.; Bousamra, M., II; Trivedi, J.R.; Li, M.; Fu, X.-A.; van Berkel, V. Normalization of Exhaled Carbonyl Compounds After Lung Cancer Resection. *Ann. Thorac. Surg.* **2016**, *102*, 1095–1100.

85. Shehada, N.; Cancilla, J.C.; Torrecilla, J.S.; Pariente, E.S.; Bronstrup, G.; Christiansen, S.; Johnson, D.W.; Leja, M.; Davies, M.P.; Liran, O.; et al. Silicon

Nanowire Sensors Enable Diagnosis of Patients via Exhaled Breath. *ACS Nano* **2016**, *10*, 7047–7057.

86. Callol-Sanchez, L.; Munoz-Lucas, M.A.; Gomez-Martin, O.; Maldonado-Sanz, J.A.; Civera-Tejuca, C.; Gutierrez-Ortega, C.; Rodriguez-Trigo, G.; Jareno-Esteban, J. Observation of nonanoic acid and aldehydes in exhaled breath of patients with lung cancer. *J. Breath Res.* **2017**, *11*, 26004.

87. Jouyban, A.; Djozan, D.; Mohammadandashti, P.; Alizadeh-Nabil, A.; Ghorbanpour, H.; Khoubnasabjafari, M.; Mohammadzadeh, M. Co-liquefaction with acetone and GC analysis of volatile compounds in exhaled breath as lung cancer biomarkers. *Bioimpacts* **2017**, *7*, 99–108.

88. Sakumura, Y.; Koyama, Y.; Tokutake, H.; Hida, T.; Sato, K.; Itoh, T.; Akamatsu, T.; Shin, W. Diagnosis by Volatile Organic Compounds in Exhaled Breath from Lung Cancer Patients Using Support Vector Machine Algorithm. *Sensors* **2017**, *17*, 287.

89. Wang, M.; Sheng, J.; Wu, Q.; Zou, Y.; Hu, Y.; Ying, K.; Wan, H.; Wang, P. Confounding effect of benign pulmonary diseases in selecting volatile organic compounds as markers of lung cancer. *J. Breath Res.* **2018**, *12*, 46013.

90. Rudnicka, J.; Kowalkowski, T.; Buszewski, B. Searching for selected VOCs in human breath samples as potential markers of lung cancer. *Lung Cancer* **2019**, *135*, 123–129.

91. Koureas, M.; Kirgou, P.; Amoutzias, G.; Hadjichristodoulou, C.; Gourgoulianis, K.; Tsakalof, A. Target Analysis of Volatile Organic Compounds in Exhaled Breath for Lung Cancer Discrimination from Other Pulmonary Diseases and Healthy Persons. *Metabolites* **2020**, *10*, 317.

92. Muñoz-Lucas, M.Á.; Jareño-Esteban, J.; Gutiérrez-Ortega, C.; López-Guijarro, P.; Collado-Yurrita, L.; Quintana-Díaz, M.; Callol-Sánchez, L. Influence of Chronic Obstructive Pulmonary Disease on Volatile Organic Compounds in Patients with Non-Small Cell Lung Cancer. *Arch. Bronconeumol.* **2020**, *56*, 801–805.

93. Chen, X.; Muhammad, K.G.; Madeeha, C.; Fu, W.; Xu, L.; Hu, Y.; Liu, J.; Ying, K.; Chen, L.; Yurievna, G.O. Calculated indices of volatile organic compounds (VOCs) in exhalation for lung cancer screening and early detection. *Lung Cancer* **2021**, *154*, 197–205.

94. Gashimova, E.; Osipova, A.; Temerdashev, A.; Porkhanov, V.; Polyakov, I.; Perunov, D.; Dmitrieva, E. Exhaled breath analysis using GC-MS and an electronic nose for lung cancer diagnostics. *Anal. Methods* **2021**, *13*, 4793–4804.

95. Li, Z.; Li, Y.; Zhan, L.; Meng, L.; Huang, X.; Wang, T.; Li, Y.; Nie, Z. Point-of-Care Test Paper for Exhaled Breath Aldehyde Analysis via Mass Spectrometry. *Anal. Chem.* **2021**, *93*, 9158–9165.

96. Long, Y.; Wang, C.; Wang, T.; Li, W.; Dai, W.; Xie, S.; Tian, Y.; Liu, M.; Liu, Y.; Peng, X.; et al. High performance exhaled breath biomarkers for diagnosis of lung cancer and potential biomarkers for classification of lung cancer. *J. Breath Res.* **2021**, *15*, 16017.

97. Zou, Y.; Wang, Y.; Jiang, Z.; Zhou, Y.; Chen, Y.; Hu, Y.; Jiang, G.; Xie, D. Breath profile as composite biomarkers for lung cancer diagnosis. *Lung Cancer* **2021**, *154*, 206–213.

98. Larracy, R.; Phinyomark, A.; Scheme, E. Infrared cavity ring-down spectroscopy for detecting non-small cell lung cancer in exhaled breath. *J. Breath Res.* **2022**, *16*, 26008.

99. Soufi, G.; Bagheri, H.; Yeganeh Rad, L.; Minaeian, S. Perylene diimide-POSS network for semi selective solid-phase microextraction of lung cancer biomarkers in exhaled breath. *Anal. Chim. Acta* **2022**, *1198*, 339550.

100. Zou, Y.; Hu, Y.; Jiang, Z.; Chen, Y.; Zhou, Y.; Wang, Z.; Wang, Y.; Jiang, G.; Tan, Z.; Hu, F. Exhaled metabolic markers and relevant dysregulated pathways of lung cancer: A pilot study. *Ann. Med.* **2022**, *54*, 790–802.

101. Schmidt, K.; Podmore, I. Current Challenges in Volatile Organic Compounds Analysis as Potential Biomarkers of Cancer. *J. Biomark.* **2015**, *2015*, 981458.

102. Brunton, N.P.; Cronin, D.A.; Monahan, F.J.; Durcan, R. A comparison of solid phase microextraction (SPME) fibers for measurement of hexanal and pentanal in cooked turkey. *Food Chem.* **2000**, *68*, 339–345.

103. Rösch, C.; Kohajda, T.; Röder, S.; Bergen, M.v.; Schlink, U. Relationship between sources and patterns of VOCs in indoor air. *Atmos. Pollut. Res.* **2014**, *5*, 129–137.

104. Li, M.; Li, Q.; Nantz, M.H.; Fu, X.-A. Analysis of Carbonyl Compounds in Ambient Air by a Microreactor Approach. *ACS Omega* **2018**, *3*, 6764–6769.

105. Fujioka, K.; Shibamoto, T. Determination of toxic carbonyl compounds in cigarette smoke. *Environ. Toxicol.* **2006**, *21*, 47–54.

106. Shahidi, F. Headspace volatile aldehydes as indicators of lipid oxidation in foods. *Adv. Exp. Med. Biol.* **2001**, *488*, 113–123.

107. Magnusson, R.; Nilsson, C.; Andersson, B. Emissions of aldehydes and ketones from a two-stroke engine using ethanol and ethanol-blended gasoline as fuel. *Environ. Sci. Technol.* **2002**, *36*, 1656–1664.

108. Kumar, S.; Nayek, M.; Kumar, A.; Tandon, A.; Mondal, P.; Vijay, P.; Bhangale, U.D.; Tyagi, D. Aldehyde, Ketone and Methane Emissions from Motor Vehicle Exhaust: A Critical Review. *Am. Chem. Sci. J.* **2011**, *1*, 1–27.

109. Cheah, N.P.; Borst, S.; Hendrickx, L.; Cremers, H.; Jansen, E.; Opperhuizen, A.; Talhout, R. Effect of Adding Sugar to Burley Tobacco on the Emission of Aldehydes in Mainstream Tobacco Smoke. *Tob. Regul. Sci.* **2018**, *4*, 61–72.

110. Domínguez, R.; Pateiro, M.; Gagaoua, M.; Barba, F.J.; Zhang, W.; Lorenzo, J.M. A Comprehensive Review on Lipid Oxidation in Meat and Meat Products. *Antioxidants* **2019**, *8*, 429.

111. Fang, J.; Zhang, H.; Yang, N.; Shao, L.; He, P. Gaseous pollutants emitted from a mechanical biological treatment plant for municipal solid waste: Odor assessment and photochemical reactivity. *J. Air Waste Manag. Assoc.* **2013**, *63*, 1287–1297.

112. Daisey, J.M.; Hodgson, A.T.; Fisk, W.J.; Mendell, M.J.; Ten Brinke, J. Volatile organic compounds in twelve California office buildings: Classes, concentrations and sources. *Atmos. Environ.* **1994**, *28*, 3557–3562.

113. Stevens, J.F.; Maier, C.S. Acrolein: Sources, metabolism, and biomolecular interactions relevant to human health and disease. *Mol. Nutr. Food Res.* **2008**, *52*, 7–25.

114. Wilson, V.L.; Foiles, P.G.; Chung, F.L.; Povey, A.C.; Frank, A.A.; Harris, C.C. Detection of acrolein and crotonaldehyde DNA adducts in cultured human cells and canine peripheral blood lymphocytes by 32P-postlabeling and nucleotide chromatography. *Carcinog.* **1991**, *12*, 1483–1490.

115. Siegel, D.A.; Fedewa, S.A.; Henley, S.J.; Pollack, L.A.; Jemal, A. Proportion of Never Smokers Among Men and Women with Lung Cancer in 7 US States. *JAMA Oncol.* **2021**, *7*, 302–304.

116. Long, E.K.; Picklo Sr, M.J. Trans-4-hydroxy-2-hexenal, a product of n-3 fatty acid peroxidation: Make some room HNE. *Free Radic. Biol. Med.* **2010**, *49*, 1–8.

117. Corradi, M.; Folesani, G.; Andreoli, R.; Manini, P.; Bodini, A.; Piacentini, G.; Carraro, S.; Zanconato, S.; Baraldi, E. Aldehydes and glutathione in exhaled breath condensate of children with asthma exacerbation. *Am. J. Respir. Crit. Care Med.* **2003**, *167*, 395–399.

118. Corradi, M.; Rubinstein, I.; Andreoli, R.; Manini, P.; Caglieri, A.; Poli, D.; Alinovi, R.; Mutti, A. Aldehydes in exhaled breath condensate of patients with chronic obstructive pulmonary disease. *Am. J. Respir. Crit. Care Med.* **2003**, *167*, 1380–1386.

119. Antus, B.; Harnasi, G.; Drozdovszky, O.; Barta, I. Monitoring oxidative stress during chronic obstructive pulmonary disease exacerbations using malondialdehyde. *Respirology* **2014**, *19*, 74–79. https://doi.org/10.1111/resp.12155.

120. Corradi, M.; Pignatti, P.; Manini, P.; Andreoli, R.; Goldoni, M.; Poppa, M.; Moscato, G.; Balbi, B.; Mutti, A. Comparison between exhaled and sputum oxidative stress biomarkers in chronic airway inflammation. *Eur. Respir. J.* **2004**, *24*, 1011–1017.

121. Bartoli, M.L.; Novelli, F.; Costa, F.; Malagrino, L.; Melosini, L.; Bacci, E.; Cianchetti, S.; Dente, F.L.; Di Franco, A.; Vagaggini, B.; et al. Malondialdehyde in exhaled breath condensate as a marker of oxidative stress in different pulmonary diseases. *Mediat. Inflamm.* **2011**, *2011*, 891752.

122. Casimirri, E.; Stendardo, M.; Bonci, M.; Andreoli, R.; Bottazzi, B.; Leone, R.; Schito, M.; Vaccari, A.; Papi, A.; Contoli, M.; et al. Biomarkers of oxidative-stress and inflammation in exhaled breath condensate from hospital cleaners. *Biomarkers* **2016**, *21*, 115–122.

123. Lee, J.S.; Choi, Y.C.; Shin, J.H.; Lee, J.H.; Lee, Y.; Park, S.Y.; Baek, J.E.; Park, J.D.; Ahn, K.; Yu, I.J. Health surveillance study of workers who manufacture multi-walled carbon nanotubes. *Nanotoxicology* **2015**, *9*, 802–811.

124. Sakhvidi, M.J.; Biabani Ardekani, J.; Firoozichahak, A.; Zavarreza, J.; Hajaghazade, M.; Mostaghaci, M.; Mehrparvar, A.; Barkhordari, A. Exhaled breath malondialdehyde, spirometric results and dust exposure assessment in ceramics production workers. *Int. J. Occup. Med. Environ. Health* **2015**, *28*, 81–89.

125. Pelclova, D.; Zdimal, V.; Kacer, P.; Komarc, M.; Fenclova, Z.; Vlckova, S.; Zikova, N.; Schwarz, J.; Makes, O.; Navratil, T.; et al. Markers of lipid oxidative damage among office workers exposed intermittently to air pollutants including nanoTiO2 particles. *Rev. Environ. Health* **2017**, *32*, 193–200.

126. Gong, J.; Zhu, T.; Kipen, H.; Wang, G.; Hu, M.; Ohman-Strickland, P.; Lu, S.-E.; Zhang, L.; Wang, Y.; Zhu, P.; et al. Malondialdehyde in exhaled breath condensate

and urine as a biomarker of air pollution induced oxidative stress. *J. Expo. Sci. Environ. Epidemiol.* **2013**, *23*, 322–327.

127. Larstad, M.; Ljungkvist, G.; Olin, A.C.; Toren, K. Determination of malondialdehyde in breath condensate by high-performance liquid chromatography with fluorescence detection. *J. Chromatogr. B* **2002**, *766*, 107–114.

128. Manini, P.; Andreoli, R.; Sforza, S.; Dall'Asta, C.; Galaverna, G.; Mutti, A.; Niessen, W.M. Evaluation of Alternate Isotope-Coded Derivatization Assay (AIDA) in the LC-MS/MS analysis of aldehydes in exhaled breath condensate. *J. Chromatogr. B* **2010**, *878*, 2616–2622.

129. Kartavenka, K.; Panuwet, P.; Greenwald, R.; Ehret, K.M.; D'Souza, P.E.; Barr, D.B.; Ryan, P.B. Quantification of malondialdehyde in exhaled breath condensate using pseudo two-dimensional ultra-performance liquid chromatography coupled with single quadrupole mass spectrometry. *J. Chromatogr. B* **2019**, *1105*, 210–216.

130. Jafari, M.; Solhi, E.; Tagi, S.; Hasanzadeh, M.; Jouyban-Gharamaleki, V.; Jouyban, A.; Shadjou, N. Non-invasive quantification of malondialdehyde biomarker in human exhaled breath condensate using self-assembled organic-inorganic nanohybrid: A new platform for early diagnosis of lung disease. *J. Pharm. Biomed. Anal.* **2019**, *164*, 249–257.

131. Andreoli, R.; Manini, P.; Corradi, M.; Mutti, A.; Niessen, W.M.A. Determination of patterns of biologically relevant aldehydes in exhaled breath condensate of healthy subjects by liquid chromatography/atmospheric chemical ionization tandem mass spectrometry. *Rapid Commun. Mass Spectrom.* **2003**, *17*, 637–645.

132. Kozlov, E.M.; Ivanova, E.; Grechko, A.V.; Wu, W.-K.; Starodubova, A.V.; Orekhov, A.N. Involvement of Oxidative Stress and the Innate Immune System in SARS-CoV-2 Infection. *Diseases* **2021**, *9*, 17.

133. Suhail, S.; Zajac, J.; Fossum, C.; Lowater, H.; McCracken, C.; Severson, N.; Laatsch, B.; Narkiewicz-Jodko, A.; Johnson, B.; Liebau, J.; Bhattacharyya, S.; Hati, S. Role of Oxidative Stress on SARS-CoV-2 (COVID-19) Infection: A Review. *Protein J*. **2020**, 39, 644-656.

134. Delgado-Roche, L; Mesta, F. Oxidative Stress as Key Player in Severe Acute Respiratory Syndrome Coronavirus (SARS-CoV) Infection. *Arch. Med. Res*. **2020**, 51, 384-387.

R.2   CHAPTER 2 REFERENCES

1. Atreja, A.; Fu, A. Z.; Sanaka, M. R.; Vargo, J.J. Non-invasive Testing for *Helicobacter pylori* in Patients Hospitalized with Peptic Ulcer Hemorrhage: A Cost-Effectiveness Analysis. *Dig. Dis. Sci.* **2010,** *55*, 1356-1363.
2. Robroeks, C.M.; van Berkel, J.J.; Jobsis, Q.; van Schooten, F.; Dallinga, J.W.; Wouters, E.F.; Dompeling, E. *Eur. Respir. J.* **2013,** *42*, 98-106.
3. Bharucha, A.E.; Camilleri, M.; Veil, E.; Burton, D.; Zinsmeister, A.R. *Neurogastroenterol Motil.* **2013,** 25, 60-69.
4. Hanna, G.B.; Boshier, P.R.; Markar, S.R.; Romano, A. Accuracy and Methodologic Challenges of Volatile Organic Compound-Based Exhaled Breath Tests for Cancer Diagnosis. *JAMA Oncol.* **2019,** *5*(1), e182815.
5. Aberle D.R.; Adams A.M.; Berg C.D.; Black W.C.; Clapp J.D.; Fagestrom R.M.; Gareen I.F.; Gatsonis C.; Marcus P.M.; Sicks J.D. Reduced Lung-Cancer Mortality with Low-Dose Computed Tomographic Screening. *N. Engl. J. Med.* **2011,** *365*, 395-409.
6. American Cancer Society. https://www.cancer.org/cancer/lung-cancer.html (accessed September 3, 2019).
7. Jia, Z.; Patra, A.; Kutty, V. K.; Venkatesan, T. Critical Review of Volatile Organic Compound Analysis in Breath and In Vitro Cell Culture for Detection of Lung Cancer. *Metabolites* **2019,** 9, 52.
8. Reuter, S.; Gupta, S.C.; Chaturvedi, M.M.; Aggarwal, B.B. Oxidative stress, inflammation, and cancer: how are they linked? *Free Radic Biol Med.* **2010,** *49,* 1603-1616.
9. Barrera, G. Oxidative stress and lipid peroxidation products in cancer progression and therapy. *ISRN Oncology.* **2012,** 2012, 137289.
10. Van der Paal, J.; Neyts, E.C.; Verlackt, C.C.W.; Bogaerts, A. Effect of lipid peroxidation on membrane permeability of cancer and normal cells subjected to oxidative stress. *Chem Sci.* **2016,** 7, 489-498.
11. Khyshiktuev, B.S.; Aganova, I.; Zhilin, I.V. Fatty acid composition of lipids in lung tissue of patients with cancer. *Vopr Onkol.* **2000,** 46, 50-53.
12. Ayala, A.; Munoz, M.F.; Arguelles, S. Lipid Peroxidation: Production, Metabolism, and Signaling Mechanisms of Malondialdehyde and 4-Hydroxy-2-Nonenal. *Oxid Med Cell Longev.* **2014,** 2014, 1-32.
13. Cejas, P.; Casado, E.; Iniesta, C.B.; Castro, J.; Espinosa, E.; Redondo, A.; Sereno, M.; Cabezas, M.A.G.; Vara, J.A.F; Caceres, A.D.; Perona, R.; Baron, M.G. Implications of Oxidative Stress and Cell Membrane Lipid Peroxidation in Human Cancer (Spain). *Cancer Causes Control.* **2004,** 15, 707-719.
14. Hauck, A.K.; Bernlohr, D.A. Oxidative stress and lipotoxicity. *J Lipid Res.* **2016,** 57, 1976-1986.
15. Hakim, M.; Broza, Y.Y.; Barash, O.; Peled, N.; Phillips, M.; Amann, A.; Haick, H. Volatile Organic Compounds of Lung Cancer and Possible Biochemical Pathways. *Chem Rev.* **2012,** 112, 5949-5966.

16. Etsuo, N. Biomarkers of lipid peroxidation in clinical material. *Biochim Biophys Acta.* **2014,** 1840, 809-817.
17. Haick, H.; Broza, Y.Y.; Mochalski, P.; Ruzsanyi, V.; Amann, A. Assessment, origin, and implementation of breath volatile cancer markers. *Chem Soc Rev.* **2014,** 43, 1423-1449.
18. Fu, X.; Li, M.; Knipp. R.J.; Nantz, M.H.; Bousamra, M. Noninvasive detection of lung cancer using exhaled breath. *Cancer Med.* **2014,** 5, 174-181.
19. Bousamra, M.; Schumer, E.; Li, M.; Knipp, R.J.; Nantz, M.H.; van Berkel, V.; Fu, X. Quantitative Analysis of Exhaled Carbonyl Compounds Distinguishes Benign From Malignant Pulmonary Disease. *J Thorac Cardiovasc Surg.* **2014,** 148, 1074-1081.
20. Li, M.; Yang, D.; Brock, G.; Knipp, R.J.; Bousamra, M.; Nantz, M.H.; Fu, X. Breath carbonyl compounds as biomarkers of lung cancer. *Lung Cancer.* **2015,** 90, 92-97.
21. Ogunwale, M.A.; Fu, X.; Nantz, M.H. unpublished results; manuscript in preparation.
22. Nair, D.P.; Podgorski, M.; Chatani, S.; Gong, T.; Xi, W.; Fenoli, C.R.; Bowman, C.N. The Thiol-Michael Addition Click Reaction: A Powerful and Widely Used Tool in Materials Chemistry. *Chem Mater.* **2014,** 26, 724-744.
23. Senter, P.D.; Sievers, E.L. The discovery and development of brentuximab vedotin for use in relapsed Hodgkin lymphoma and systemic anaplastic large cell lymphoma. *Nat Biotechnol.* **2012,** 30, 631-637.
24. Gopal, K.L.; Kumar, R.; Chakraborti, A.K. Catalyst-Free Conjugated Addition of Thiols to α,β-Unsaturated Carbonyl Compounds in Water. *Org Lett.* **2006,** 8, 2433-2436.
25. Lourenco, C.; Turner, C. Breath analysis in disease diagnosis: methodological considerations and applications. *Metabolites.* **2014,** 4, 465-498.
26. In the following article, MBA is named TMT: DePamphilis, B.V.; Averill, B.A.; Herskovitz, T.; Que, L.; Holm, R.H. Synthetic analogs of the active sites of iron-sulfur proteins. VI. Spectral and redox characteristics of the tetranuclear clusters [Fe4S4(SR)4]2-. *J Am Chem Soc.* **1974,** 96, 4159-4167.
27. Mattingly, S.J.; Xu, T.; Nantz, M.H. Higashi, R.M. Fan, T.W.M. A carbonyl capture approach for profiling oxidized metabolites in cell extracts. *Metabolomics* **2012,**8, 989–996.
28. Das, B.; Kumar, A. S.; Ravikanth, B.; Damodar, K.; Krishnaiah, M. Rapid, efficient and selective conjugate addition of thiols to α,β-unsaturated carbonyl compounds using silica supported sodium hydrogen sulfate under solvent-free conditions. *J Sulfur Chem.* **2008,** 29, 489-494.

R.3 CHAPTER 3 REFERENCES

1. Pavia, D.; Lampman, G.M.; Kriz, G.S.; Vyvyan, J.R. Introduction to Spectroscopy. **2015**. Stamford, CT: Cengage Learning.
2. Sidman, J. W. Electronic transitions due to nonbonding electrons carbonyl, aza-aromatic, and other compounds. *Chem. Rev.* **1958**, 58, 689-713.
3. Perkampus, H. H. UV-VIS Spectroscopy and Its Applications. **1992**. Berlin, Germany: Springer.
4. Pauling, L.; Robinson, A.B.; Teranishi, R.; Cary, P. Quantitative Analysis of Urine Vapor and Breath by Gas-Liquid Partition Chromatography. *Proc Nat Acad Sci.* **1971,** 68, 2374-2376.
5. Berna, A. Z.; Odom John, A. R. Breath Metabolites to Diagnose Infection. *Clin. Chem.* **2022**, 68, 43–51. https://doi.org/10.1093/clinchem/hvab218
6. Phillips, M.; Gleeson, K.; Hughes, J.M.B.; Greenberg, J.; Cataneo, R.N.; Barker, L.; McVay, W.P. Volatile Organic Compounds in Breath as Markers of Lung Cancer: A Cross-Sectional Study. *Lancet.* **1999,** 353, 1930-1933.
7. Jia, Z.; Patra, A.; Kutty, V.K.; Venkatesan, T. Critical Review of Volatile Organic Compound Analysis in Breath and In Vitro Cell Culture for Detection of Lung Cancer. *Metabolites.* **2019,** 9, 52.
8. Hanna, G.B.; Boshier, P.R.; Markar, S.R.; Romano, A. Accuracy and Methodologic Challenges of Volatile Organic Compound-Based Exhaled Breath Tests for Cancer Diagnosis: A Systematic Review and Meta-Analysis. *JAMA Oncol.* **2019,** 5(1), e182815.
9. Amann, A.; Miekisch, W.; Schubert, J.; Buszewski, B.; Ligor, T.; Jezierski, T.; Pleil, J.; Risby, T. Analysis of Exhaled Breath for Disease Detection. *Annu Rev Anal Chem.* **2014,** 7, 455-482.
10. Buszewski B.; Kesy M.; Ligor T.; Amann A. Human exhaled air analytics: biomarkers of diseases. *Biomed Chromatogr.* **2007**, 21, 553-566.
11. Miekisch, W.; Schubert, J.K.; Noeldge-Schomburg, G.F.E. Diagnostic Potential of Breath Analysis–Focus on Volatile Organic Compounds. *Clin. Chim. Acta.* **2004**, 347, 25-39.
12. Leemans M.; Bauër P.; Cuzuel V.; Audureau E.; Fromantin I. Volatile Organic Compounds Analysis as a Potential Novel Screening Tool for Breast Cancer: A Systematic Review. *Biomark Insights.* **2022**, 17:11772719221100709.
13. Sutaria, S.R.; Gori, S.S.; Morris, J.D.; Xie, Z.; Fu, X.-A.; Nantz, M.H. Lipid Peroxidation Produces a Diverse Mixture of Saturated and Unsaturated Aldehydes in Exhaled Breath That Can Serve as Biomarkers of Lung Cancer—A Review. *Metabolites.* **2022**, 12, 561.
14. Selvaraj, R.; Vasa, N.J.; Nagendra, S.M.S.; Mizaikoff, B. Advances in Mid-Infrared Spectroscopy-Based Sensing Techniques for Exhaled Breath Diagnostics. *Molecules.* **2020**, *25*, 2227.
15. Ibrahim B.; Marsden P.; Smith J.A.; Custovic A.; Nilsson M.; Fowler S.J. Breath metabolomic profiling by nuclear magnetic resonance spectroscopy in asthma. *Allergy.* **2013**, 68, 1050–1056.

16. Kudo, Y.; Kino, S.; Matsuura, Y. Vacuum Ultraviolet Absorption Spectroscopy Analysis of Breath Acetone Using a Hollow Optical Fiber Gas Cell. *Sensors*. **2021**, 21, 478.

17. Iwata, T.; Katagiri, T.; Matsuura, Y. Real-Time Analysis of Isoprene in Breath by Using Ultraviolet-Absorption Spectroscopy with a Hollow Optical Fiber Gas Cell. *Sensors.* **2016**, *16*, 2058.

18. Fu, X.; Li, M.; Biswas, S.; Nantz, M.H.; Higashi, R.M. A Novel Microreactor Approach for Analysis of Ketones and Aldehydes in Breath. *Analyst.* **2011,** 136,4662-4666.

19. Li, M.; Biswas, S.; Nantz, M.H.; Higashi, R.M.; Fu, X. Preconcentration and Analysis of Trace Volatile Carbonyl Compounds. *Anal Chem.* **2012,** 84, 1288-1293.

20. Li, M.; Biswas, S.; Nantz, M.H.; Higashi, R.M.; Fu, X. A Microfabricated Preconcentration Device for Breath Analysis. *Sens Actuator B-Chem.* **2013,** 180, 130-136.

21. Fu, X.; Li, M.; Knipp. R.J.; Nantz, M.H.; Bousamra, M. Noninvasive Detection of Lung Cancer Using Exhaled Breath. *Cancer Med.* **2014,** 3, 174-181.

22. Bousamra, M.; Schumer, E.; Li, M.; Knipp, R.J.; Nantz, M.H.; van Berkel, V.; Fu, X. Quantitative Analysis of Exhaled Carbonyl Compounds Distinguishes Benign from Malignant Pulmonary Disease. *J Thorac Cardiovasc Surg.* **2014,** 148, 1074-1081.

23. Knipp, R.J.; Li, M.; Fu, X.; Nantz, M.H. A Versatile Probe for Chemoselective Capture and Analysis of Carbonyl Compounds in Exhaled Breath. *Anal Methods.* **2015,** 7, 6027-6033.

24. Li, M.; Yang, D.; Brock, G.; Knipp, R.J.; Bousamra, M.; Nantz, M.H.; Fu, X. Breath Carbonyl Compounds as Biomarkers of Lung Cancer. *Lung Cancer.* **2015,** 90, 92-97.

25. Schumer, E.M.; Trivedi, J.R.; van Berkel, V.; Black, M.C.; Li, M.; Fu, X.-A.; Bousamra, M. High sensitivity for lung cancer detection using analysis of exhaled carbonyl compounds. *J. Thorac. Cardiovasc. Surg.* **2015**, *150*, 1517–1524.

26. MacNee, W. Oxidative stress and lung inflammation in airways disease. *Eur. J. Pharmacol.* **2001**, 429, 195-207.

27. Anderson, J.C. Measuring breath acetone for monitoring fat loss: Review. *Obesity*. **2015**, 23, 2327-2334.

28. Corradi, M.; Poli, D.; Banda, I.; Bonini, S.; Mozzoni, P.; Pinelli, S.; Alinovi, R.; Andreoli, R.; Ampollini, L.; Casalini, A.; et al. Exhaled breath analysis in suspected cases of non-small-cell lung cancer: A cross-sectional study. J. Breath Res. 2015, 9, 027101.

29. Lamers, M. M.; Haagmans, B. L. SARS-CoV-2 pathogenesis. *Nat Rev Microbiol* **2022**, 20, 270–284.

30. Ogunwale, M.A.; Fu, X.; Nantz, M.H. unpublished results; manuscript in preparation.

31. Suhail, S.; Zajac, J.; Fossum, C.; Lowater, H.; McCracken, C.; Severson, N.; Laatsch, B.; Narkiewicz-Jodko, A.; Johnson, B.; Liebau, J.; Bhattacharyya, S.; Hati, S. Role of

Oxidative Stress on SARS-CoV-2 (COVID-19) Infection: A Review. *Protein J*. **2020**, 39, 644-656.

32. Kozlov, E.M.; Ivanova, E.; Grechko, A.V.; Wu, W.-K.; Starodubova, A.V.; Orekhov, A.N. Involvement of Oxidative Stress and the Innate Immune System in SARS-CoV-2 Infection. *Diseases* **2021**, *9*, 17.

33. Delgado-Roche, L.; Mesta, F. Oxidative Stress as Key Player in Severe Acute Respiratory Syndrome Coronavirus (SARS-CoV) Infection. *Arch. Med. Res*. **2020**, 51, 384-387.

34. Centers for Disease Control and Prevention. https://covid.cdc.gov/covid-data-tracker/#variant-proportions (accessed 07/25/2022).

35. Hakim, M.; Broza, Y.Y.; Barash, O.; Peled, N.; Phillips, M.; Amann, A.; Haick, H. Volatile organic compounds of lung cancer and possible biochemical pathways. *Chem. Rev.* **2012**, *112*, 5949–5966.

36. Cornelius M.E.; Loretan C.G.; Wang T.W.; Jamal A.; Homa D.M. Tobacco Product Use Among Adults — United States, 2020. MMWR Morb Mortal Wkly Rep. **2022**, 71, 397–405.

37. Chen, H.; Qi, X.; Zhang, L.; Li, X.; Ma, J.; Zhang, C.; Feng, H.; Yao, M. COVID-19 Screening Using Breath-Borne Volatile Organic Compounds. *J. Breath Res*. **2021**, 15, 047104.

38. Grassin-Delyle, S.; Roquencourt, C.; Moine, P.; Saffroy, G.; Carn, S.; Heming, N.; Fleuriet, J.; Salvator, H.; Naline, E.; Couderc, L.J.; Devillier, P.; Thévenot, E.A.; Annane, D. Metabolomics of Exhaled Breath in Critically Ill COVID-19 Patients: A Pilot Study. *EBioMedicine*. **2021**, 63, 103154.

39. Ruszkiewicz, D.M.; Sanders, D.; O'Brien, R.; Hempel, F.; Reed, M.J.; Riepe, A.C.; Bailie, K.; Brodrick, E.; Darnley, K.; Ellerkmann, R.; Mueller, O.; Skarysz, A.; Truss, M.; Wortelmann, T.; Yordanov, S.; Thomas, C.L.P.; Schaaf, B.; Eddleston, M. Diagnosis of COVID-19 by Analysis of Breath with Gas Chromatography-Ion Mobility Spectrometry – a Feasibility Study. *EClinicalMedicine*. **2020**, 29-30, 100609.

40. Liangou, A.; Tasoglou, A.; Huber, H.J.; Wistrom, C.; Brody, K.; Menon, P.G.; Bebekoski, T.; Menschel, K.; Davidson-Fiedler, M.; DeMarco, K.; Salphale, H.; Wistrom, S.; Lee, R.J. A Method for the Identification of COVID-19 Biomarkers in Human Breath Using Proton Transfer Reaction Time-of-Flight Mass Spectrometry. *EClinicalMedicine*. **2021**, 42, 101207.

R.4   CHAPTER 4 REFERENCES

1.   University of Louisville Superfund Research Center. https://louisville.edu/enviromeinstitute/superfund (accessed 08/13/2022).
2.   Latriano, L.; Goldstein, B.D.; Witz, G. Formation of muconaldehyde, an open-ring metabolite of benzene, in mouse liver microsomes: an additional pathway for toxic metabolites. *Proc. Natl. Acad. Sci.* **1986**, 83, 8356-8360.
3.   Oshiro, Y.; Balwierz, P.S.; Witz, G. Micronucleus formation in mouse bone marrow cells in vivo in response to trans, trans-muconaldehyde. *Toxicol. Lett*. **2001**, 121, 159-166.
4.   Snyder, R. Xenobiotic metabolism and the mechanism(s) of benzene toxicity. *Drug Metab. Rev*. **2004**, 36, 531-547.
5.   Whysner, J.; Reddy, M.V.; Ross, P.M.; Mohan, M. Lax, E.A. Genotoxicity of benzene and its metabolites. *Mutat. Res*. **2004**, 566, 99-130.
6.   Ghigo, G.; Tonachini, G. From Benzene to Muconaldehyde: Theoretical Mechanistic Investigation on Some Tropospheric Oxidation Channels. *J. Am. Chem. Soc*. **1999**, 121, 8366-8372.
7.   Liu, C.; Zhang, X.; Wang, Q.; Shi, K. Role of $PM_{2.5}$ in the photodegradation of the atmospheric benzene. *Environ. Pollution* **2019**, 247, 447-456.
8.   Wang, L.; Wu, R.; Xu, C. Atmospheric Oxidation Mechanism of Benzene. Fates of Alkoxy Radical Intermediates and Revised Mechanism**.** *J. Phys. Chem. A* **2013**, 117, 14163-14168.
9.   Vosburg, D.A.; Weiler, S.; Sorensen, E.J. Concise stereocontrolled routes to fumagillol, fumagillin, and TNP-470**.** *Chirality* **2003**, 15, 156-166.
10.   Märkl, G.; Aschenbrenner, N.; Baur, A.; Rastorfer, C.; Kreitmeier, P. Synthese von Polymethintetrathiafulvalenen durch Dimerisierung von ω-(1,3-Dithiol-2-yliden)polyenalen mit dem *Lawesson*-Reagens: Carotinoide und supracarotinoide Tetrathiafulvalene. *Helv. Chim. Acta* **2003**, 86, 2589-2609.
11.   Craig, G.S.W.; Cohen, R.E.; Schrock, R.R. Esser, A; Schrof, W. Synthesis and Nonlinear Optical Characterization of Spin-Coated Films of Triblock Copolymers Containing Durham Polyacetylene. *Macromolecules* **1995**, 28, 2512-2518.
12.   Epiotis, N.D.; Yates, R.L. Correlation diagrams and the mechanism and stereochemistry of the photochemical Diels-Alder reaction. *J. Org. Chem*. **1949**, 39, 3150-3153.
13.   Karrer, P.; Eugster, C.H.; Perl, S. Isolierung von Thymin und Dimethylsulfon aus Equisettum palustre. *Helv. Chim. Acta.* **1949**, 32, 957-960.
14.   Kossmehl, G.; Bohn, B. Notiz über eine einfache Synthese von Mucondialdehyd. *Chem. Ber.* **1974**, 107, 710-711.
15.   Davies, S.G.; Whitham, G.H. Benzene oxide-oxepin. Oxidation to muconaldehyde. *J. Chem. Soc. Perkin Trans.* **1977**, 1, 1346-1347.
16.   Golding, B.T.; Kennedy G.; Watson, W.P. Simple syntheses of isomers of muconaldehyde and 2-methylmuconaldehyde. *Tetrahedron Lett*. **1988**, 29, 5991-5993.

17. Kurteva, V.B.; Afonso, C.A.M. *J. Molec. Catal.* A study on the intramolecular catalytic aldol cyclodehydration of 3,4-disubstituted 1,6-dialdehydes. *A: Chem.* **2005**, 234, 159-167.

18. Chen, X.; Zhang, Y.; Wan, H.; Wang, W.; Zhang, S. Stereoselective organocatalytic oxidation of alcohols to enals: a homologation method to prepare polyenes. *Chem. Commun*. **2016**, 52, 3532-3535.

19. Murray, M.M.; Kaszynski, P.; Kaisaki, D.A.; Chang, W.; Dougherty, D.A. Prototypes for the Polaronic Ferromagnet. Synthesis and Characterization of High-Spin Organic Polymers. *J. Am. Chem. Soc*., **1994**, 116, 8152-8161.

20. Cha, J.S. *Org.* RECENT DEVELOPMENTS IN THE SYNTHESIS OF ALDEHYDES BY REDUCTION OF CARBOXYLIC ACIDS AND THEIR DERIVATIVES WITH METAL HYDRIDES. A REVIEW. *Prep. Proc. Int*. **1989**, 21, 451-477.

21. Cha, J.S.; Brown, H.C. Exceptionally facile reduction of acid chlorides to aldehydes by sodium tri-tert-butoxyaluminohydride. *J. Org. Chem.* **1993**, 58, 4732-4734.

22. Fujisawa, T.; Mori, T.; Tsuge, S.; Sato, T. Direct and chemoselective conversion of carboxylic acids into aldehydes. *Tetrahedron Lett.* **1983**, 24, 1543-1546.

23. Nahm, S.; Weinreb, S.M. N-methoxy-n-methylamides as effective acylating agents. *Tetrahedron Lett.*, **1981**, 22, 3815-3818.

24. Graham, J.M.; Shireman, B.T.; Maddux, T.M.; Brandstedt, C.M.; Zeller, W.E. DIC-Mediated Coupling of Carboxylic Acids to (4R, 5S)-4-Methyl-5-Phenyl-2-Oxazolidinone, *Synth. Commun.* **2000**, 30, 1221-1226.

25. Bach J.; Blachère, C.; Bull, S.D.; Davies, S.G.; Nicholson, R.L.; Price, P.D.; Sanganee, H.J.; Smith, A.D. N-Acyl-5,5-dimethyloxazolidin-2-ones as latent aldehyde equivalents. *Org. Biomol. Chem.* **2003**, 1, 2001-2010.

26. Anglada, J.M.; Campos, T.; Camps, F.; Moretó, J.M.; Pagès, L. *N,N'*-Cyclization of Carbodiimides with 2-(Bromomethyl)acrylic Acid. A Direct Entry to the System 5-Methylene-6*H*-Pyrimidine-2,4-dione, A New Class of Thymine Analogues. *J. Heterocyclic Chem.* **1996**, 33, 1259-1270.

27. Ramazani, A.; Nasrabadi, F.Z.; Rezaei, A.; Rouhani, M.; Ahankar, H.; Asiabi, P.A.; Joo, S.W.; Ślepokura, K.; Lis, T. Synthesis of N-acylurea derivatives from carboxylic acids and N,N'-dialkyl carbodiimides in water. *J. Chem. Sci*. **2015** 127, 2269-2282.

28. Eyley, S.; Thielemans, W. Surface Modifications of Cellulose Nanocrystals. *Nanoscale* **2014**, 6, 7764-7779.

29. Quyyumi, A.A. Endothelial function in health and disease: new insights into the genesis of cardiovascular disease. *Am. J. Med*. **1998**, 105, 32S-39S.

30. Malovichko, M.V.; Abplanalp, W.T.; McFall, S.A.; Taylor, B.S.; Wickramasinghe, N. S.; Sithu, I. D.; Zelko, I. N.; Uchida, S.; Hill, B.G.; Sutaria, S.R.; Nantz, M.H.; Bhatnagar, A.; Conklin, D. J.; O'Toole, T. E.; Srivastava, S. Subclinical Markers of Cardiovascular Toxicity of Benzene Inhalation in Mice. *Toxicol. Appl. Pharmacol*. **2021**, 431, 115742.

R.5   CHAPTER 5 REFERENCES

1.   Khromov-Borisov, N.V.; Gmiro, V.E.; Magazanik, L.G. Synthesis of medicinal substances with controllable length of action (In the case of curare-like compounds). *Pharm Chem. J.* **1969**, 3**,** 325–330.
2.   Breton, G.W. Selective Monoacetylation of Unsymmetrical Diols Catalyzed by Silica Gel-Supported Sodium Hydrogen Sulfate. *J. Org. Chem.* **1997**, 62, 8952-8952.
3.   Kim, Y.J.; Lek, M. T.; Schramm, M.P. pH Influenced molecular switching with micelle bound cavitands. *Chem. Commun.* **2011**, 47, 9636-9638.
4.   Li, M.; Biswas, S.; Nantz, M.H.; Higashi, R.M.; Fu, X. Preconcentration and Analysis of Trace Volatile Carbonyl Compounds. *Anal Chem.* **2012,** 84, 1288-1293.
5.   Biswas, S.; Huang, X.; Badger, W. R.; Nantz, M.H. Nucleophilic cationization reagents. *Tetrahedron Letters* **2010**, 51, 1727-1729.
6.   Knipp, R.J.; Li, M.; Fu, X.; Nantz, M.H. A Versatile Probe for Chemoselective Capture and Analysis of Carbonyl Compounds in Exhaled Breath. *Anal Methods.* **2015,** 7, 6027-6033.
7.   Baker, R.; Castro, J.L. The Total Synthesis of (+)-Macbecin I. *J. Chem. Soc.* **1990**, 1, 47-65.
8.   Patel, P.; Anumolu, J.R.; Powell, W.S.; Rokach, J. 5-Oxo-15-HETE: Total synthesis and bioactivity, *Bioorg. Med. Chem. Lett*. **2011**, 21, 1857-1860.
9.   Davies, S.G.; Whitham, G.H. Benzene oxide-oxepin. Oxidation to muconaldehyde. *J. Chem. Soc. Perkin Trans.* **1977**, 1, 1346-1347.

APPENDIX A

SPECTRA

A.1 <u>Index of NMR Spectra</u>

Section

133

¹HNMR *S*-(4-(Dimethylamino)phenyl)ethanethioate 400 MHz (CDCl₃)
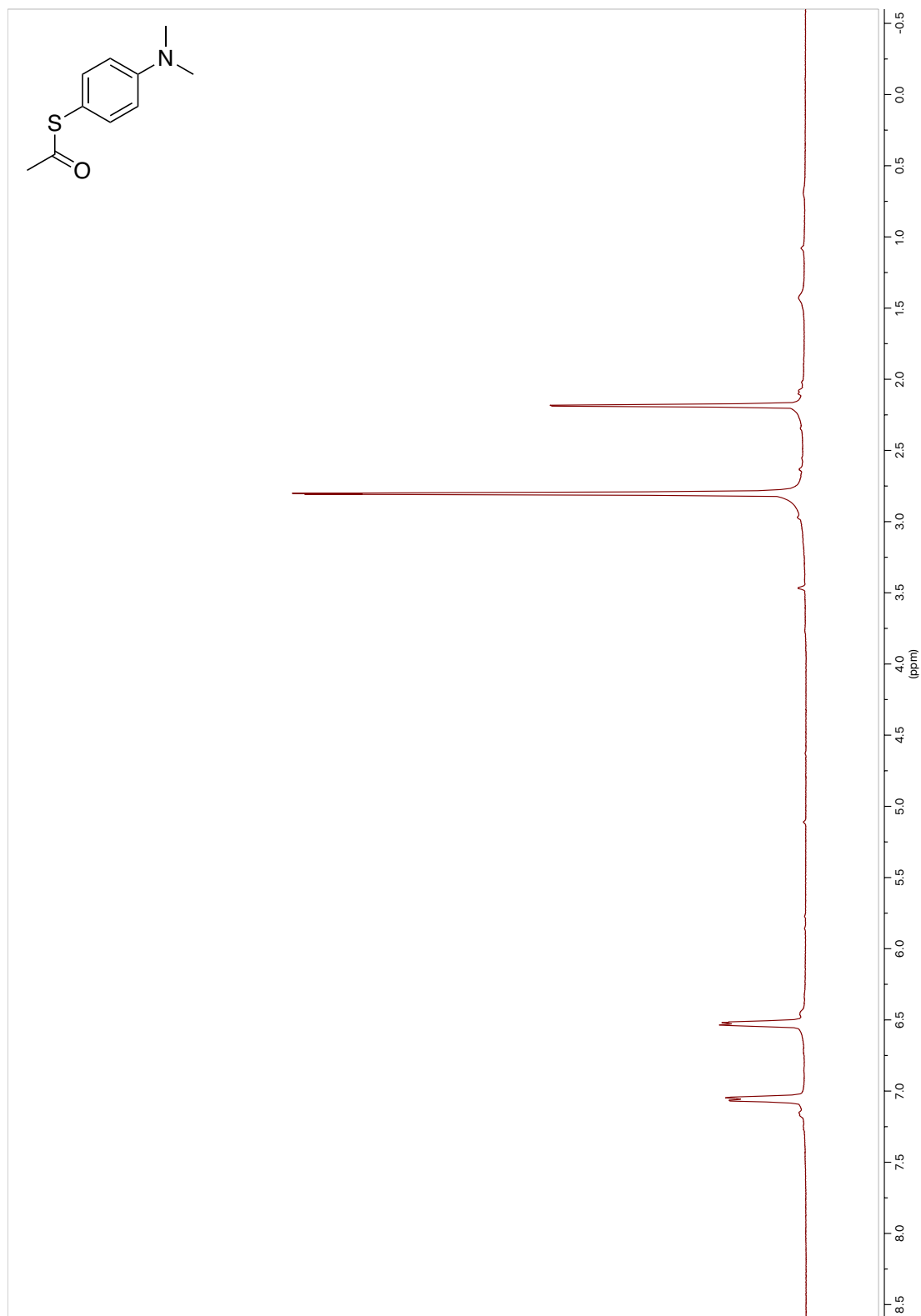
¹³CNMR *S*-(4-(Dimethylamino)phenyl)ethanethioate 100 MHz (CDCl₃)
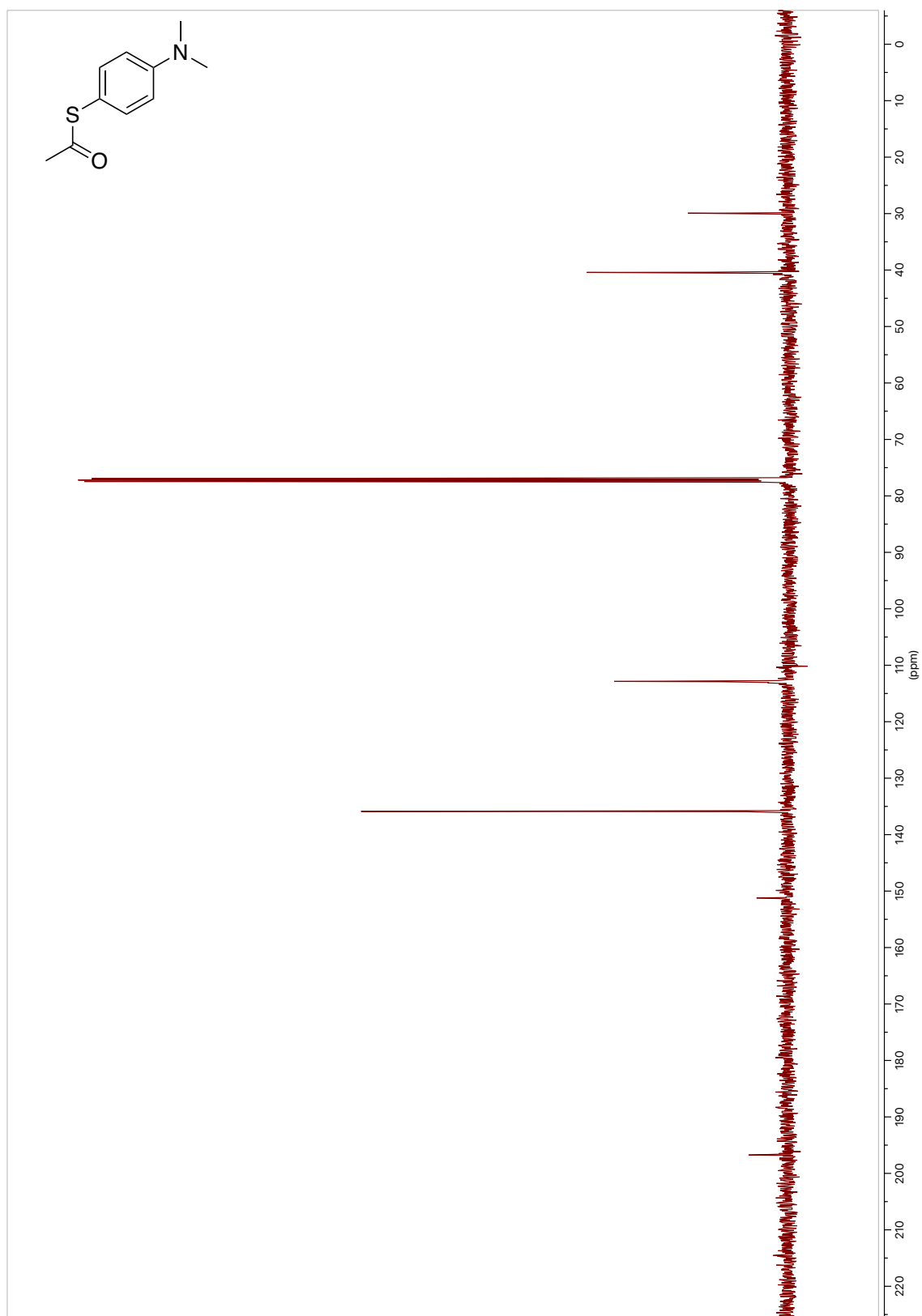
¹H NMR 4-(Acetylthio)-*N,N,N*-trimethylbenzenammonium iodide 400 MHz (CD₃CN)
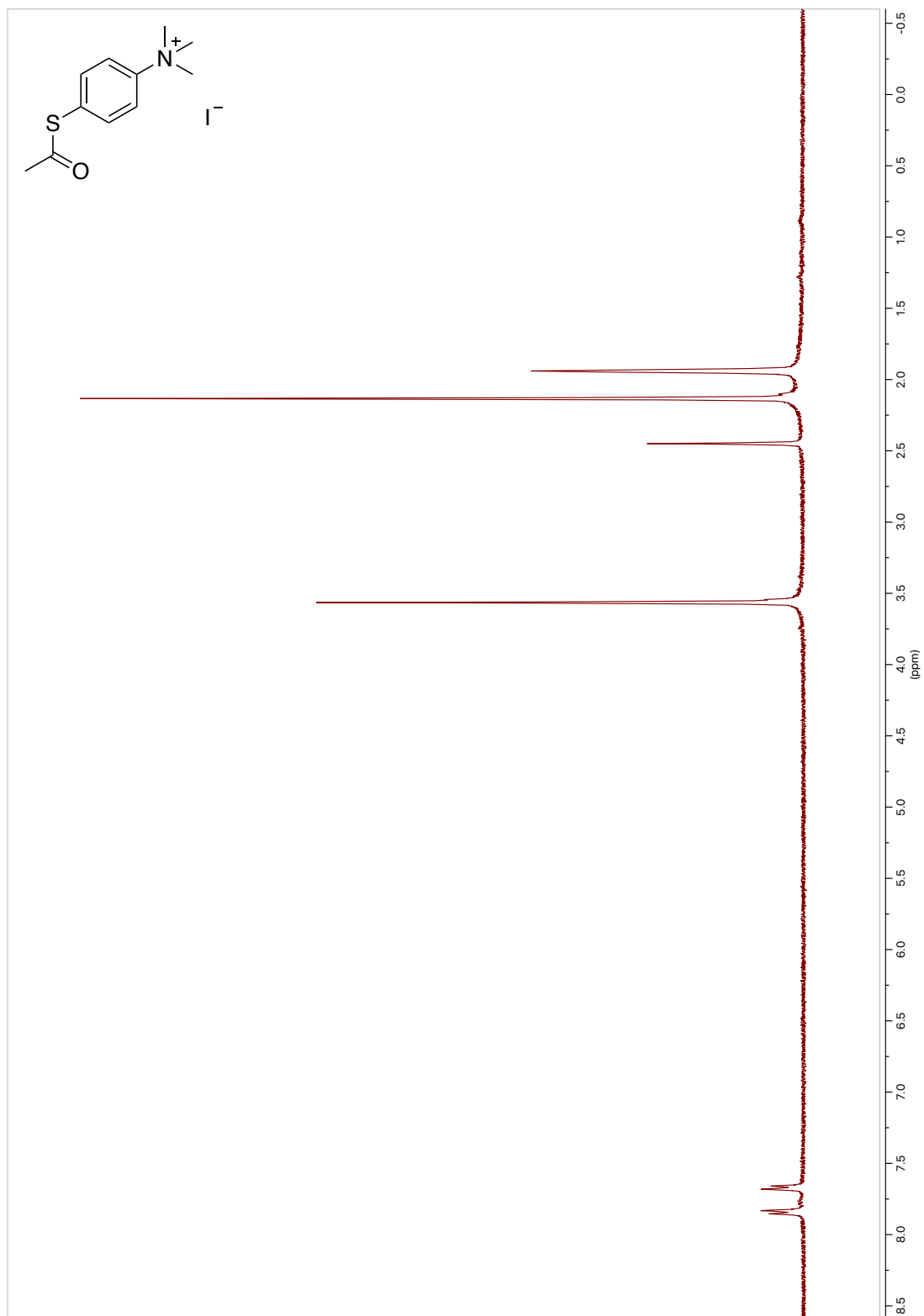
^{13}C NMR 4-(Acetylthio)-*N,N,N*-trimethylbenzenammonium iodide 100 MHz (CD$_3$CN)
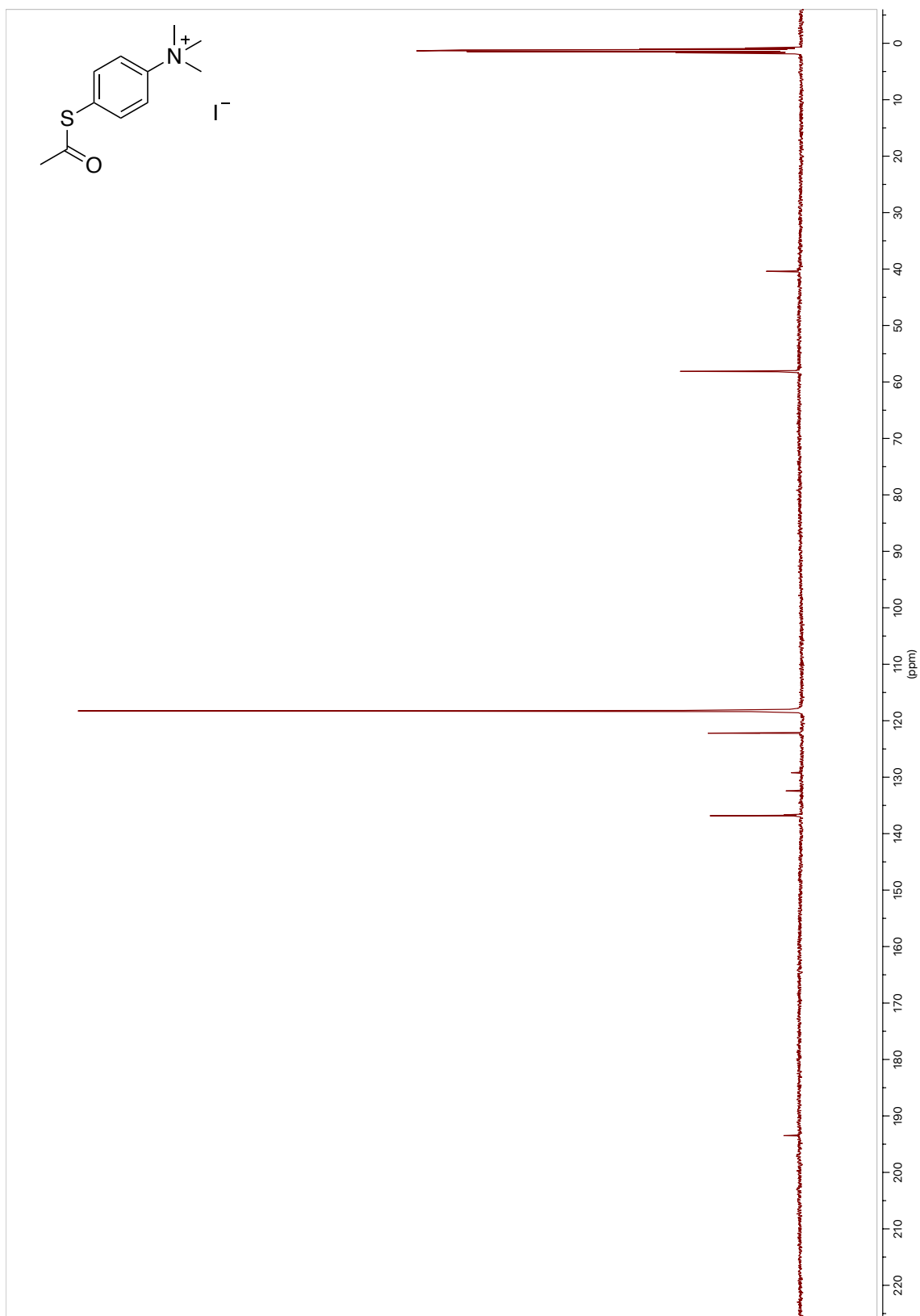
¹H NMR ATM•OTf 400 MHz (CD₃OD)
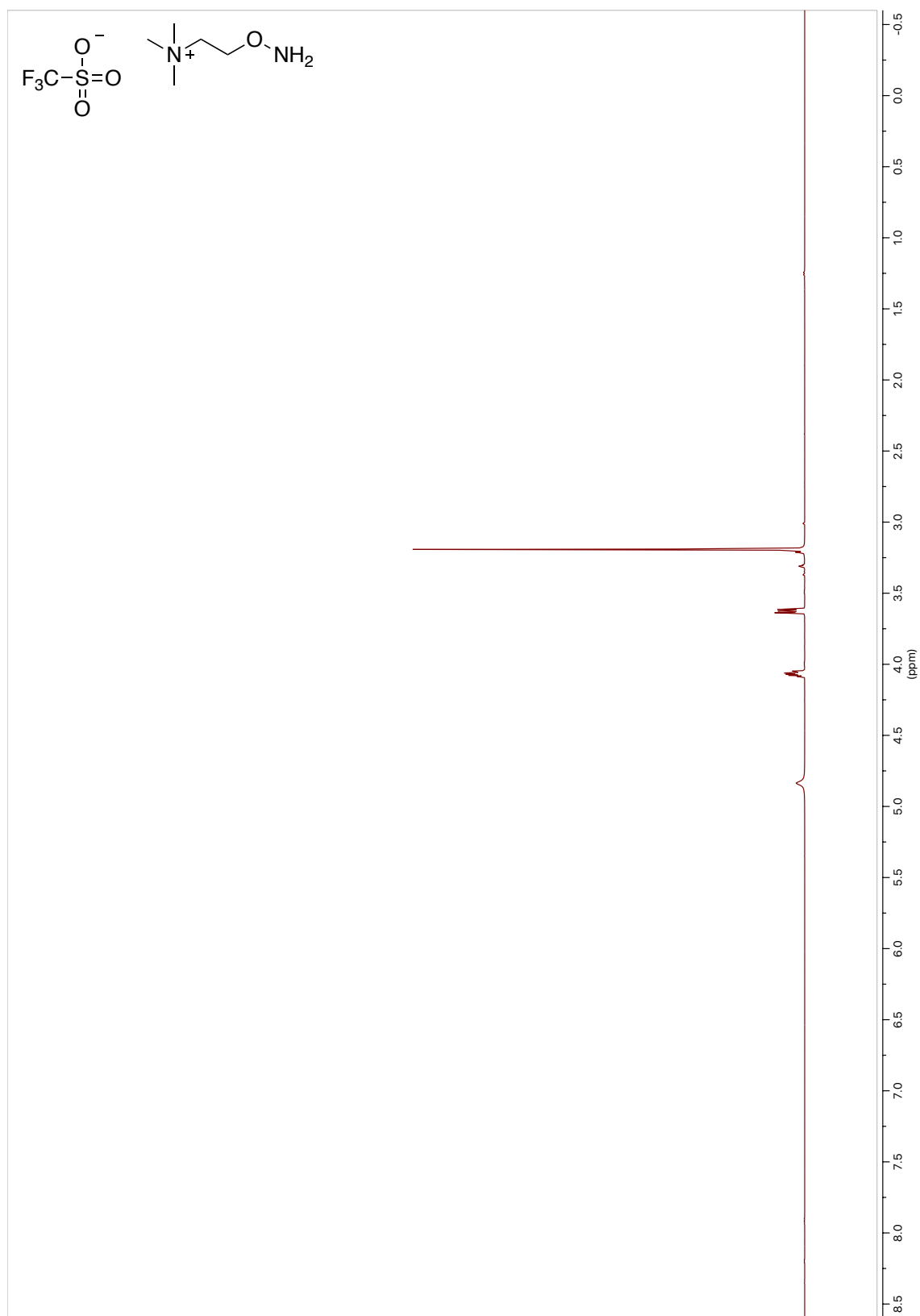
¹³C NMR ATM•OTf 100 MHz (CD₃OD)
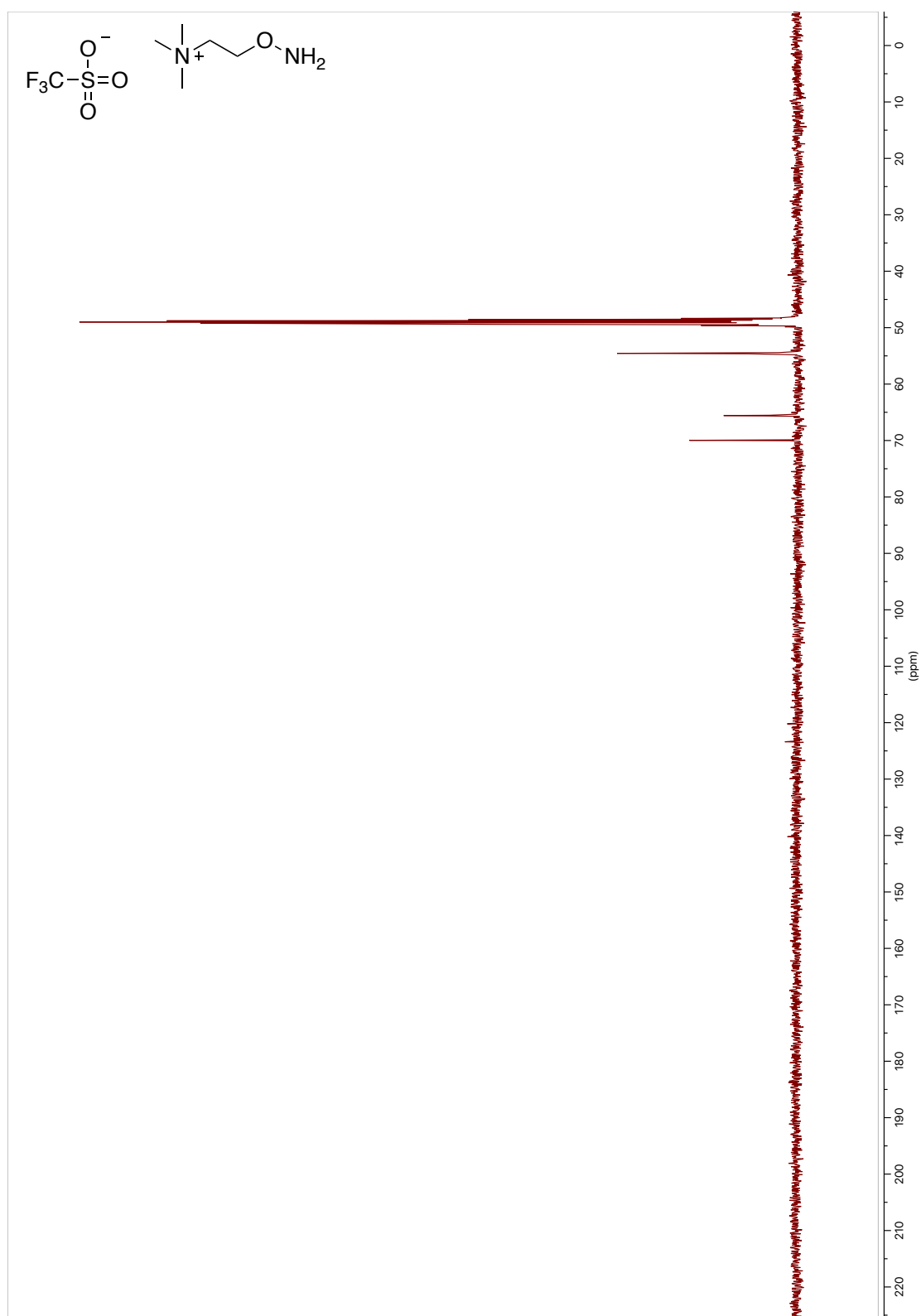
^{19}F NMR ATM•OTf 376 MHz (CD$_3$OD)
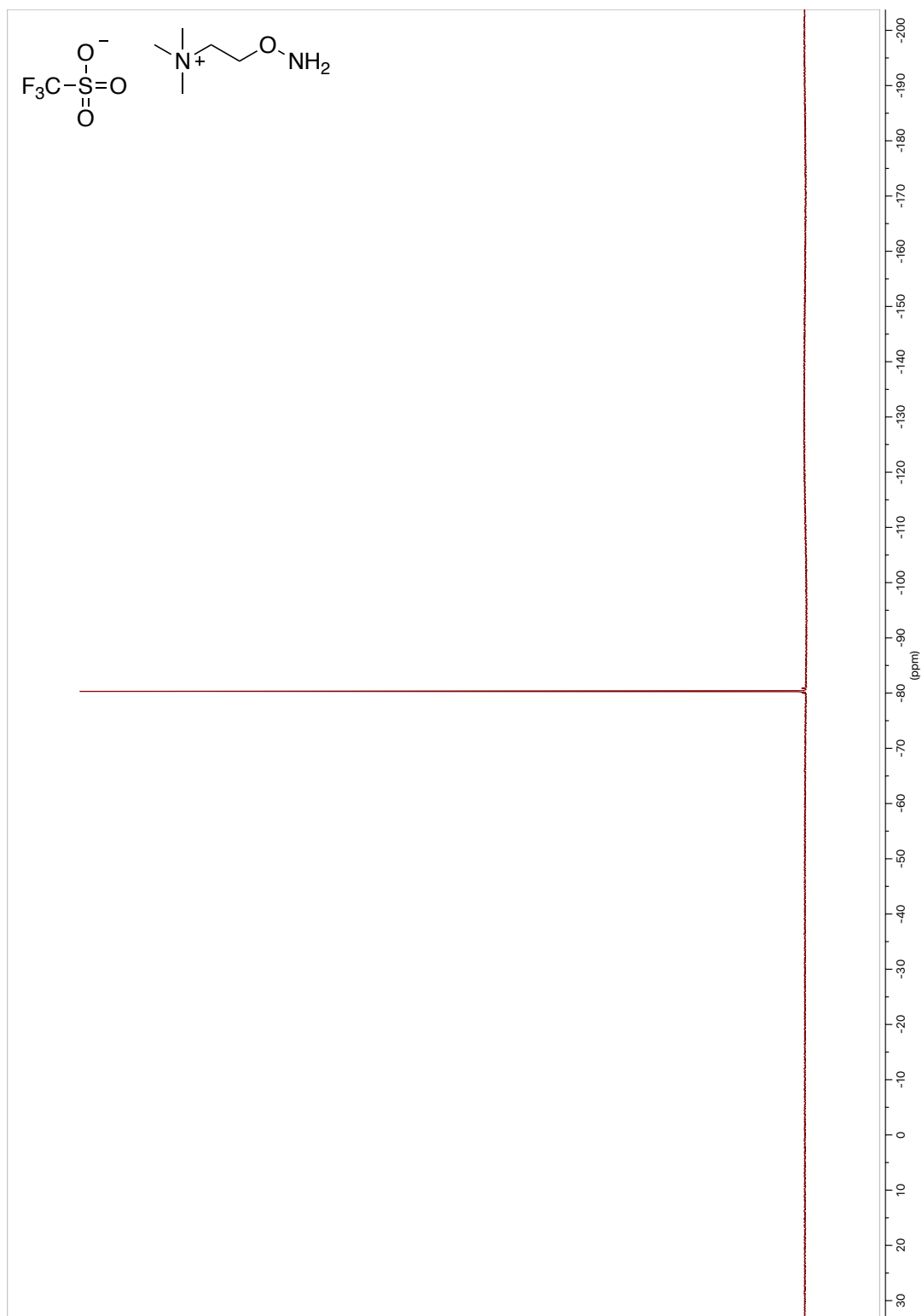
¹H NMR AMAH-hexanal chloride 400 MHz (CD₃OD)
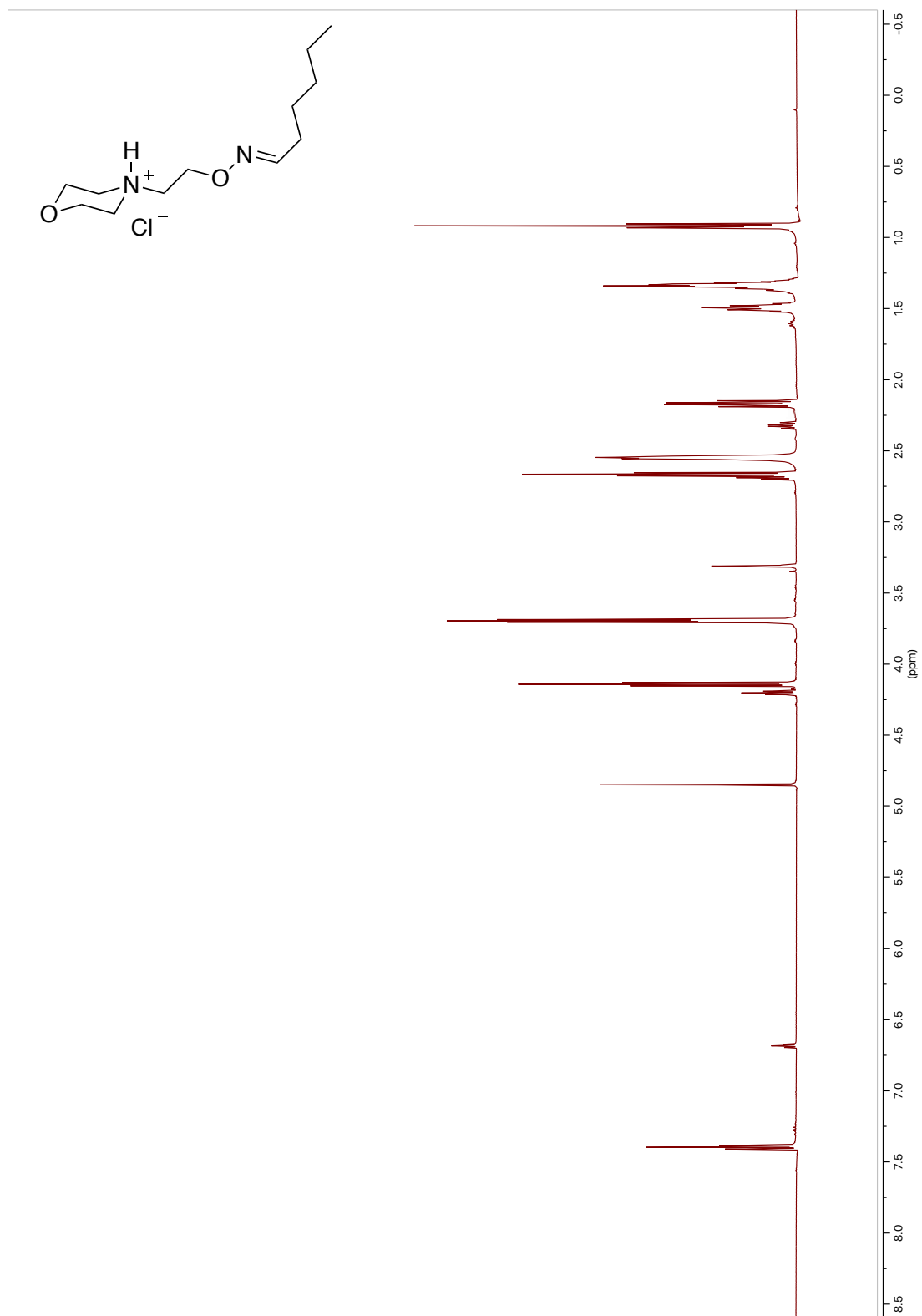
¹³C NMR AMAH-hexanal chloride 100 MHz (CD₃OD)
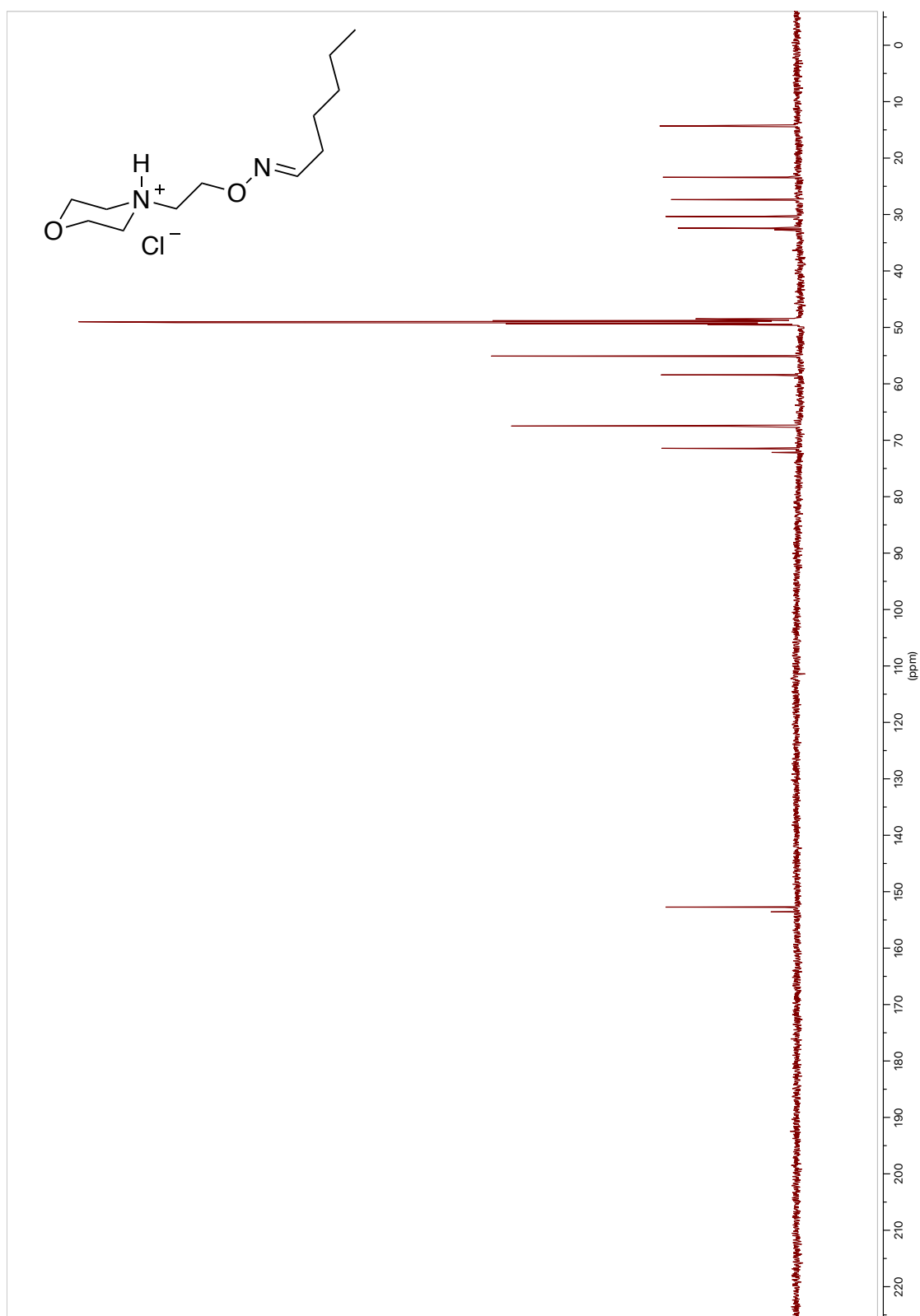
¹H NMR AMAH-2-hexenal chloride 400 MHz (CD₃OD)
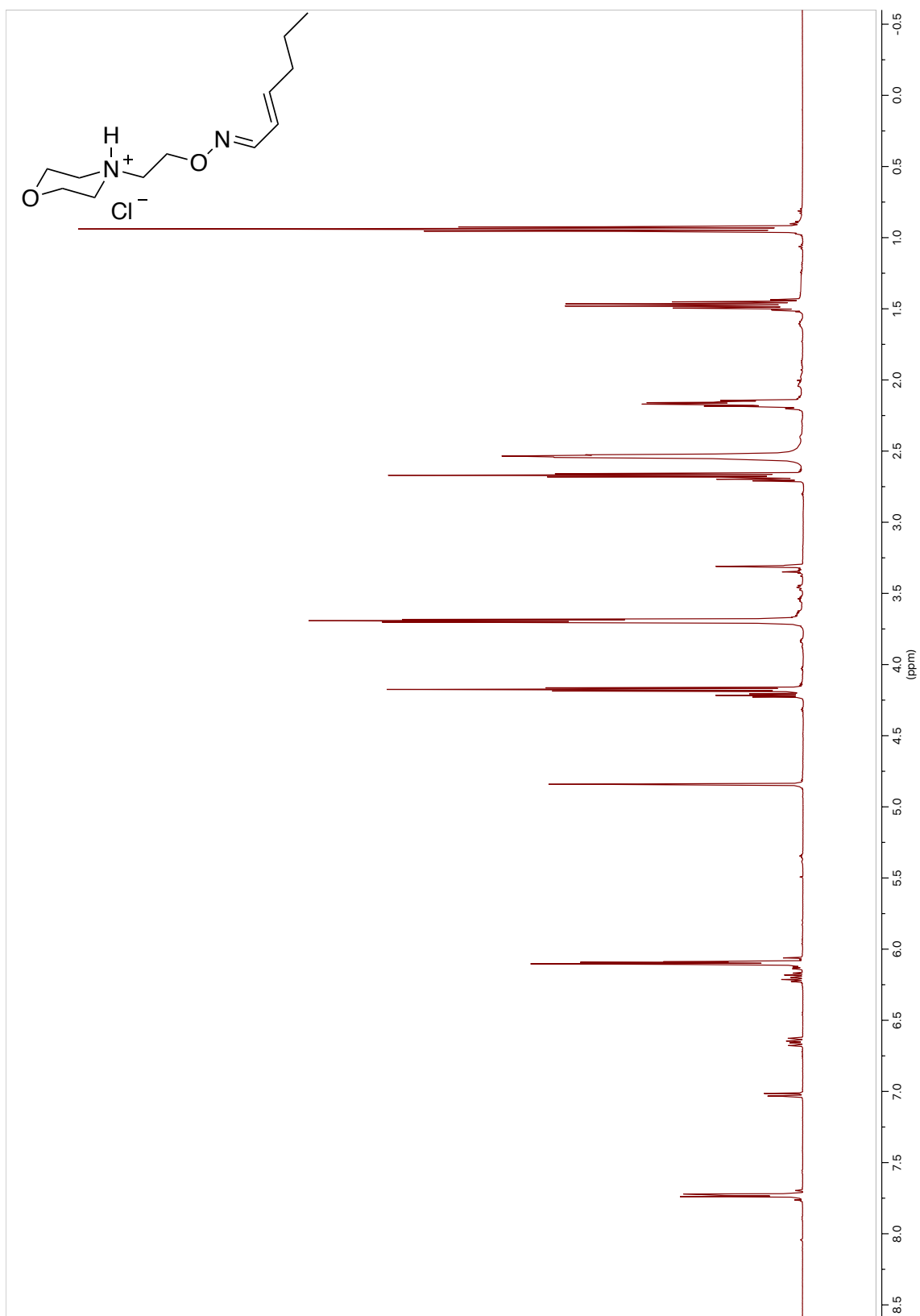
¹³C NMR AMAH-2-hexenal chloride 100 MHz (CD₃OD)
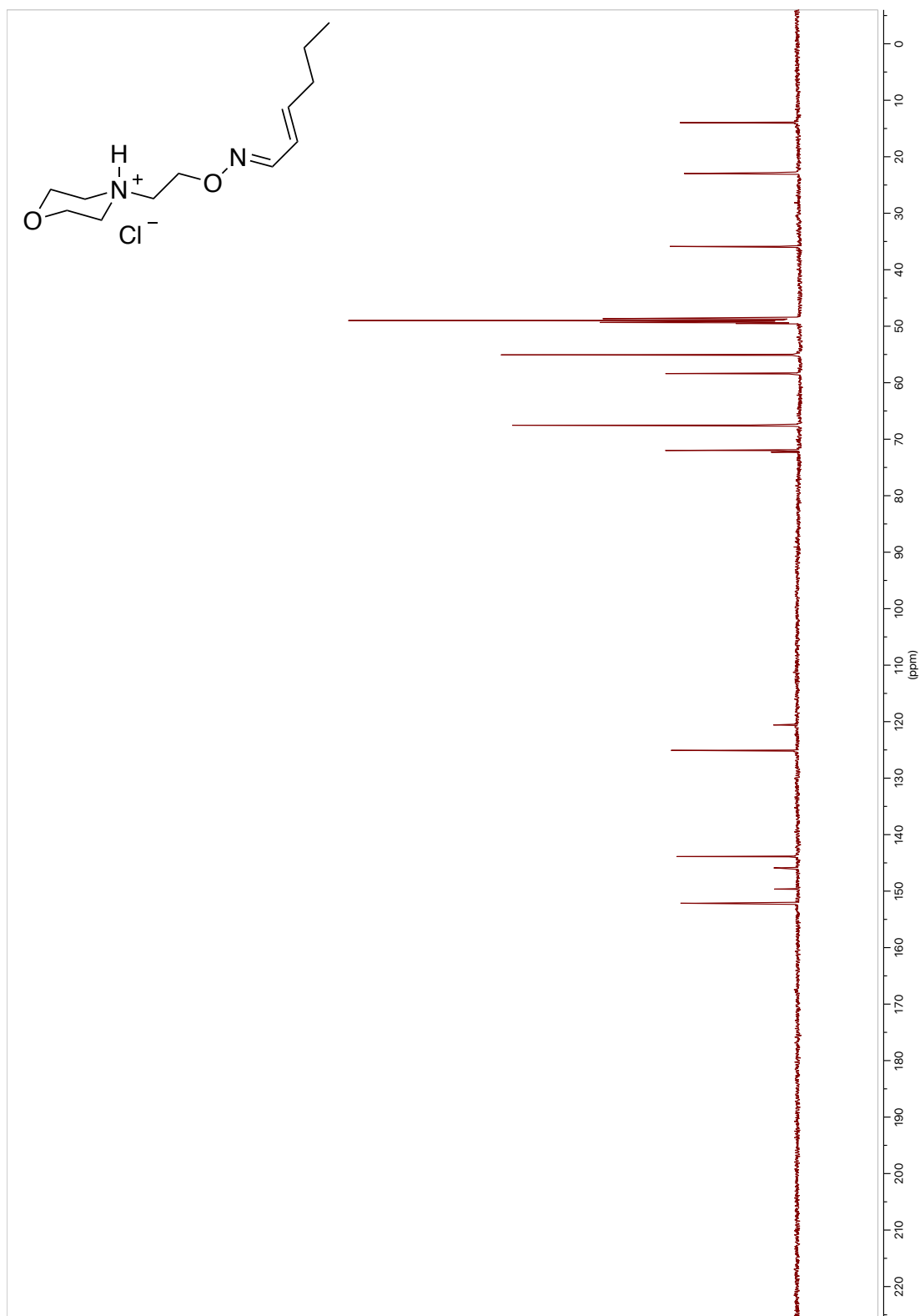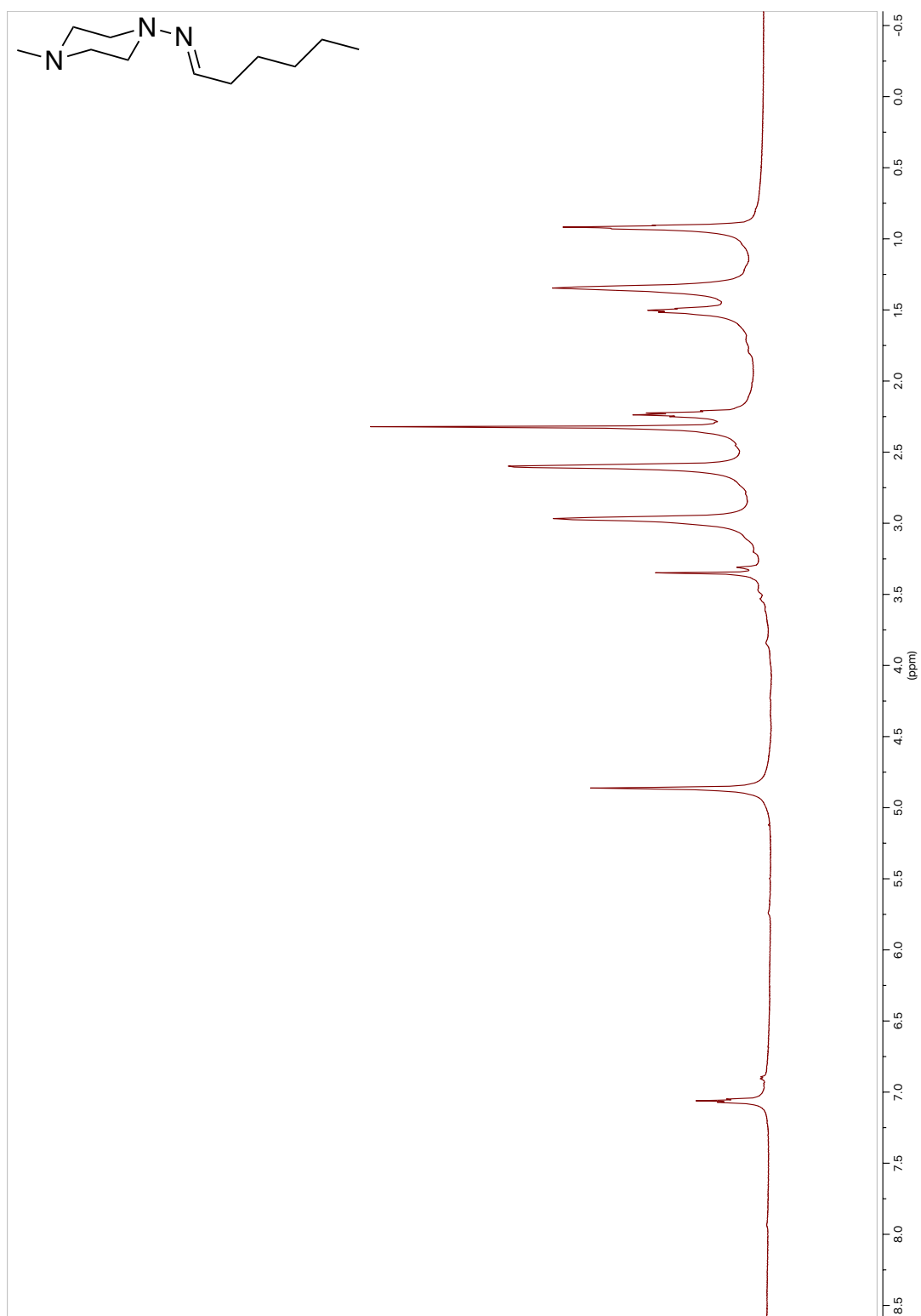
¹³C NMR AMP-hexanal 100 MHz (CD₃OD)
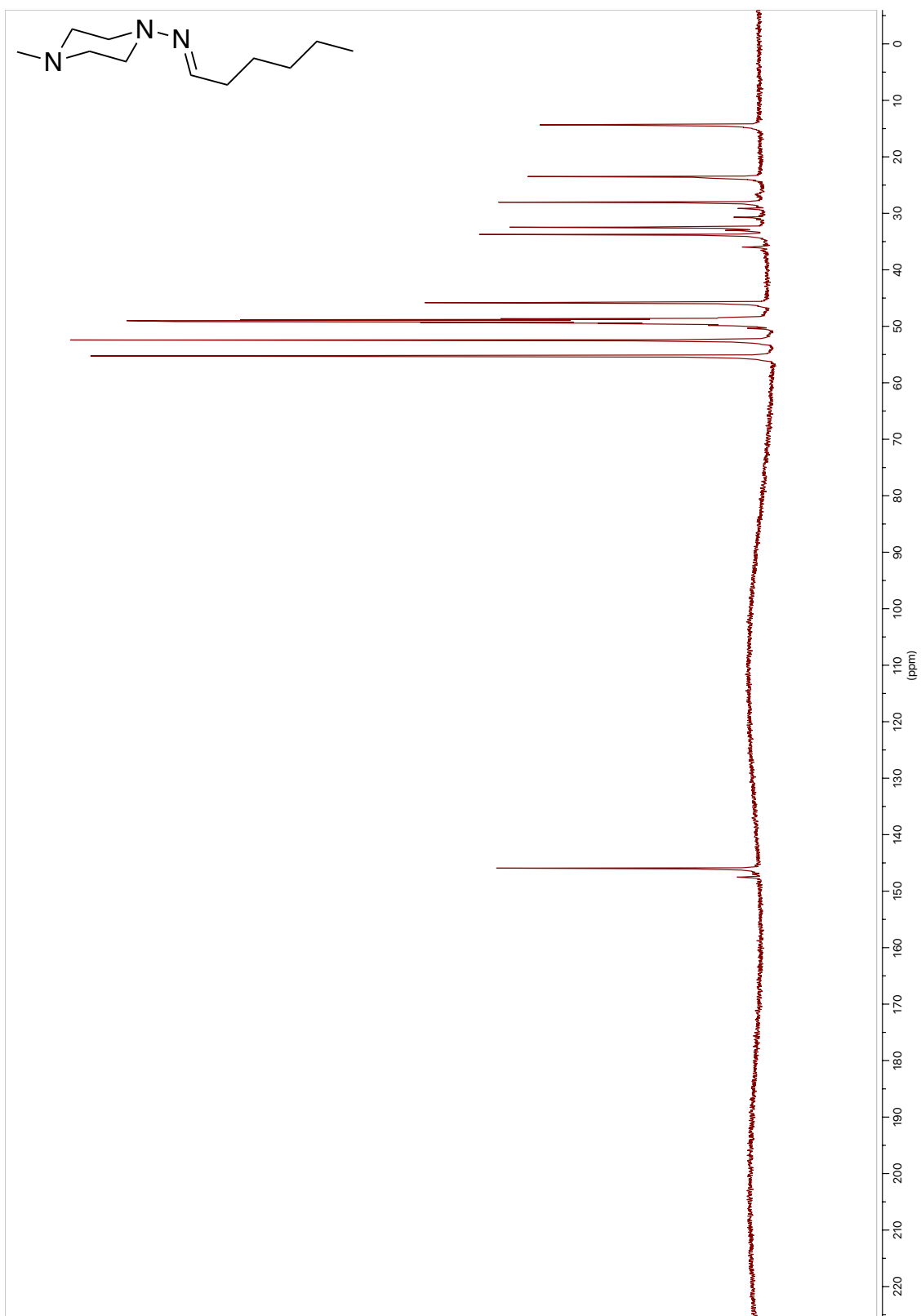
¹H NMR AMP-2-hexenal 400 MHz (CD₃OD)

^{13}C NMR AMP-2-hexenal 100 MHz (CD$_3$OD)
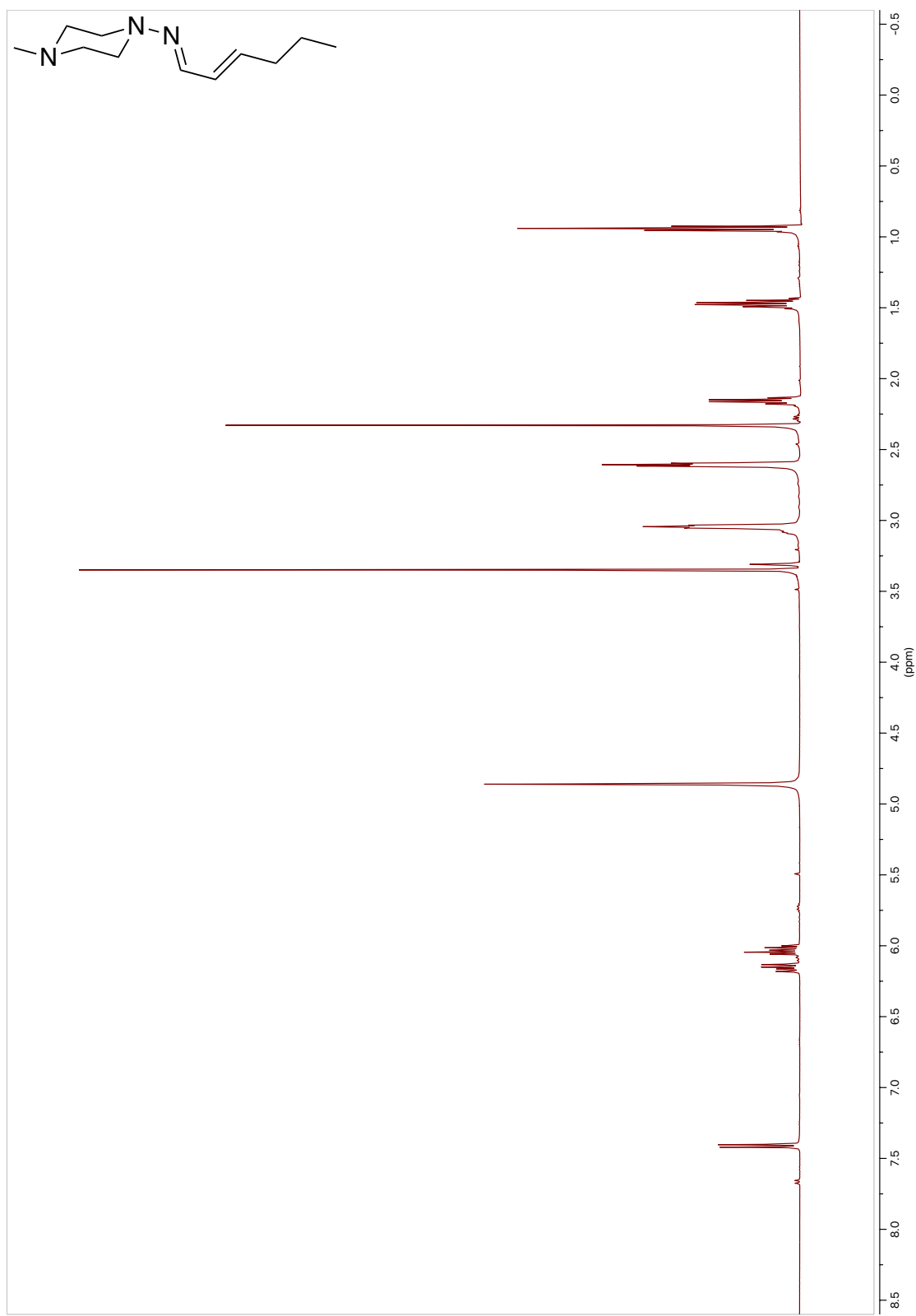
¹H NMR ATM-acetone triflate 400 MHz (CD₃OD)
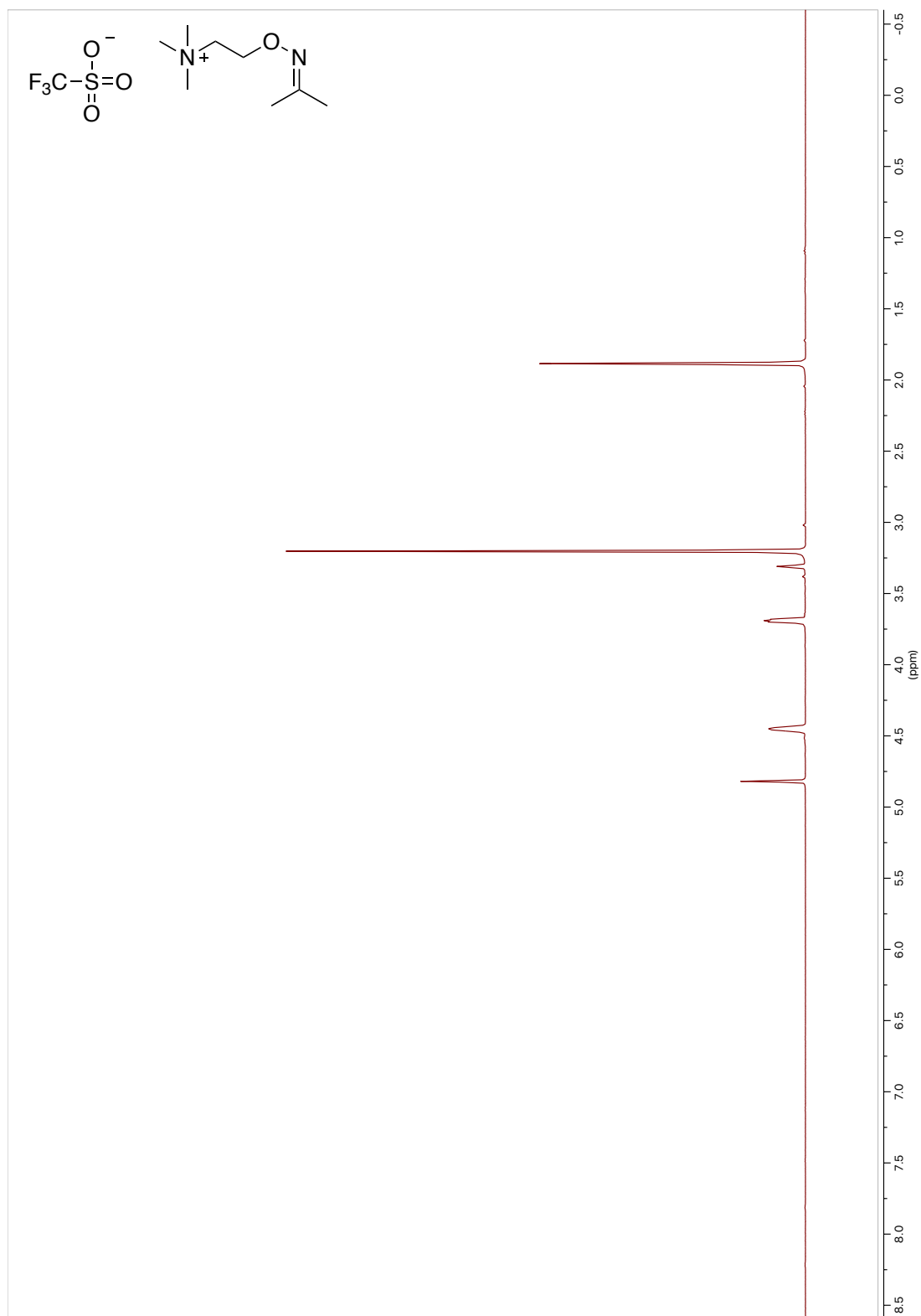
¹³C NMR ATM-acetone triflate 100 MHz (CD₃OD)
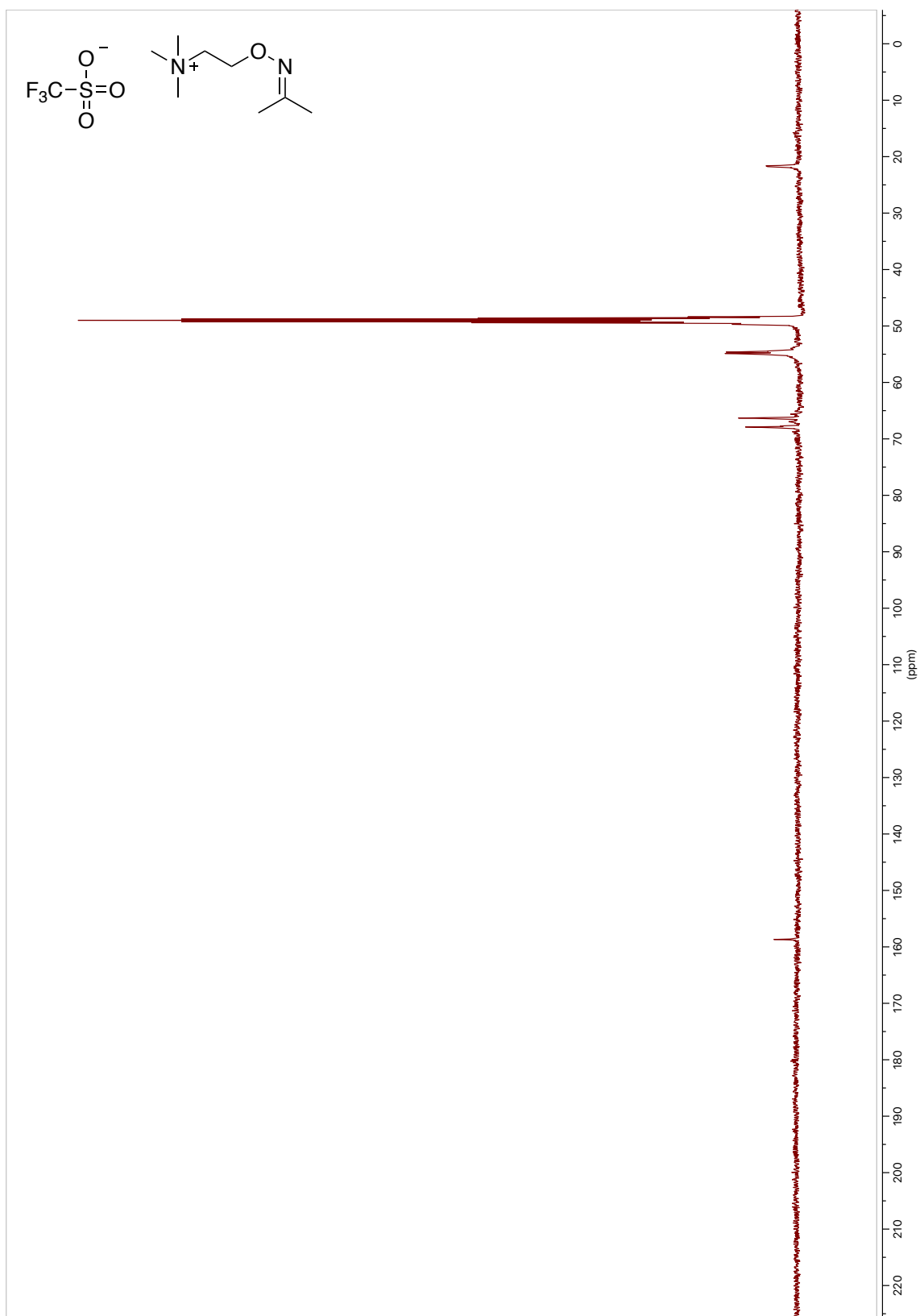
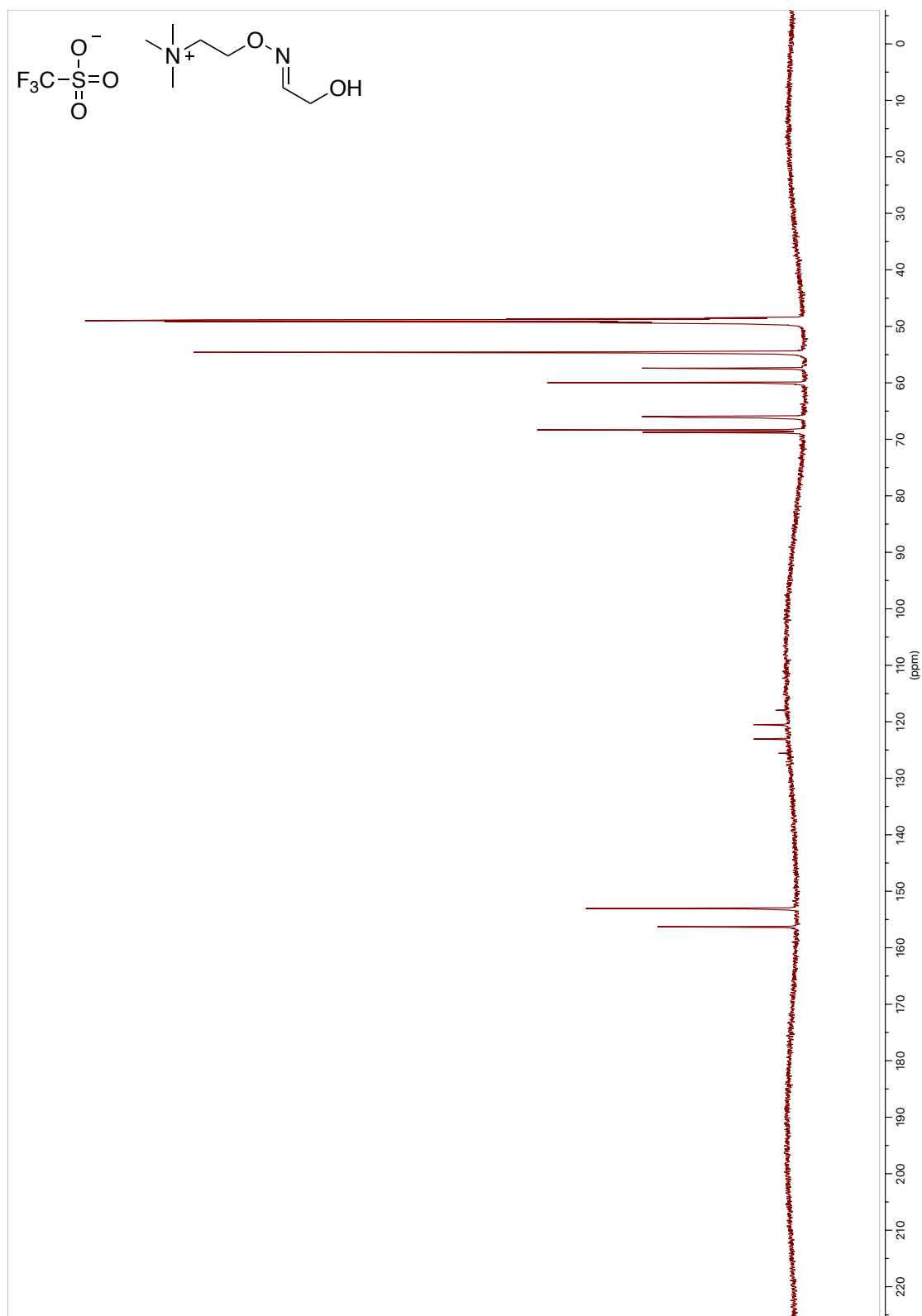# ¹H NMR ATM-butan-2-one triflate 400 MHz (CD₃OD)
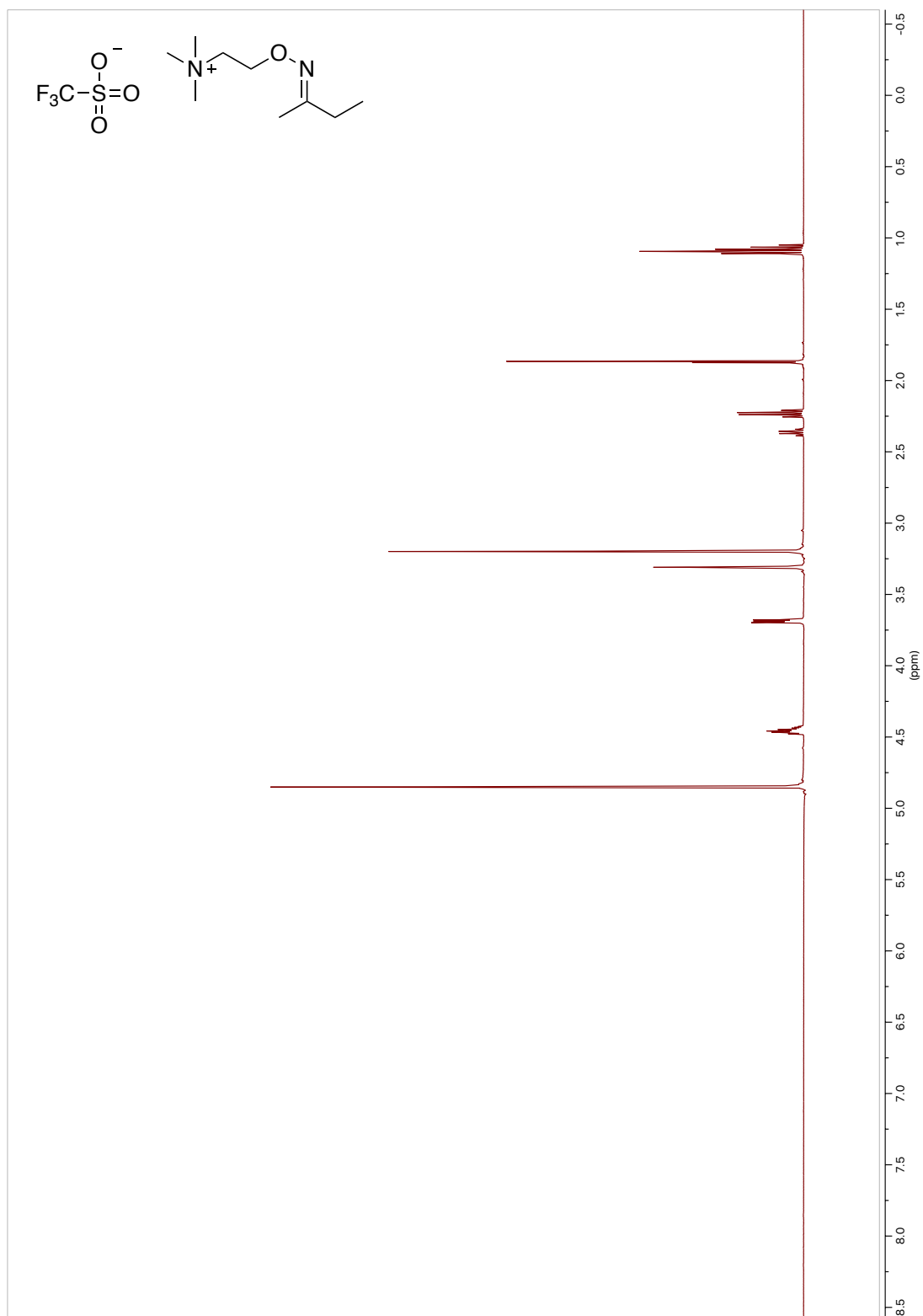
¹³C NMR ATM-butan-2-one triflate 100 MHz (CD₃OD)
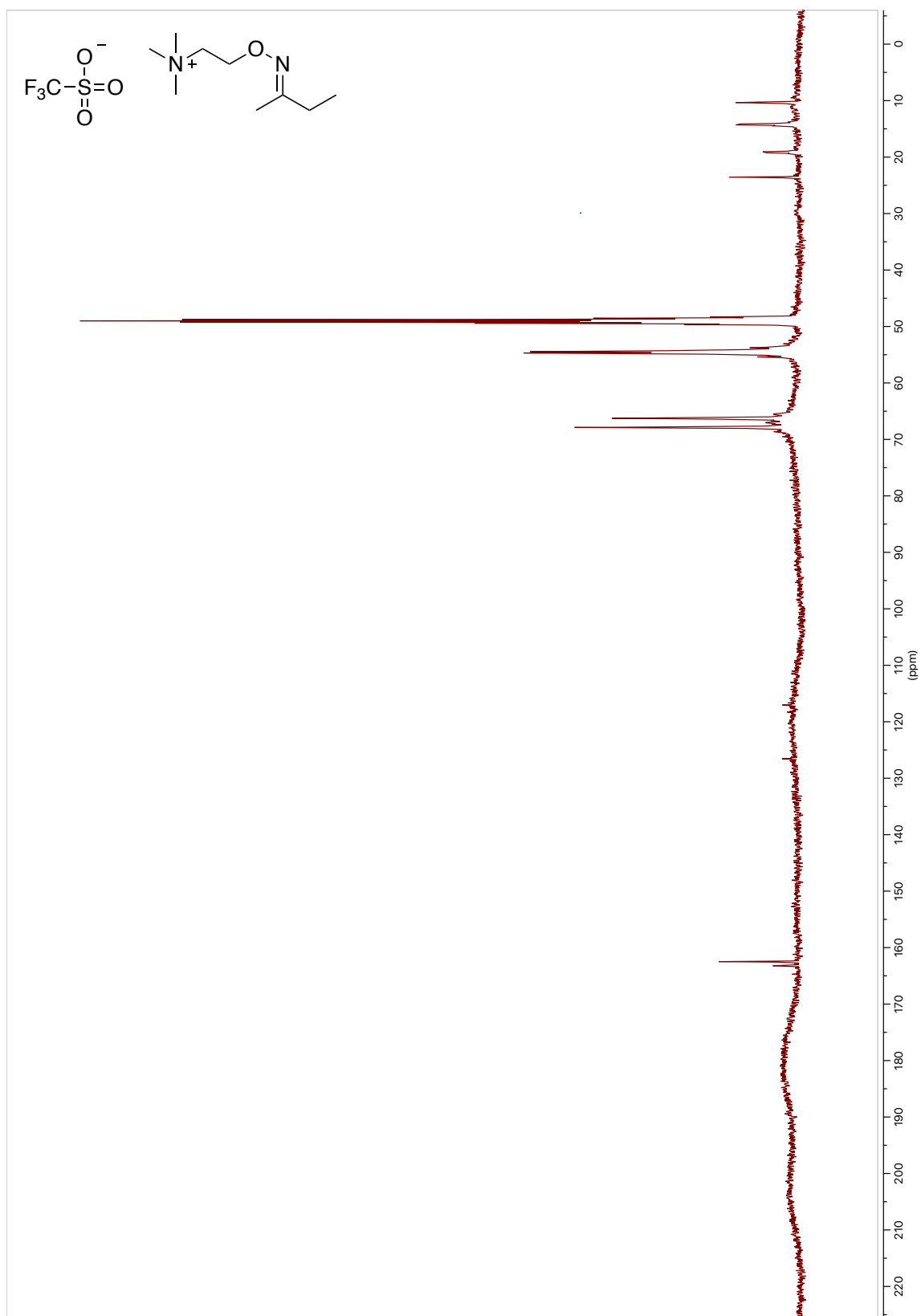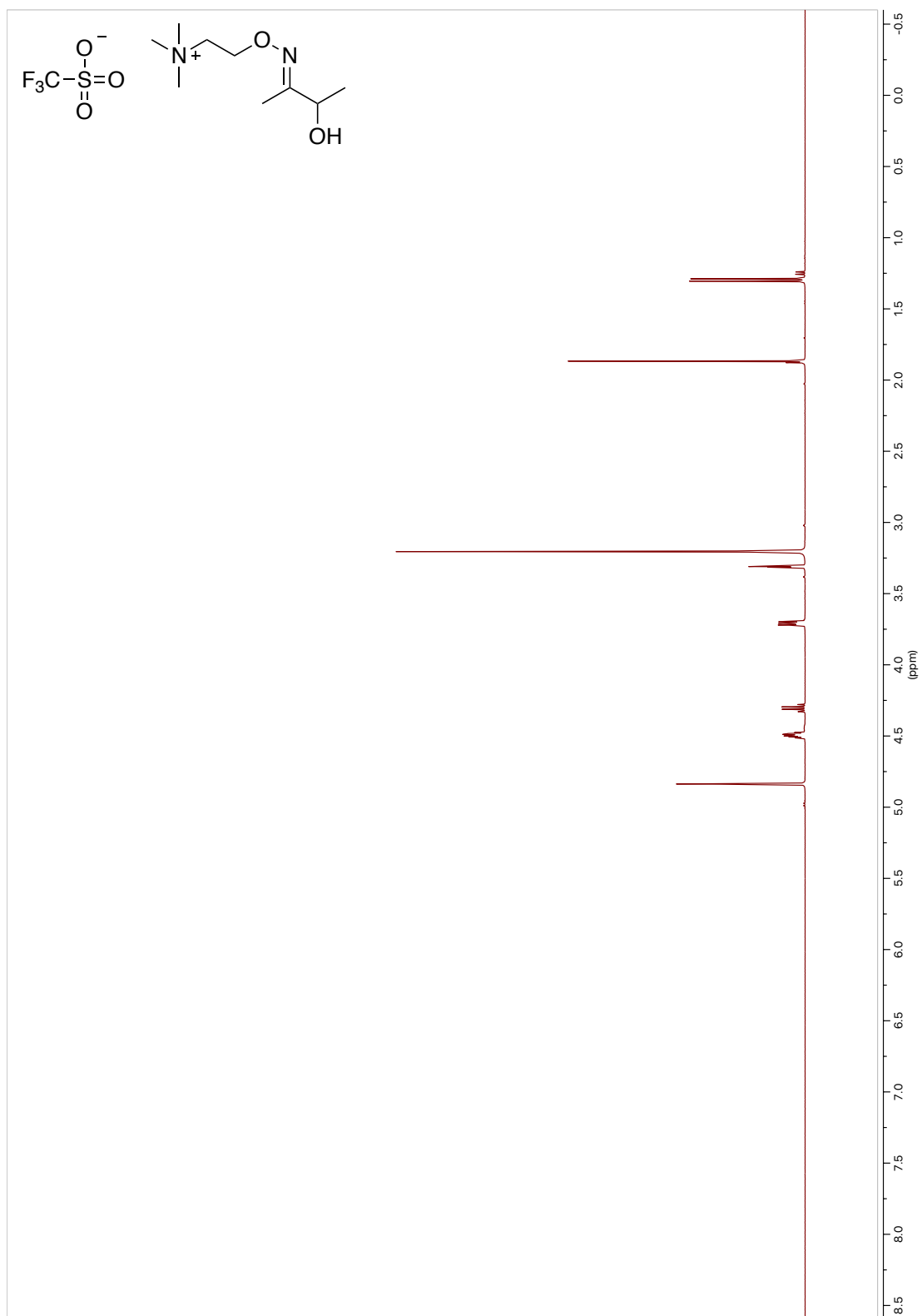

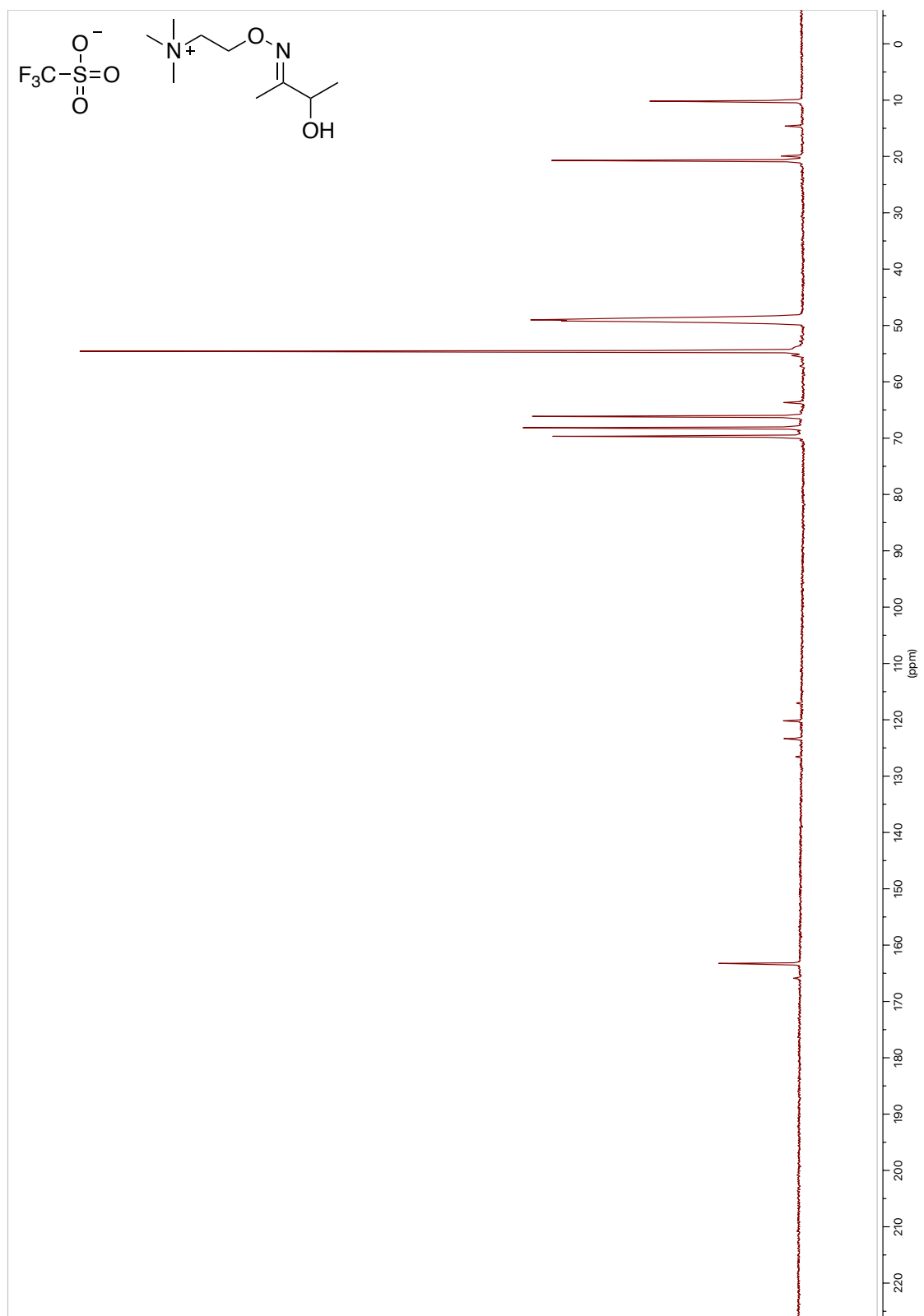^{1}H NMR ATM-2-hydroxyacetaldehyde triflate 400 MHz (CD$_3$OD)

¹³C NMR ATM-2-hydroxyacetaldehyde triflate 100 MHz (CD₃OD)
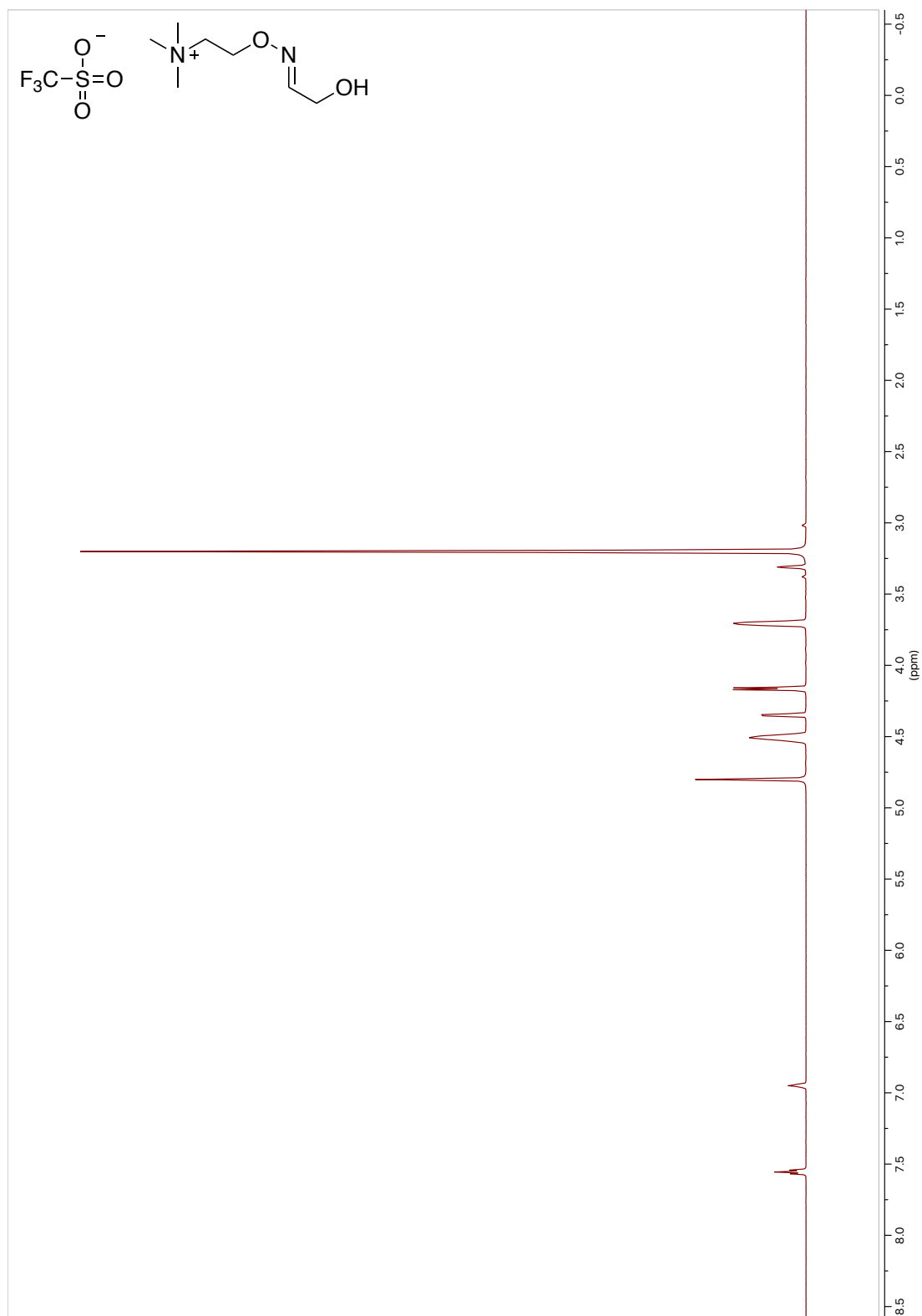
^{13}C NMR ATM-2-hydroxyacetaldehyde triflate 100 MHz (CD₃OD)
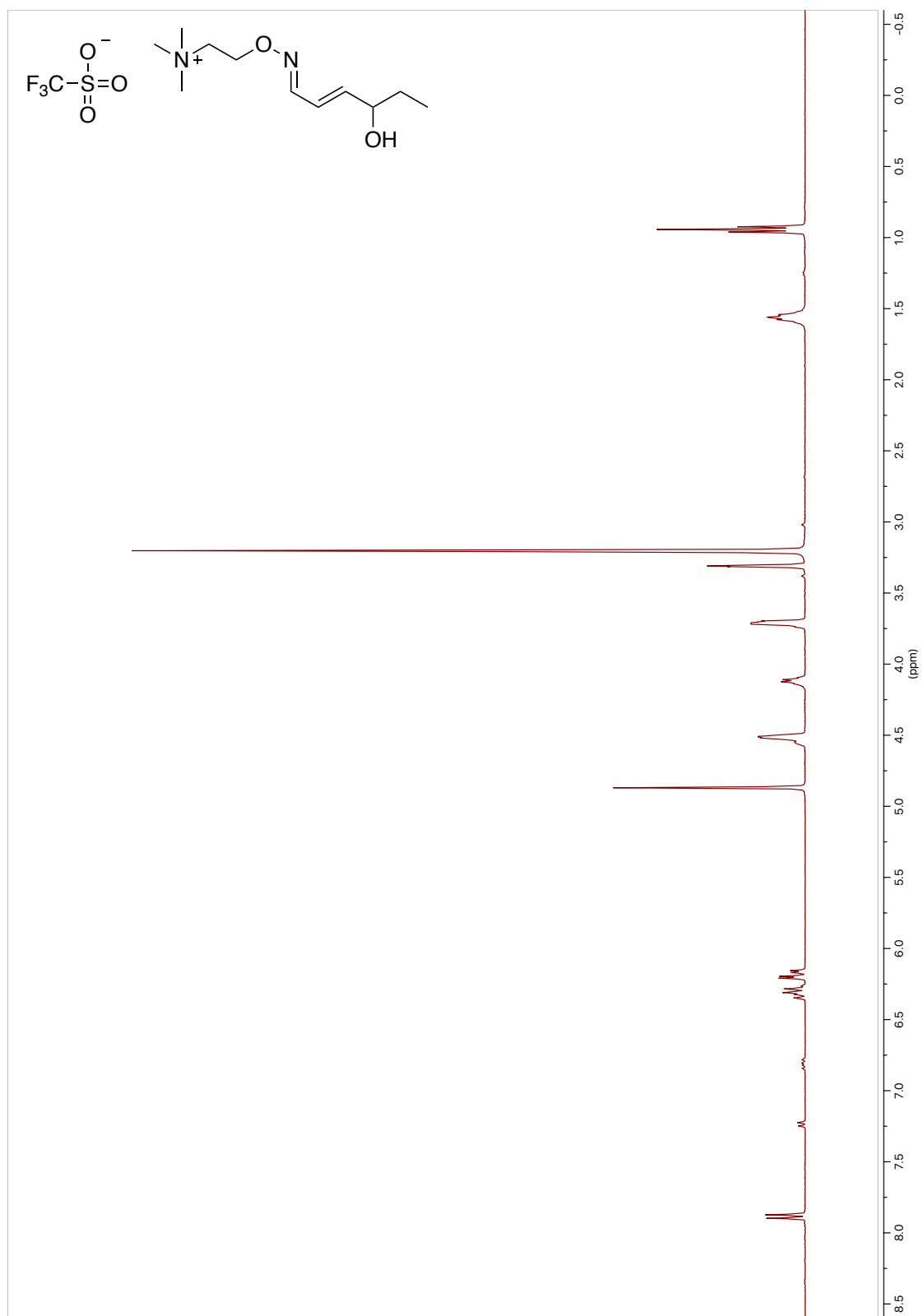
^{1}H NMR ATM-3-hydroxybutan-2-one triflate 400 MHz (CD$_3$OD)
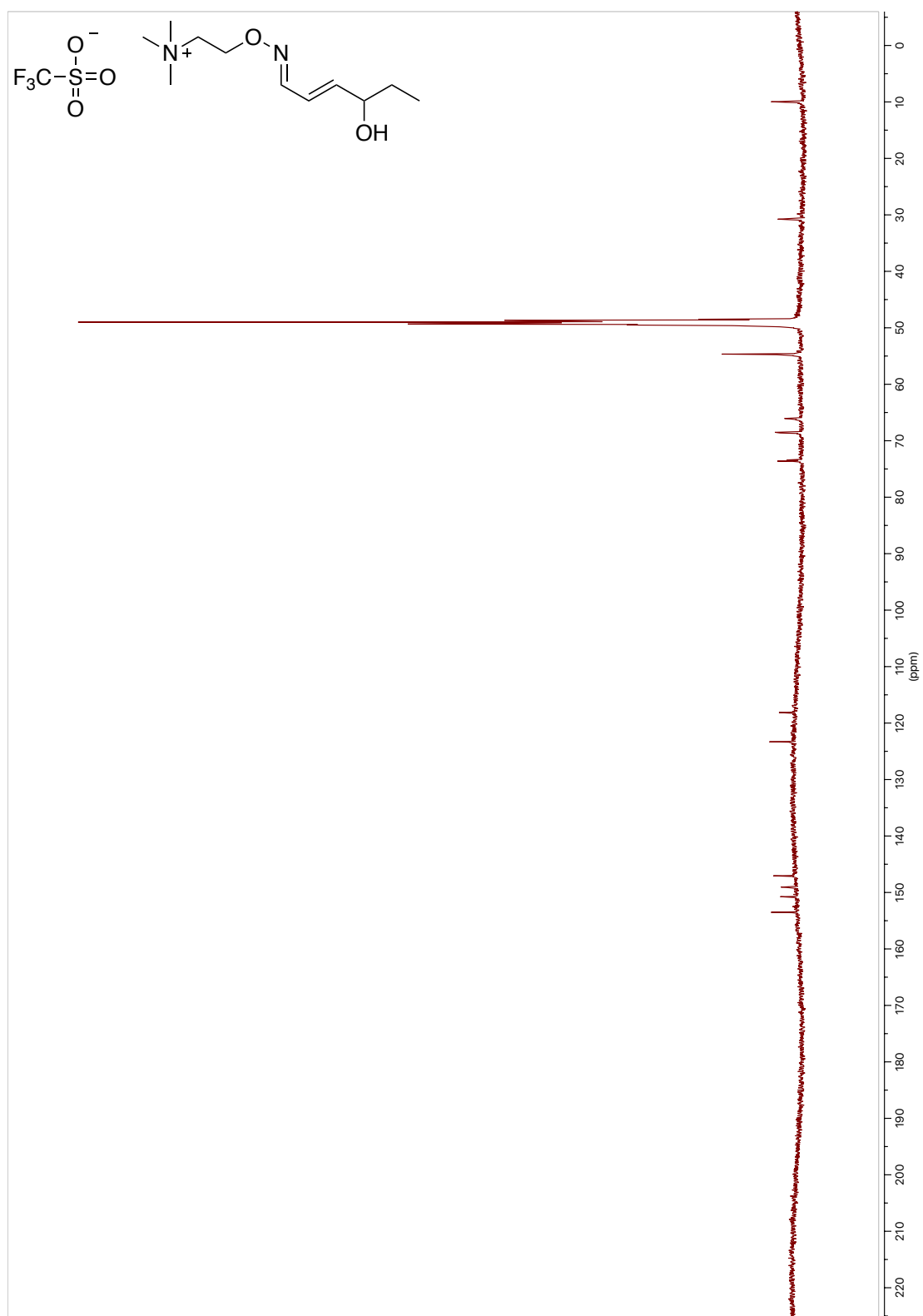
¹³C NMR ATM-3-hydroxybutan-2-one triflate 100 MHz (CD₃OD)
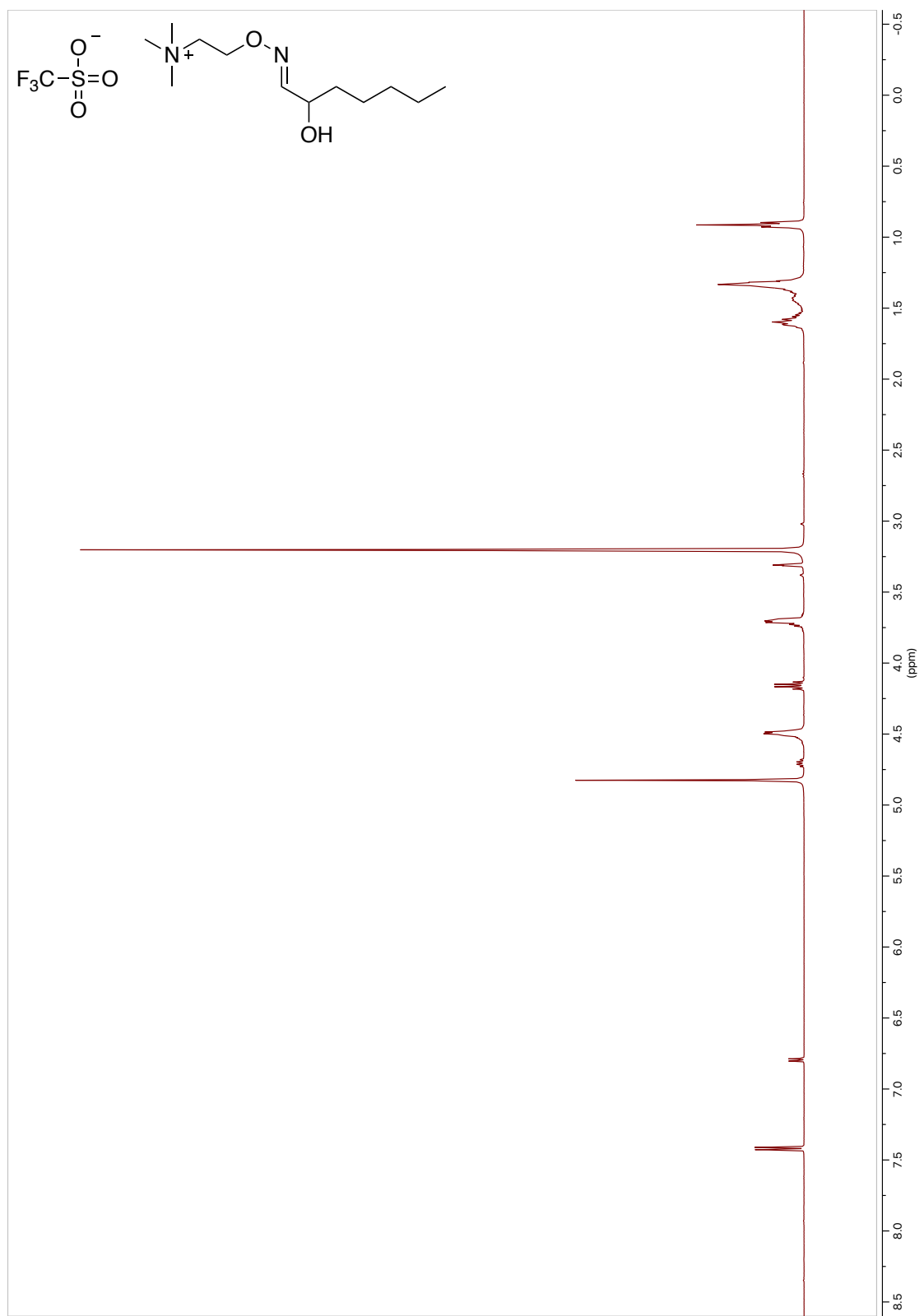
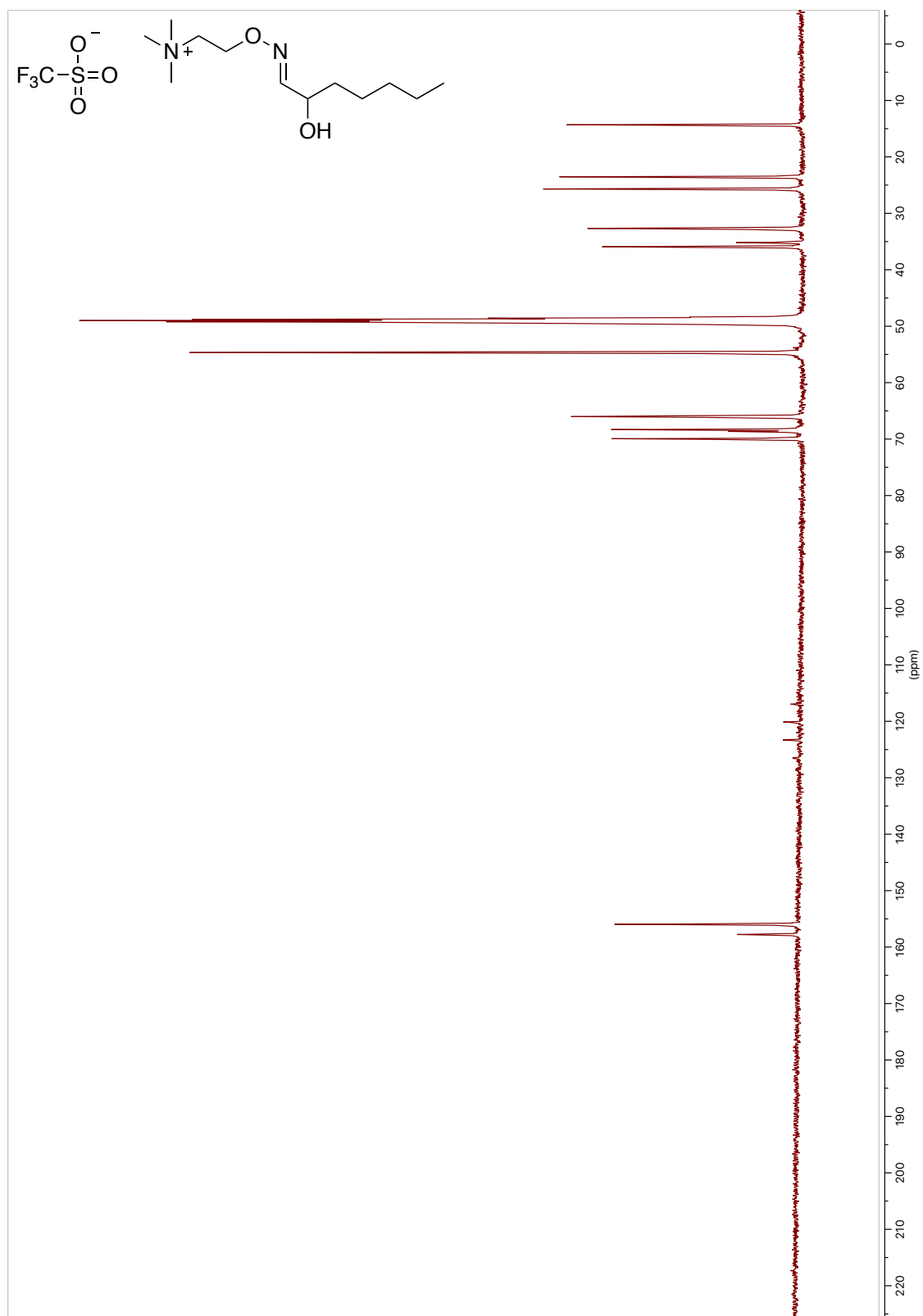# ^{1}H NMR ATM-4-hydroxyhex-2-enal triflate 400 MHz (CD$_3$OD)

¹³C NMR ATM-4-hydroxyhex-2-enal triflate 100 MHz (CD₃OD)

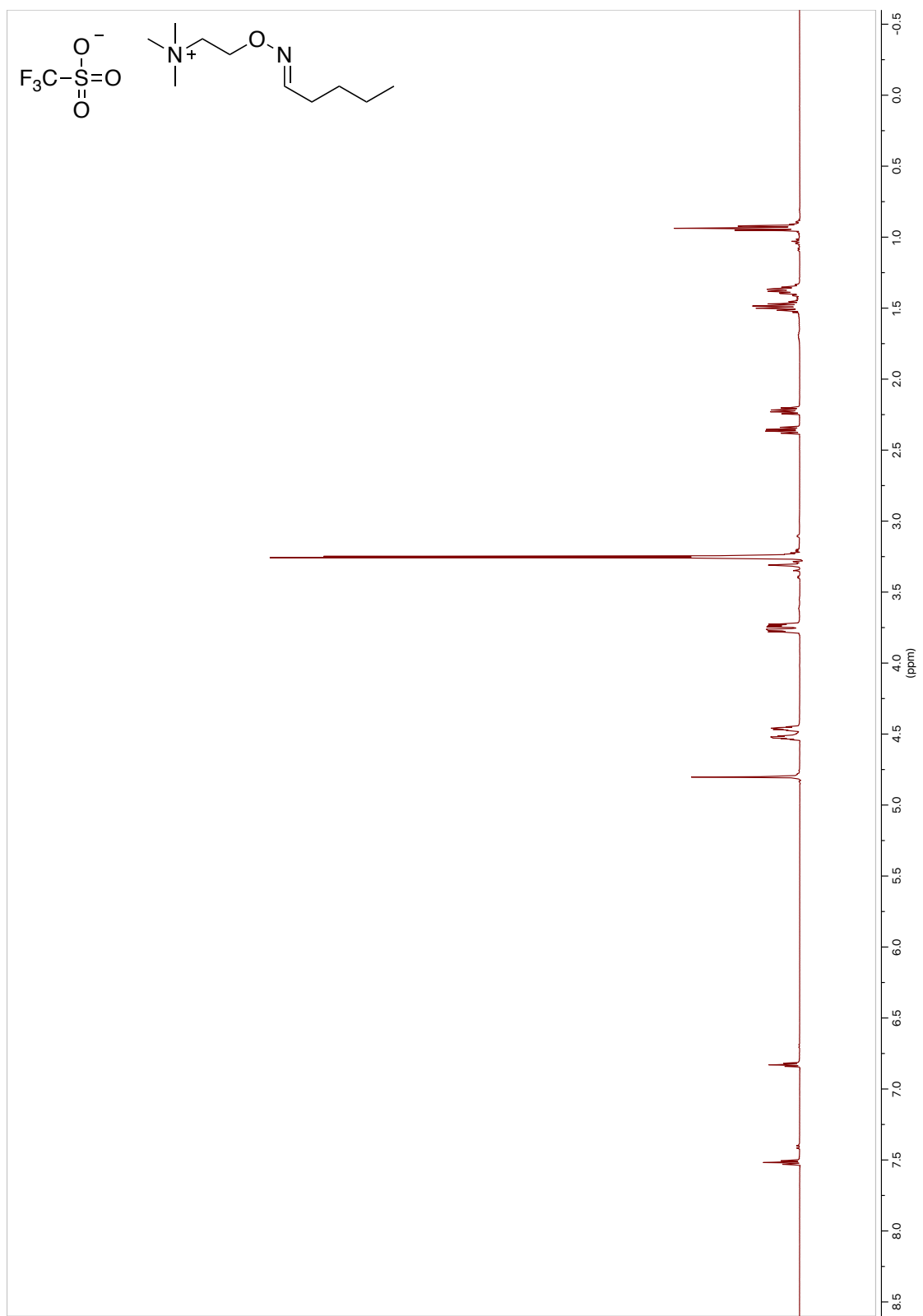# ¹H NMR ATM-2-hydroxyheptanal triflate 400 MHz (CD₃OD)

¹H NMR ATM-2-hydroxyheptanal triflate 400 MHz (CD₃OD)

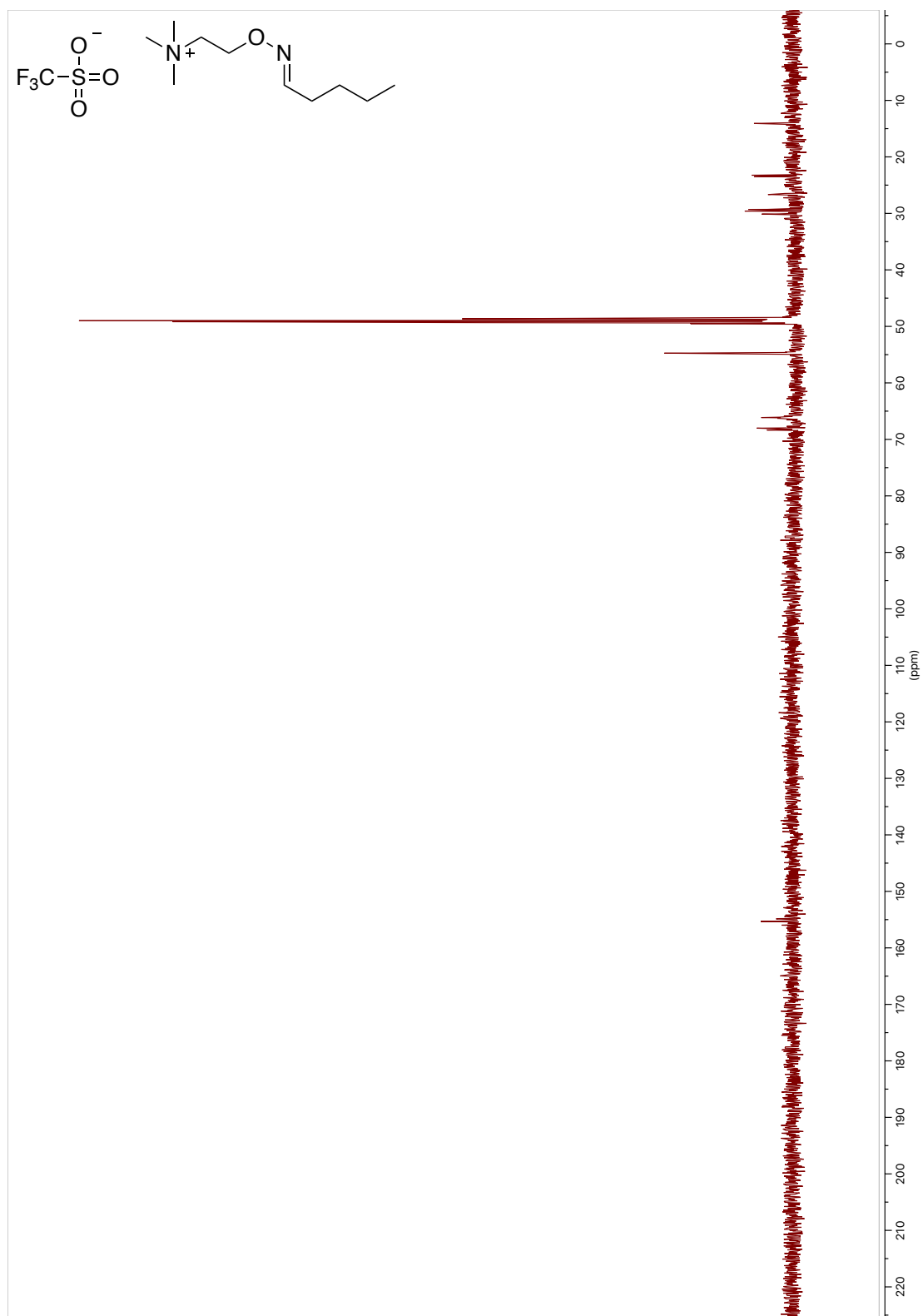## ^{13}C NMR ATM-2-hydroxyheptanal triflate 100 MHz (CD$_3$OD)

¹H NMR ATM-pentanal triflate 400 MHz (CD₃OD)

^{13}C NMR ATM-pentanal triflate 100 MHz (CD$_3$OD)
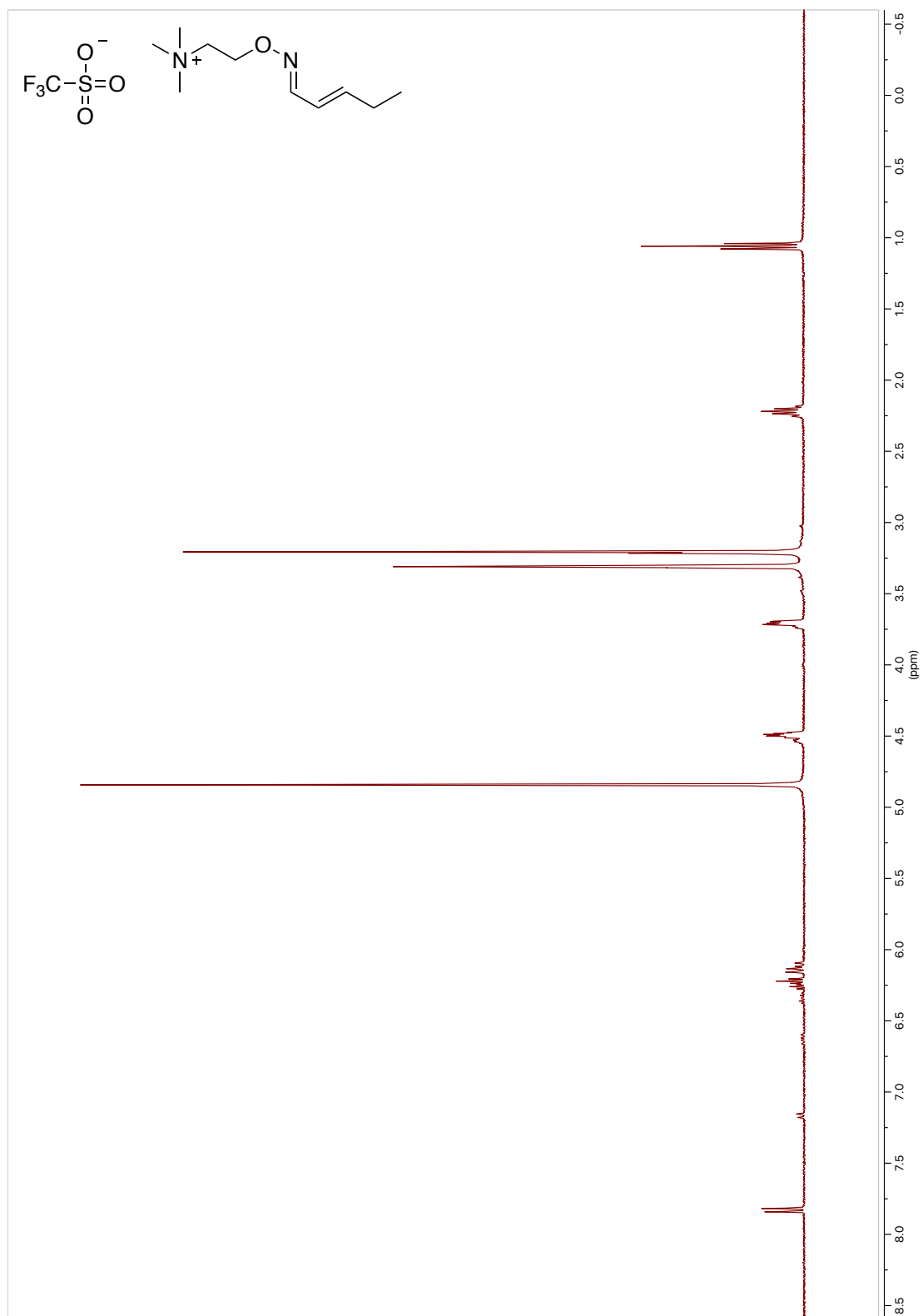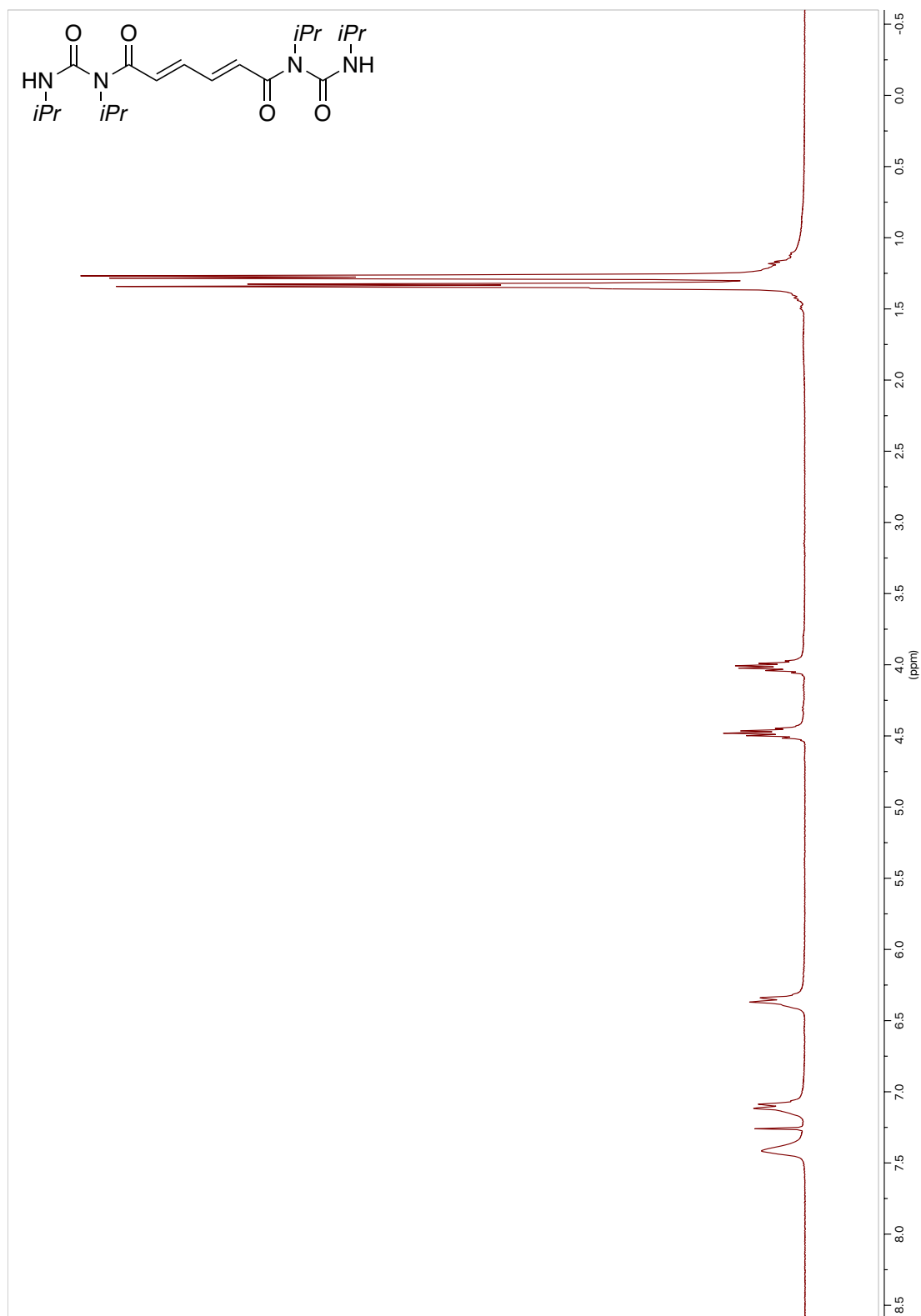
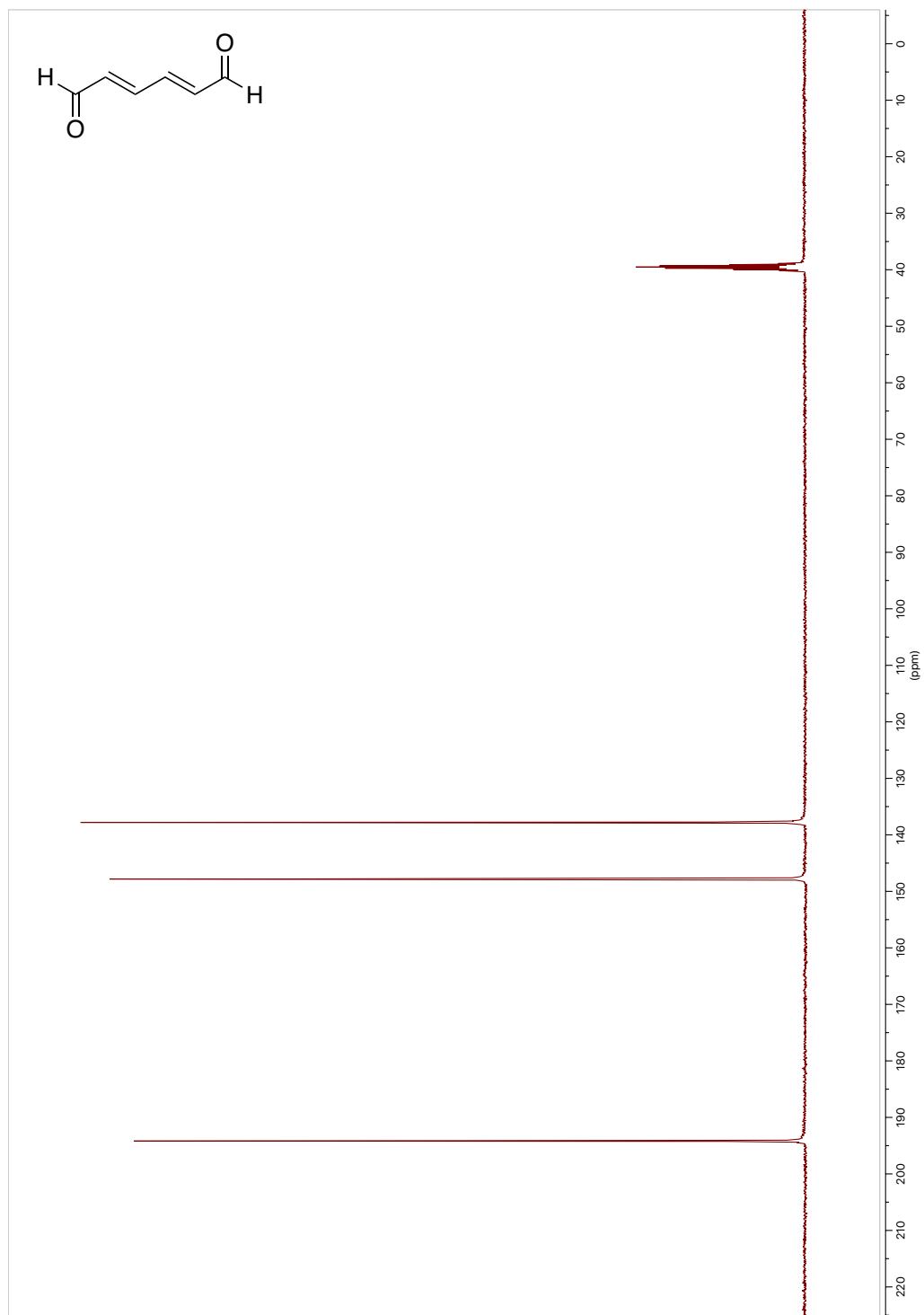¹³C NMR ATM-2-pentenal triflate 100 MHz (CD₃OD)
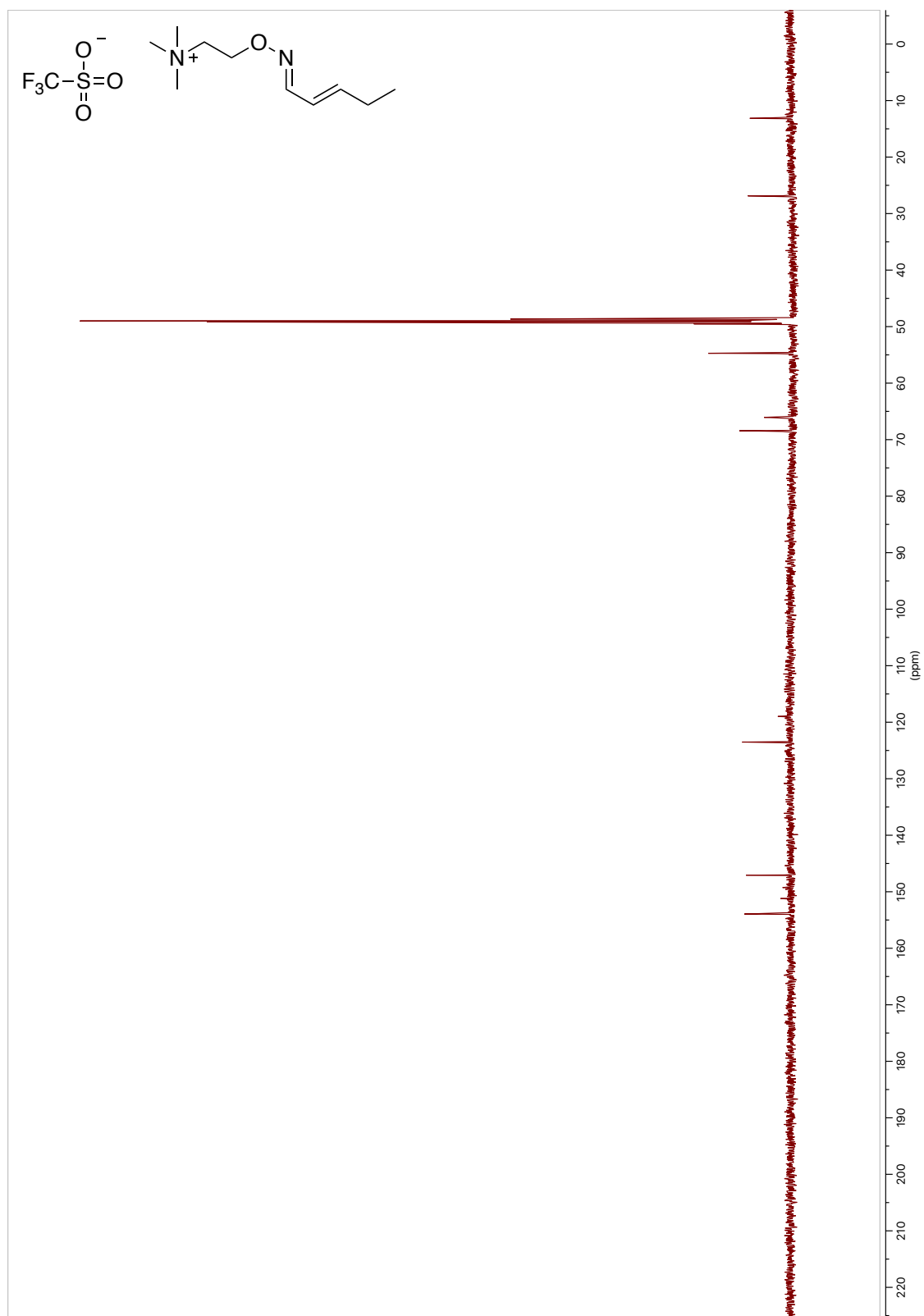
¹HNMR (2*E*,4*E*)-*N*¹,*N*⁶-diisopropyl-*N*¹,*N*⁶-bis(isopropylcarbamoyl)hexa-2,4-dienediamide.
400 MHz (CDCl₃)

¹³CNMR Muconaldehyde 100 MHz (DMSO)

APPENDIX B

LIST OF PUBLICATIONS

This dissertation is the culmination and summary of the research completed in pursuit of a Ph.D. from University of Louisville, College of Arts and Sciences, Department of Chemistry, from Fall 2017 to Fall 2022. Listed below are the peer-reviewed publications and manuscript of said work.

<u>Publications:</u>

1. Sutaria, S.R.; Gori, S.S.; Morris, J.D.; Xie, Z.; Fu, X.A. and Nantz, M.H. Lipid Peroxidation Produces a Diverse Mixture of Saturated and Unsaturated Aldehydes in Exhaled Breath That Can Serve as Biomarkers of Lung Cancer—A Review. *Metabolites*, **2022**, 12, 561. [Chapter 1]
2. Sutaria, S.R.; Huang, J.; Fu, X.A. and Nantz, M.H. UV Spectroscopy of Chemo-selectively Preconcentrated Exhaled Breath as Novel COVID-19 Screening Method. Manuscript prepared. [Chapter 3]
3. Sutaria, S.R. and Nantz, M.H. A Convenient Preparation of Muconaldehyde Using a One-Pot Acid-to-Aldehyde Reduction Protocol. *Organic Preparations and Procedures International*, **2021**, 53, 488-492. [Chapter 4]
4. Malovichko, M.V.; Abplanalp, W.T.; McFall, S.A.; Taylor, B.S.; Wickramasinghe, N. S.; Sithu, I. D.; Zelko, I. N.; Uchida, S.; Hill, B.G.; Sutaria, S.R.; Nantz, M.H.; Bhatnagar, A.; Conklin, D. J.; O'Toole, T. E.; Srivastava, S. Subclinical Markers of Cardiovascular Toxicity of Benzene Inhalation in Mice. *Toxicol. Appl. Pharmacol*. **2021**, 431, 115742. [Chapter 4]

CURRICULUM VITAE

Saurin Sutaria
srsuta01@louisville.edu
linkedin.com/in/saurin-
sutaria-90521b1a3

Education:	**University of Louisville,** Louisville, KY	December 2022
	Ph.D. in chemistry	
	Dissertation title: α,β-Unsaturated Aldehydes: The Underrepresented Markers of Disease	
	University of Louisville, Louisville, KY	September 2019
	M.S. in chemistry	
	Indiana University Southeast, New Albany, IN	May 2017
	B.S. in chemistry	

Research: Developed derivatization reagents for detection of trace carbonyl metabolites from exhaled breath by mass spectrometry and uv-vis spectroscopy, to create noninvasive breath diagnosis techniques.
Developed a new acid-to-aldehyde reduction protocol to synthesize an important analyte muconaldehyde, in fewer steps and higher yield than any previous synthesis.

Teaching Experience:

University of Louisville, Louisville, KY   May 2022 – August 2022
Department of Chemistry
  Part Time Lecturer
• Instructor of record for first and second semester organic chemistry lecture. Responsibilities include delivering 1.5-hour lectures five days a week, making quizzes and exams weekly, and grading

University of Louisville, Louisville, KY   August 2017 – May 2022
Department of Chemistry
  Graduate Teaching Assistant
• Recitation and lab instructor for 300-500 level chemistry courses. Responsibilities include teaching, grading, and making quizzes and exams (7 semesters)

Jefferson Community and Technical College, Louisville, KY   Fall 2020
Department of Chemistry
  Adjunct Faculty Instructor
• Instructor of record for first semester organic chemistry lecture and labs. Responsibilities include delivering biweekly lectures, making quizzes and exams, and grading

Indiana University Southeast, New Albany, IN   August 2016 – May 2017
    Supplemental Instructor
- Conducted study and review session the hour before lectures, in which I administer practice questions and answer student's questions on material for intro chemistry and organic chemistry courses

Indiana University Southeast, New Albany, IN   August 2015 – May 2017
    Tutor
- Tutored many students, in a variety of disciplines of Chemistry and Mathematics

Publications: Pawel Lorkiewicz; Daniel W Riggs; Rachel J Keith; Daniel J Conklin; Zhengzhi Xie; Saurin R. Sutaria; Blake Lynch; Sanjay Srivastava and Aruni Bhatnagar. Comparison of Urinary Biomarkers of Exposure in Humans Using Electronic Cigarettes, Combustible Cigarettes, and Smokeless Tobacco. *Nicotine & Tobacco Research*, Volume 21, Issue 9, May 2018, Pages 1228–1238, 10.1093/ntr/nty089.

Saurin R. Sutaria and Michael H. Nantz. A Convenient Preparation of Muconaldehyde Using a One-Pot Acid-to-Aldehyde Reduction Protocol. *Organic Preparations and Procedures International*, Volume 53, Issue 5, July 2021, Pages 488-492, 10.1080/00304948.2021.1953889.

Marina V. Malovichko; Wesley T. Abplanalp; Samantha A. McFall; Breandon S. Taylor; Nalinie S. Wickramasinghe; Israel D. Sithu; Igor N. Zelko; Shizuka Uchida; Bradford G. Hill; Saurin R. Sutaria; Michael H. Nantz; Aruni Bhatnagar; Daniel J. Conklin; Timothy E. O'Toole and Sanjay Srivastava. Subclinical Markers of Cardiovascular Toxicity of Benzene Inhalation in Mice. *Toxicology and Applied Pharmacology*, Volume 431, 115742, November 2021, 10.1016/j.taap.2021.115742.

Saurin R. Sutaria; Sadakatali S. Gori; James D. Morris; Zhenzhen Xie; Xiao-An Fu and Michael H. Nantz. Lipid Peroxidation Produces a Diverse Mixture of Saturated and Unsaturated Aldehydes in Exhaled Breath That Can Serve as Biomarkers of Lung Cancer—A Review. *Metabolites*, Volume 12, 561, June 2022, 10.3390/metabo12060561.

Conference Presentations: <u>Sutaria, S.R.</u>; Khan, H.; Nantz, M.H. *Convenient preparation of muconaldehyde using one-pot acid-to-aldehyde reduction protocol.* **Talk** 279, presented at 2021 Midwest Regional Meeting of the American Chemical Society, Springfield, MO; October 22, 2021.

Awards: **Best Laboratory Graduate Teaching Assistant Award 2022**
Award presented by University of Louisville Chemistry Department

Work Experience: **University of Louisville,** Louisville, KY   August 2015 – May 2017
    School of Medicine, Department of Cardiology, Analytical Chemistry Core
      Research Lab Tech
- Review and Analyze data from various Chemical Measurement Instruments, for example output
from UPLC-MS

Subway Sandwich Shop DBA Saurin Inc., Louisville, KY   2005 – 2015
    Franchisee/Owner/Operator

- Managed all in store day to day operations, as well as handling all accounting, payroll, and taxes

Film and Television Productions, Louisville, KY   2012 – 2015
  Producer/Coordinator
- Worked on a variety of Film and Television projects, in almost every capacity

Student Activities: **Indiana University Southeast**, New Albany, IN   May 2016 – May 2017
  Organic Chemistry Research with Dr. Enoch Mensah
- Completed various organic chemistry reactions, work ups and purifications, all contributing towards a scholarly journal article

  University of Louisville, Louisville, KY   August 2003 – May 2005
  Student at Speed School of Engineering
- Completed 120 hours of various volunteer work and community service with Tau Kappa Epsilon